UNIVERSITY OF NOTTINGHAM

School of Chemical, Environmental and Mining Engineering

NOVEL AMPEROMETRIC GAS SENSORS

by

Kirsi Wallgrén, BSc.

Thesis submitted to the University of Nottingham
for the degree of Doctor of Philosophy, January 2005

Abstract

The electrochemistry of oxygen and methanol at solid polymer electrolyte (SPE)-based amperometric sensors, fabricated according to an all-planar design concept, has been investigated. The solid protonic conductors used were Nafion®-117 membranes and Polybenzimidazole (PBI) films. The working and counter electrodes were non-porous gold and/or platinum layers (300-1500 nm thick), sputtered on the same face of the solid electrolyte, separated by a gap of the ionic conductor (10-1 mm wide) and in contact with the gas sample. Such all-planar solid-state devices could offer potential advantages over sandwich-type gas sensors namely, reduction in precious metal electrode area and simplified fabrication.

Sensors based on both materials exhibited near-linear response to oxygen concentration changes (in the 0.1-21% v/v range) and response times comparable to those of commercially available sensors, irrespective to sample relative humidity, but the magnitude of the signal did depend on the latter even after ohmic correction or at low currents.

A systematic study of the effect of humidity on oxygen reduction and gold surface electrochemistry reveals, that the fall in the oxygen signal with decreasing humidity cannot be explained simply in terms of decreasing membrane conductivity and increased ohmic losses, but is related to the effect of water on the number of electroactive sites, their catalytic activity and oxygen reduction mechanism in general. The latter is further supported by the unusually high Tafel slopes obtained both on gold and platinum electrodes with decreasing levels of test gas humidification.

The shape of the oxygen reduction current-potential curves observed at open all-planar gold-based devices and the magnitude of current at both gold- and platinum-based ones, when compared to those of sandwich- and capillary-type arrangements, point to high mass transport rates and a thin or porous mass transport barrier. Current distribution considerations supported by surface electrochemistry estimates suggest that parts of the deposit closer to the reference and counter electrodes contribute more to the observed currents. Further experimentation by varying the deposit thickness and progressive masking of working electrode areas, revealed that the test gas reacted both at the line formed by the gas/solid electrolyte/metal layer interface (diffusion from the gas phase) and underneath the deposit (diffusion from the back of the sensor and through the Nafion® membrane), but not through the metal layer.

For monitoring of dissolved methanol (0.5-3 M) in acidic solutions using bare platinum microdisc electrodes and of methanol vapours (in equilibrium with 2-10% w/w or ca. 0.6-3 M aqueous solutions of methanol) using Nafion®-based all-planar platinum sensors, a simple amperometric method was developed. For both types of sensors a clear voltammetric picture was obtained with a good separation of methanol oxidation and oxygen reduction curves. The amperometric response could be correlated to the variations in methanol concentration, demonstrating the suitability of the method for crude monitoring of dissolved methanol levels in a range applicable to the feed of direct methanol fuel cells.

Acknowledgements

To Dr Sotirios Sotiropoulos without whom none of this would have been possible.

To City Technology Ltd for their financial contribution and technical expertise.

To Prof. Barry Azzopardi who agreed to supervise a project beyond his research interests.

To L3 workshop technicians for taking care of one of their own.

And to Bill.
I told you I would finish one day.

CONTENTS

LIST OF PICTURES

LIST OF TABLES

LIST OF FIGURES

CHAPTER 1

Introduction

The basic human desire to monitor and control our environment has created a fertile ground for sensor research. The real benefit in sensors is their ability to provide immediate feedback on the world around us just like our own five senses. The research in sensors is also one of the more free-spirited fields where new approaches and concepts are often embraced and explored eagerly.

Chemical sensors are used to gain information about the chemical nature of the environment, and their applications are almost limitless. The sensors can be small, probe-like and they can be used to monitor dynamic fluctuations. By adding a signal feedback they can be upgraded to control devices. Chemical sensors can be used in solid, liquid or gas phases, for analyte concentrations down to parts per trillion levels.

New environmental monitoring legislation brings new demands and challenges to sensor development and there has been a fast growth in sensor technology during the past three decades. Toxic gas and vapour monitoring (e.g. domestic carbon monoxide sensor or fertiliser run-offs from fields in contaminated natural waters) have opened huge markets.

Professor Janata and co-authors (Janata et al. 1988, Janata 1990, Janata 1992, Janata et al. 1994, Janata et al. 1998) have reviewed chemical sensors in regular intervals and growing number of publications, not only on specialist papers but also in scientific and engineering publications, prove the vitality of the chemical sensing field. Understanding of chemical sensors requires some knowledge on several academic areas creating a very interdisciplinary field.

1.1 Electrochemical gas sensors

Electroanalytical techniques are particularly attractive in view of their selectivity and sensitivity. They offer instantaneous in-situ measurements in the analyte environment and they provide direct relationship between the concentration of the analyte and the electrical output. Considering the benefits it is understandable that electrochemical sensors became the largest and oldest group of chemical sensors.

Electrochemical sensors are normally small, lightweight and personalised devices, that have a low power requirement, are cheap to manufacture and easy to use. They are easily adaptable to miniaturisation with high degree of robustness and reliability. These sensors can be found in very diverse applications:

Automotive industry – engine management, emissions monitoring
Aerospace industry – operating systems, air quality monitoring
Agriculture – modified atmospheres
Chemical industry – emissions, product quality
Safety – gas detection
Environmental monitoring – pollutants
Medicine – anaesthetic gases, metabolites

Challenges existing in electrochemical sensor research include the lack of selectivity when compared to other analytical techniques such as chromatography. The sensors also require a reference electrode that needs to maintain a constant half-cell potential over the course of the measurement (Heineman 1989).

An ideal electrochemical sensor does not actually exist as sensor characteristics are always a function of application, but certain properties should be expected:

1. Signal linearity

   The sensor should provide a direct relationship between the concentration of the analyte measured and the electrical output of the sensing device or at least it should be able to be calculated with simple mathematics
2. No hysterisis

   The signal should always return back to the same value using same pathway after switching off the sensor or changing back the analyte concentration.
3. Fast response time

   Sensor should react rapidly to changes in concentration – especially important in safety monitoring
4. Selectivity

   Sensor should be able to measure the analyte required without interfering signals
5. Sensitivity

   Detection limit of the sensor is the smallest change in the concentration that causes a significant change in sensor signal. For linear sensors this should remain constant.
6. Low residual signal

   The signal measured in an analyte-free medium. The smallest measurable concentration is determined by sensitivity together with intensity and stability of the residual current.
7. Wide operation range (dynamic range)

   The sensor should operate satisfactorily in as a wide analyte concentration range as possible.
8. Stability

   This refers to sensor performance over long periods assuming that the external conditions do not change. For devices with liquid electrolytes the lifetime is often determined by the drying out of the electrolyte.

9. Accuracy and reproducibility
10. Rugged construction

As it is difficult to develop a device matching the highest standards for all of the above characteristics, a working sensor generally represents a compromise between the properties and the real specific needs. For example, commercially available systems can be used to monitor from near 100% oxygen in medical and gas purity applications to around 20% for general air quality and hypoxia warning. Others can measure from a few per cent in flue gas analysis down to a few parts per million in some process control and gas purity applications (Hobbs et al. 1991).

Chemical sensors have had regular reviews since 1988 by Janata and various co-authors. In the first review (Janata & Bezegh 1988) the combined electrochemical sensors covered 80% of the total sensor publications. The research showed vigorous growth, particularly on amperometric micro sensors and on solid-state potentiometric sensors. By 1990 (Janata 1990) the trend towards miniaturisation was clearly visible within the electrochemical sensor group. Intensive basic research in microelectrodes was especially reflected in the strength of interest in amperometric sensors. A review in 1992 (Janata 1992) showed no particularly remarkable change in the distribution of sensor papers by type with potentiometric sensors together with ion-selective electrodes remaining the strongest group and the trend towards miniaturisation continuing. By the time of the next review in 1994 (Janata et al. 1994) the number of publications covering chemical sensors had increased by 45%. Although electrochemical sensors still remained the largest group of chemical sensors with the number of publications remaining steady, they had continued to decline relative to the total. In the 1998 review by Janata et al. (1998) electrochemical sensors were still the largest group, but now consisted only 49% of the published papers. It was discovered that the number of papers explaining sensing of individual species far exceeded the species themselves. This was attributed to the variety of applications with unique requirements that demanded individual characteristics. The reviewers emphasised that this practise requires authors to publish the limitations of their system as well as the benefits.

2002 gave electrochemical sensors their own review by Bakker and Telting-Diaz. They noted that even within electrochemical sensing field the diversity of electrochemical principles is quite large and that the research in electrochemical gas sensors is mostly driven by engineers and materials scientists. This can lead to engineering aspects being solved before the chemistry is fully understood, which in turn can lead to over-optimistic and uncritical attitude.

The majority of oxygen, and gas sensors in general, are electrochemical detectors (amperometric, coulometric, potentiometric, conductimetric and semiconductor sensors). The construction is based on cells whose output is directly related to the concentration or the partial pressure of the analysis gas. The other major class of common gas sensors, used mainly with flammable gases, is that of catalytic combustion sensors called microcalorimeters or pellistors. Flammable gases generally cannot be detected at ambient temperatures electrochemically, so the design is based on a Wheatstone bridge arrangement where the sensor can be heated to an operating temperature of ~500°C. The detector element of the bridge is coated with a noble metal coating that promotes combustion of flammable gases increasing the resistance of the coil while the compensator element remains unreactive giving output, that is directly related to the concentration of flammable gases in the atmosphere (Willett 1999).

1.2 Oxygen electrochemical sensors

The need for accurate measurement of oxygen increases as new industries are formed and existing technologies develop. Applications for oxygen measurement can be:

Medical – anaesthesia, incubators, controlled environments
Biological – fermentation, fruit storage, food packaging
Industrial – gas purity, safe operation of chemical plants
Energy management – optimal car fuel/air ratio
Area monitoring – hazardous areas, aircraft atmosphere

The demand for oxygen sensors in US by 2000 was ~40 million units and in Europe the market had grown to 25 million units by 2002. Although the market in these continents is believed to have reached saturation point, the tightening emission regulations in other countries ensure growing demand for oxygen sensors (Ramamoorthy et al. 2003).

1.2.1 General

Early methods for analysing oxygen included volumetric methods, such as the Orsat equipment, catalytic combustion and the measurement of inferential thermal conductivity (Kocache 1986). Analysis methods can also be based on the physical properties of oxygen. With methods based on the electrochemical properties of oxygen, the sensors can be found in all major classes of electrochemical detectors:

- Potentiometric
- Conductimetric
- Amperometric

Potentiometric sensors are the oldest and largest sensor field and one of the most studied. They detect the composition of a sample by measuring the potential difference between the sensing and the reference electrodes and the potential depends on the ratio of the partial pressures of the gas at each electrode. Zirconium oxide sensors, such as Rapidox by Cambridge Sensotec Ltd or a flue gas sensor by Apollo solutions are few examples of commercially available potentiometric sensors.

Conductimetric devices are utilising changes on the electrolyte conductivity to measure gas concentration. The simplest form of conductimetric sensor is a solution conductivity cell where the analyte gas is admitted to a cell where it can react with the appropriate electrolyte solution. The change in the liquid conductivity can then be measured (Hamann et al. 1998). Solid state conductometric sensors are based on semiconductors and can only be operated on elevated temperatures (300°C and above). Titanium dioxide (TiO_2) is one of the most widely studied semiconductors for oxygen sensors. Another promising material is Niobium pentoxide (Nb_2O_5) (Ramamoorthy et al. 2003).

1.2.2 Amperometric oxygen sensors

Amperometric gas sensors detect the composition of a sample with respect to the analyte gas by measuring the current produced by the electrochemical transformation of the gas. However, there is no conceptual difference between aqueous or gaseous amperometric sensors. Compared with laboratory analysis, amperometric sensors are simple instruments that can be mass-produced and sometimes even used as disposable sensors. As amperometric gas sensors are developing rapidly the field is often reviewed both generally and with respect to special types (Alber et al. 1997, Bontempelli et al. 1997, Opekar & Štulík 1999).

The operating principle is based on oxidation or reduction of species at a potential, which is characteristic of that species. At that potential the signal is proportional to the concentration and the information is obtained from the concentration – current relationship.

One of the two main types of electrochemical gas sensors is membrane-covered amperometric or galvanic devices. For oxygen sensing, the former is generally based on fuel cell technology and the latter on metal-air battery principles. In the UK the main manufacturers of amperometric oxygen sensors are Alphasense, Analox and City Technology Ltd. The operating principle of these sensors is based on a gas permeable membrane through which the gas diffuses to a noble metal cathode. The cell is completed with a lead anode and a liquid electrolyte. The electrolyte is usually potassium hydroxide with a pH of 10-12, but acids are used if the sensor is to operate in high carbon dioxide atmospheres. Sensor lifetime depends on the lead anode as the sensor dies after all the lead is oxidised. The electrodes and electrolyte are sealed in a metal or plastic container to prevent leakage and provide resistance to chemicals. However, as the lead anode oxidises during use, it occupies more volume than pure lead and the overall volume inside the cell expands. If the container is not properly designed, internal pressure build-up can split the sensor and cause leakage. For amperometric oxygen sensors, although mature devices, there are still plenty of research challenges left.

1.2.2.1 Sensor structure

The most common structures for amperometric gas sensors are:

- Clark cell

  Early amperometric sensors consisted purely of bare metal wires that could only be operated in conducting media and suffered from fouling-up of the electrode surfaces (Janata 1989). In 1959 L.J. Clark patented his cell where the sample was separated from the electrode compartment, which contains the electrodes and an internal electrolyte solution by a gas permeable membrane. This electrode is still an important instrument for the determination of dissolved oxygen, particularly in environmental studies.

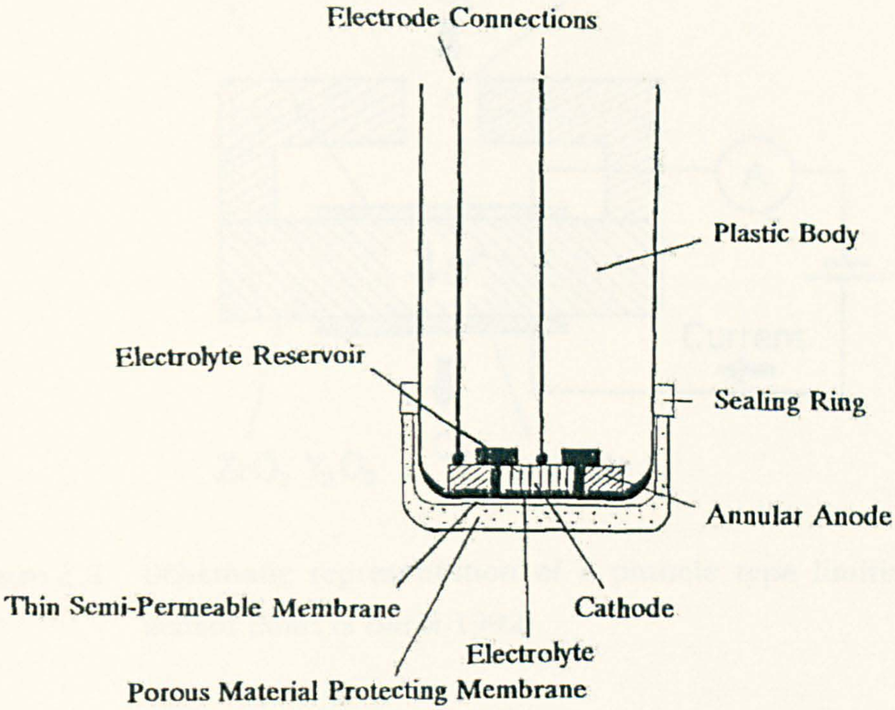

Figure 1.1 Schematic representation of a later Clark sensor (Sotiropoulos 1994)

- Metallised membrane sensors

  These sensors are similar to Clark type sensors but there is no diffusion through solution to the sensing electrode. This design improves response time.

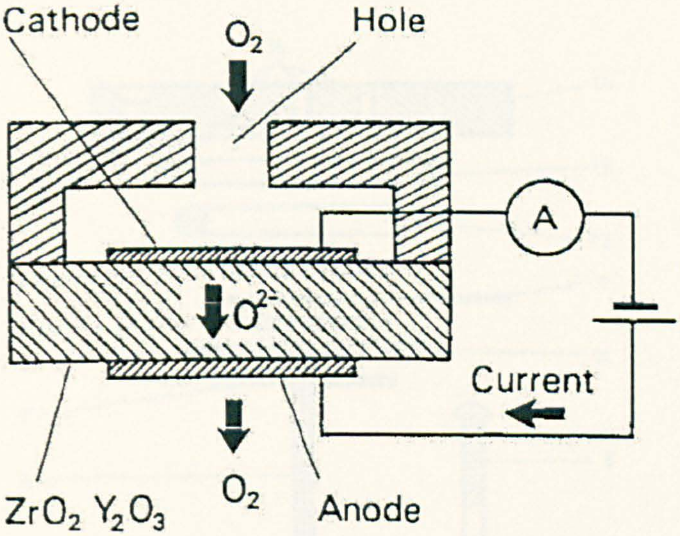

Figure 1.2 Schematic representation of a pinhole type limiting current sensor (Mari & Barbi 1992)

- Limiting current type sensor

The major application of limiting-current type oxygen sensors is in the exhaust system of modern cars, also known as λ-sensor, and hundreds of thousands of sensors are produced each year for this purpose. In these high-temperature sensors as the oxygen is reduced at the cathode, oxide ions diffuse through a zirconia layer to the anode where they are oxidised to oxygen. The electric current, which flows through the circuit, is limited by the oxygen flux to the cathode. In practical sensors the mass-transport is limited by creating a barrier (Janata 1989).

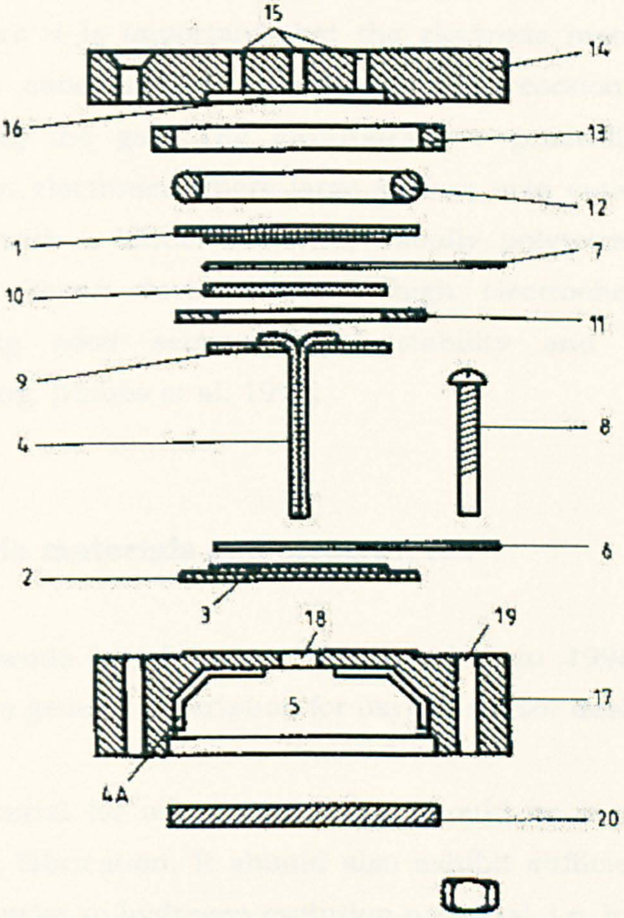

Figure 1.3 Commercial fuel cell acid electrolyte electrochemical sensor: 1 sensing electrode; 2 counter electrode; 3 counter electrode wick hole; 4 wick; 4A wick extension; 5 electrolyte reservoir, expansion chamber; 6,7 contacts; 8 terminal bolts; 9,10 separators; 11 gasket; 12 O-ring; 13 retaining ring; 14 top plate; 15 capillaries; 16 cavity; 17 bottom plate; 18 wick hole; 19 terminal post holes; 20 cover plate. (Hobbs et al. 1991)

- Fuel cells

Sensors with fuel cell principles with aqueous electrolytes are widely adopted to meet the growing demand for reliable and cheap devices in safety and process control applications. In its simplest form a fuel cell electrochemical sensor is built of a diffusion barrier, a gas permeable sensing electrode within an easy access for the analyte gas, electrolyte and a counter electrode deep within the cell interior. The principal rate controlling step should be diffusion through the barrier. Therefore it is important that the electrode material has high enough catalytic activity towards the reactions involved in detecting the gas. The electrodes are generally porous gas diffusion electrodes where large surface area catalyst powder is mixed with a binder material, usually polytetrafluoroethylene (PTFE). These electrodes have high electrochemical activity ensuring good sensor signal stability and resistance to poisoning. (Hobbs et al. 1991)

1.2.2.2 Electrode materials and electrolytes

Probe choice depends largely on application, but in 1998 Linek et al. attempted to give a general description for oxygen sensor design.

The cathodic material for oxygen reduction should be inert and flexible enough to permit fabrication. It should also exhibit sufficient plateau for oxygen reduction prior to hydrogen evolution potential, i.e. have reasonably fast electron transfer kinetics. Only the pure metals of gold, silver and platinum are used in oxygen sensors as they meet best the criteria required. Platinum is the most commonly used metal, as it exhibits good catalytic activity and follows the direct pathway on oxygen reduction. However the reaction at platinum is complicated and the electrodes can suffer from poisoning by sulphur compounds. Silver electrodes provide long-term stability and are even better catalyst for H_2O_2 reduction (see also below), but are still sensitive to poisoning. Gold is best at resisting the poisoning and has a long operating time over a wider potential range, but has to go through two-step reduction with a stable H_2O_2 intermediate

The use of liquid internal electrolyte restricts the design options and automated fabrication. It is essential that the electrolyte permit both anodic and cathodic reactions and also the transport of ions without extra reactions or side effects. In aqueous solutions and inorganic substances the side effects are suppressed by using additives. Neutral or alkaline electrolytes have predominated over the acidic ones. Large electrolyte reservoirs are preferred to avoid drying, when the measuring gases are not saturated with water vapour. But this increases the possibility of evaporation of the electrolyte or corrosion within the instrument, if sensors have leaked.

1.2.3 Oxygen electrochemistry

Cathodic reduction of oxygen is one of the most widely studied electrochemical reactions. Several experimental techniques have been used resulting in equally numerous theories to explain the observed results. The mechanism of oxygen reduction itself still remains a controversial topic and many of the aspects are not fully understood even after extensive research. In 1968 Hoare wrote a monograph to try to present a consensus of what was known about the oxygen electrode at that time and in 1992 Kinoshita brought together the latest knowledge in his book about electrochemical oxygen technology.

The kinetics and mechanism of oxygen reduction are a function of many experimental factors including the cathode material and the electrolyte, but in general the oxygen reduction is considered to follow two pathways:

a) Direct pathway or the four-electron reduction whereby oxygen is reduced directly into water.

Acid solutions:

$$O_2 + 4H^+ + 4e^- \rightarrow 2H_2O$$

Alkaline solutions:

$$O_2 + 2H_2O + 4e^- \rightarrow 4OH^-$$

b) Indirect pathway or the peroxide pathway.

Acid solutions:

$O_2 + 2H^+ + 2e^- \rightarrow H_2O_2$

$H_2O_2 + 2H^+ + 2e^- \rightarrow 2H_2O$

or

$2H_2O_2 \rightarrow 2H_2O + O_2$

Alkaline solutions:

$O_2 + H_2O + 2e^- \rightarrow HO_2^- + OH^-$

$HO_2^- + H_2O + 2e^- \rightarrow 3OH^-$

or

$2HO_2^- \rightarrow 2OH^- + O_2$

The direct pathway may also involve adsorbed peroxide intermediate, but there is no hydrogen peroxide in the solution phase. Pathway a) is predominant on noble-metal electrocatalysts (platinum, palladium, silver) and on metal oxides. The pathway b) is predominant on graphite, most carbons, gold and mercury and on most oxide covered metals (Kinoshita 1992).

There have been numerous studies of oxygen reduction in aqueous electrolytes with various reaction intermediates and rate-determining steps being proposed. A summary of possible reactions was compiled by Gnanamuthu and Petrocelli in 1967. They concluded, that different rate-determining steps for noble metals were possible depending on the overall reaction pathway, providing further evidence of the complexity of the mechanism for oxygen reduction. One of the most difficult problems with oxygen reduction study is the presence of a stable intermediate, H_2O_2. In most cases, rotating ring disk electrode is used to study the oxygen reduction as it proceeds via a complicated mechanism and depends amongst other things on cathode materials and chosen electrolyte. The chosen cathode must be a good electron transfer catalyst and a good peroxide decomposing catalyst at the same time. Experimental factors such as the condition of the electrode surface or impurities in the electrolytic solution can also affect the experimental data.

Platinum is the usual choice of electrode material as it follows direct four-electrode reduction in both acid and alkaline media. Most studies in platinum have been on acidic media but recently there has been increased interest to alkaline solutions as oxygen reduction kinetics are more rapid in alkaline than acid electrolytes (Kinoshita 1992).

In 1961 Lingane studied oxygen reduction at a platinum wire cathode. He considered the results of his experiments to prove that in both acidic and alkaline solutions oxygen is reduced all the way to water by a four-electron step without a hydrogen peroxide step. Later, researchers have suggested that with his experimental set-up he was not actually measuring the oxygen reduction but rather the amount of absorbed oxygen present on the electrode surface (Hoare 1968). Müller and Nekrassow (1964) presented evidence that the reduction of oxygen on smooth platinum in acid and alkaline solutions occurs in two stages with hydrogen peroxide as an intermediate product. Kosawa (1964) came to the same conclusion that the oxygen reduction on platinum required at least two processes including reactions of $O_2 + H_2O + 2e \rightarrow OOH^- + OH^-$ in alkaline and $O_2 + 2H^+ + 2e \rightarrow H_2O_2$ in acidic solutions. He also added that the proportion of peroxide formation depended on surface condition of the electrode. In 1966 Damjanovic et al. disputed previous findings with their studies using rotating ring disk electrode where any peroxide formed will diffuse to the ring electrode where it can be measured. They concluded, that the hydrogen peroxide step in acidic solutions is not an intermediate product but rather due to side reaction arising from the adsorption of residual impurities at the platinum surface. However preliminary studies in alkaline solutions showed that hydrogen peroxide was formed as an intermediate.

Later studies have concentrated on smaller details of the oxygen reduction reaction, as understanding and improving the reaction mechanisms on platinum catalysts are essential in fuel cell industry. In 1997 Tammeveski et al. studied electrochemical reduction of oxygen on thin film platinum electrodes in 0.1M KOH solutions using rotating disk electrode technique. They saw no essential change in mechanism for oxygen reduction on platinum films down to 1 nm thickness, but they did observe a decrease in specific activity with the film thickness that could be directly correlated to the particle size. However the studies of Geniès et al. (1998) on platinum nanoparticles in alkaline media using ring disk electrodes showed only slight effect (up to a factor of 3) with decreasing particle size. Most oxygen reduction studies have been either on pure metal electrodes or on poorly characterised alloy surfaces. To establish the influence of the surface structure on the reduction reaction researchers are turning on to studies on single crystals. In 2003 Schmidt et al. used single crystal platinum to study temperature effects on oxygen reduction reaction. They found the reduction reaction to be highly structure-sensitive and suggested that the reaction rate is mainly determined by the potential/temperature dependent surface coverage by OH_{ad}.

Gold is a very attractive electrode material when studying oxygen reduction, as it is the only precious metal that has an oxide free surface at oxygen reduction potentials. In acidic solutions oxygen and hydrogen peroxide reduction processes can interfere with each other. When a stable concentration of peroxide is achieved in the solution oxygen reduces directly to water via four-electron process (Bianchi et al. 1966). Studies in alkaline solutions have indicated the absence of direct four-electron reduction with hydrogen peroxide as a stable intermediate (Wroblowa et al. 1976). In 2001 Sarapuu et al. studied oxygen reduction on thin film gold electrodes using rotating disc electrode. They observed no change in the mechanism of oxygen reduction when varying the gold film thickness from 0.25 nm to bulk gold electrode, but the reduction of H_2O_2 on gold electrodes was very slow. In 2002 El-Deab and Ohsaka[1] continued studying oxygen reduction on gold electrodes in acidic media. Again with bulk gold electrodes the 2-electron reaction to H_2O_2 was observed, but further reactions interfered with hydrogen evolution. With addition of gold nanoparticles into the electrodeposited gold electrodes they observed enhanced catalytic activity with results indicating a change to two-step 4-electron reduction pathway: the first step being two-electron reduction of O_2 to H_2O_2 and the second reduction of H_2O_2 to H_2O. Further studies (El-Deab and Ohsaka[2] 2002) using gold nanoparticles - electrodeposited gold rotating disk electrodes showed no well-defined limiting currents indicating mixed control diffusion and kinetic limitations.

For kinetic studies of oxygen reduction, Tafel-slopes are used as they can take on characteristic values for various mechanisms. If the kinetics are determined purely by electron transfer, a linear Tafel-plot can be measured over current range of several orders of magnitude (Pletcher 1991). However, determining the reaction mechanisms should not be based on Tafel-slopes alone without additional independent data. For platinum and gold, in acidic solutions, the Tafel-value has been found to be 100 mV and 110 mV respectively. For silver the measurements in acidic solutions are more difficult due to metal dissolution. At relatively high current densities Tafel-slope has been measured to be 112 mV. In all of these cases the rate-determining step according to Hoare (1968) is most likely to be:

$$(O_2)_{ads} + e \rightarrow (O_2^{\bullet -})_{ads}$$

1.3 Methanol electrochemical sensors

1.3.1 General

Methanol is used in a variety of applications that can be divided roughly to three categories (Cheng & Kung 1994):

- feedstock for other chemicals
- fuel use
- other direct uses such as solvent, antifreeze, inhibitor or substrate

Simple organic compounds are regarded highly as a source of fuel. Mostly they are relatively non-toxic, easy to store, handle and produce and should have easy and straightforward reaction mechanism when compared to other possible organic fuels. Methanol specifically has been considered globally for a variety of fuel uses with direct applications such as power generation, internal combustion engines and fuel cells and with indirect use via derivatives (Short 1994). The recent changes in environmental policies concerning car exhaust gases increased interest in synthesising methanol to ethers producing Methyl tert-butyl ether (MTBE) and Tert-amyl methyl ether (TAME) which are used as oxygenates in reformulated gasoline (Kung & Smith 1994).

Sensitive and selective alcohol sensors are in demand in biomedical, chemical, drug and food industries. Morisawa et al. (2001) introduced a plastic optical fibre sensor for detecting vapour phase alcohol. The swelling of certain resins when exposed to alcohol vapour changes their polymer refractive index and the light intensity depended on the vapour pressure. The method produced a fast, stable and reproducible sensor that could be used as a gas leakage sensor for fuel cells or an atmosphere monitor in a brewery. Fuel cell research is one of the major driving forces to methanol sensor research, as practical operation of a fuel cell requires accurate monitoring and control of methanol concentration. A viable methanol sensor should have a sensitivity of ±0.02M over the range of 0.1-2M with a response time of less than 1 s. The sensor should also be robust and amenable for miniaturisation (Narayanan et al. 2000). In 1998 Barton et al. introduced an amperometric methanol concentration sensor based on current output being limited by methanol diffusion through a Nafion® 117 membrane. In their cell the reactant solution was introduced on the cathode side of the membrane and had to diffuse through a current collector, cathode and the membrane to oxidise at the anode. The output of the sensor was correlated within ±0.1M over a concentration range of 0-3M and a temperature range of 40 to 80°C. The response times varied from 10 to 50 s depending primarily on temperature, which they considered adequate for systems that operate with a constant load. Narayanan et al. (2000) were also researching a sensor for direct methanol fuel cell that would analyse the liquid methanol feed into the cell. They considered several techniques for methanol sensing including density, refractometry and ultraviolet (UV) light absorptivity, but these methods did not satisfy their design criteria. Eventually they designed a sensor based on same principles of methanol electro-oxidation as Barton (Barton et al 1998), but improved the cell design to enhance sensitivity and decrease response time. In their design the methanol is introduced first to the anode side with the transport of methanol to the Pt-Ru/Nafion® interface occurring through the backing and electrocatalyst layer. The changes improved sensitivity to 0.01M with response times of no longer than 0.2 s.

While the previous sensors were designed for liquid feed fuel cells, some fuel cell use gasified methanol. In 2001 Umeda[1] et al. introduced a detection of methanol vapour by using ultramicroelectrode-based electrochemical method. By covering the ring electrode with Nafion®-membrane they enhanced the methanol vapour detection efficiency by ~ 200 times compared to a bare electrode.

1.3.2 Methanol electrochemistry

Of all small organic molecules, methanol has been the most studied. Before 1980s the mechanism of methanol oxidation had not been agreed upon and even after 30 years of fundamental studies, the mechanism is still not fully understood.

In 1988 Parsons and Van der Noot wrote a survey of the fuel cell related research, making a clear distinction for papers published before and after 1980. Before 1980s many groups had worked on the subject, but the researchers had been divided on the oxidation mechanism into two groups depending on the species responsible for the poisoning effect. After 1980 the groups studying methanol oxidation used more rigorous methods and better-controlled experimental conditions. Improvements on the spectroscopic methods allowed clearer identification of the absorbed intermediates making many of the older work obsolete.

In the review (Parsons and Van der Noot 1988) it was accepted that platinum seemed to be the only sufficiently active catalyst in acidic solutions and various researchers preferred alkaline solutions for methanol oxidation as other materials were equally active when compared to platinum electrodes. There are still problems with the alkaline electrolyte namely progressive carbonation of the solution due to CO_2 retention that needed solving. Some researchers had also studied reactions on gold electrodes in basic solutions and observed better activity than with platinum or platinum-palladium alloys without signs of electrode poisoning. Beden et al. (1981) tested series of platinum alloys with tin, lead, rhenium and ruthenium. They discovered that platinum-ruthenium alloy displayed greater activity than pure platinum electrode under all the experimental conditions. The other alloys were catalytic only under certain conditions. Overall Parsons and Van der Noot (1988) concluded that gas diffusion anodes seemed to be the best anodes for organic fuel cells. They provide high current densities by making efficient use of the catalyst and only small amounts of electrolyte is required reducing the risks on handling corrosive liquids. However the electrodes still need platinum based catalyst, making them relatively expensive.

For a complete oxidation methanol has to go through a six-electron reaction:

$$CH_3OH + H_2O \rightarrow CO_2 + 6H^+ + 6e^-$$

Direct electro-oxidation is difficult and the actual reactions are complicated as several steps or parallel reactions are occurring with several products or intermediates. The knowledge of the different steps is however important to identify the reason for electrode poisoning. In 2001 Léger discussed methanol oxidation mechanisms based on work carried out in his laboratory and on other published results describing in detail the different steps of oxidation on platinum based electrocatalysts. The total oxidation pattern of the parallel reactions was summarised by Iwasita (2002) as:

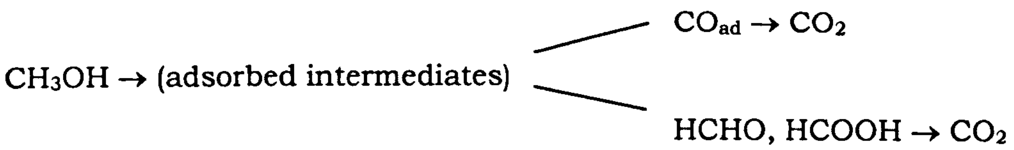

The concentration of the various oxidation products was found to depend on methanol concentration, temperature, electrode roughness and on the time of the electrolysis. In 1984 Ota et al. studied methanol oxidation in sulphuric acid solutions and they discovered that HCOOH & HCHO was mainly produced during the initial period of the reaction. Also, by increasing the roughness factor of the electrode they could improve methanol oxidation. In 1996 Lin et al studied the role of water in the electrocatalysis of methanol oxidation, by introducing the methanol either in the gas-fed or in the electrolyte-fed mode. They found difference on the mechanism of methanol oxidation depending on the feeding mode with electrolyte mode leading to the formation of a –CO or –COH species whereas the vapour phase mode seemed to enhance direct oxidation to CO_2. In 2001 Umeda [2] et al. continued gas-phase methanol oxidation studies using ultramicroelectrodes in the presence and in the absence of water molecules. They also discovered the oxidation peak potential to be water dependent with water reducing the overpotential of the reaction at platinum electrode. This all leads to difficulties when trying to understand the mechanisms of methanol oxidation.

1.4 Solid electrolytes

"The distinction between conductors and insulators is often not well-defined but is, to a certain extent, a matter of choice." Colomban P & Novak A. 1992.

Ionic conduction is common in liquids, but it is relatively rare in solids. Still the field of solid-state electrochemistry is not a new one and has its origins, as so much in electrochemistry, with Michael Faraday. He discovered that PbF_2 and Ag_2S were good conductors and established the first solid electrolyte in 1838 (Bruce 1995). In one of the first applications, solid electrolytes were used to measure thermodynamic properties of solid compounds in high temperatures. From there on the developments were steady until 1960s, when initial reports of gas sensors employing solid-state electrochemical techniques were made. The oil crisis in the early 1970s and growing environmental concerns also increased interest in solid-state ionics for batteries, fuel cells and gas sensors.

Solid polymer amperometric gas sensors were first introduced in 1972, but a nominally dry solid-state amperometric gas sensor was not reported until 1984 (Alber et al. 1997). Since then the development of solid-state amperometric sensors has been reviewed regularly (Alber et al. 1997, Opekar F. & Štulík K. 2002).

Classic electrochemical sensors are usually rather bulky and awkward. The use of liquid electrolyte lead to leakage, corrosion and limited lifetime of the sensors. One of the important approaches to replacing the liquid electrolyte was to use solid polymers that exhibit ionic conductivity. An important class of such polymers is ion permeable membranes, designed to pass selectively either anions or cations. So far the most successful ones are manufactured from one of two classes of polymer: styrene/divinylbenzene copolymers (Neosepta®, Selemion®) or copolymers of a perfluorinated alkene and a substituted perfluorinated alkene (Aciplex®, Nafion®) (Davis et al. 1997). Ion permeable membranes can also be used in a number of applications and where they can combine the roles of separator and solid electrolyte. The most successful of the applications is probably a fuel cell.

So far solid-state physical sensors have been a commercial success, but less so their chemical analogues. However to prove the potential for solid state gas sensors, one only has to look high-temperature potentiometric zirconia-based sensors that are well established for monitoring exhaust gases in automotive industry. In 1992, nearly 75% of solid oxygen sensors were used in the automobiles (Azad et al. 1992).

1.4.1 Solid protonic conductors and solid oxides

A range of materials has exhibited solid electrolyte behaviour and considerable number of mobile ions have been a target for research. West (1995) did a survey of solid electrolytes and found silver ion conductors numerically to be the most common and generally to have the highest conductivity. Sodium ion was also common because of the known properties of beta-aluminas and NASICONs. A third much sought after mobile ion is lithium because of the high voltages and power densities that can be obtained with lithium batteries. In the case of solid oxide conductors, their conductivity is due to the mobility of the oxygen anion at elevated temperatures. Stabilised zirconia was the first material discovered to exhibit oxide ion conductivity (Yamamoto 1995) and has been found applications both in sensor research (λ-sensor, Ivers-Tiffée et al. 2001) and in Solid Oxide Fuel Cells (SOFC). Despite much research since the early 1960s stabilised zirconia still remains one of the best materials for a SOFC (Yamamoto 1995).

Protonic conduction is a particular case of ionic conduction. Materials can be classified as solid proton conductors if protons can be transferred through the solid (Colomban 1992). They include glasses (Nogami et al. 2003), crystals (Chen et al. 1998), ceramics (Minh 1993) and organic and inorganic polymers. Solid protonic conductors were reviewed recently by Alberti and Casciola (2001). The materials can be classified in various ways depending on purpose, but for this review Alberti and Casciola decided to divide the conductors by operating temperatures. A majority of present materials operating below 100°C and with conductivity over 10^{-3} S cm^{-1} were already known 20 years ago and the progress in materials and applications has been low. However they felt great optimism for the prospects of solid state protonic conductors, as tightening environmental legislation and high fuel prices force industry to look for alternatives at the time the present knowledge is maturing and the problems relating to protonic membranes are near to being solved.

All solid electrochemical gas sensors incorporating organic or inorganic solid ionic conductors, such as hydrogen uranyl phosphate (HUP) (Lyon & Fray 1983, Lyon & Elgbar 1989), antimonic acid (Miura et al. 1984, Chivruk et al. 1997), beta-aluminas (Nāfe 1994, Davies et al. 1995, He et al. 1999) and zirconium phosphates and phosphonates (Alberti & Palombari 1989, Alberti et al. 1995) have been tested extensively. Although the conductivities of 10^{-4} to 10^{-2} S cm^{-1} are modest, they still seem to be sufficient for chemical sensing devices.

1.4.2 Solid polymer electrolytes

New developments were exclusively in inorganic solids and glasses until the early 1970s when a new material, polymer electrolyte, was introduced by Wright (1973) and Armand et al. (1978). Traditionally polymers were considered only as insulators and the conductivity was undesired property. However, the research to the thermodynamic and kinetic properties of ion conducting polymers prepared the ground for wide use in power sources, sensors and all solid devices. These polymer electrolytes could be fabricated as soft films of only a few micron thick.

The polymer electrolytes can have either positively or negatively charged ions covalently attached to the polymer backbone and therefore only the unattached counter ion has long-range mobility. Since the polyelectrolytes contain only one type of mobile ion, the interpretation of conductivity data is greatly simplified. (Bruce 1995)

Polymer electrolytes have found applications in almost all areas of modern electrochemical technology such as fuel cells (Ticianelli et al. 1988, Lufrano et al. 2001), batteries (Brodd et al. 2000, Kalhammer 2000), sensors (Opekar F. 1992, Bouchet R.[2] 2001), electrodialysis (Bazinet et al. 1998, Koter & Warszawski 2000) and most industrial electrosynthetic processes

(Kordali et al. 2000). The solid electrochemical devices based on polymer electrolytes offer several advantages, which apart from improved compactness include high power densities in the case of fuel cells and batteries and absence of problems related to corrosion and electrolyte leakage. It can also simplify product separation and purification and diminish any unwanted side reactions.

1.4.3 Solid polymer electrolyte sensors

Solid polymer electrolyte based sensors can be divided into two main groups: sensors containing a liquid phase and all-solid state sensors. In liquid phase sensors, the sensing electrode is mounted on the polymer facing the detection side. The other side is in contact with an electrolyte solution together with the reference and counter electrodes. These electrodes can be used for detection in both liquid and gas phases. Solid-state sensors are mostly used for detection in a gaseous phase (Opekar & Štulík 1999) and they are usually of a "sandwich" type arrangement where the electrolyte separates the sensing electrode from the reference and counter electrodes.

In polymer electrolyte sensors the indicator electrode is created directly onto the surface of the polymer or is in intimate contact with it. With these sensors the geometry can be designed on detection demands. They can be used in environments unsuitable for standard electrochemical measurements e.g. non-conducting liquids or gases, and it is not necessary to use a diffusion barrier since usually either the thin electrode layer or the polymer itself (depending on whichever is in contact with the analyte) serves as the mass transport barrier. Also in contrast to most solid electrolyte sensors, polymer electrolyte sensors operate in ambient temperatures.

The first reports of solid polymer gas sensors were written in the early 1960s, but amperometric gas sensors were not introduced until 1972 (Alber et al. 1997). In 1997 Bontempelli et al. reported a survey of electroanalytical sensors where porous electrodes were supported on perfluorinated ion-exchange membranes. They discussed the basic operative mechanisms and described the procedures for preparing the electrodes and the general strategies followed in sensor assembly. The basic design of these sensors had the sensing electrode, which is chemically or mechanically embedded into the membrane, facing the analyte while the uncoated side faced an internal compartment containing a suitable electrolyte and the reference and counter electrodes. The membranes were acting as ion-pumps that release or take up ions. The charges are quickly balanced by ion migration through the membrane and the electrolyte is required to transfer the charged species to counter electrode to restore the ionic content of the membrane. These researchers also discovered that the electrolyte was needed to maintain the membrane moist enough to make possible the ion transport inside the membrane. A wide variety of organic and inorganic electroactive analytes such as CO, CO_2, H_2S and SO_2 were reported in both electrolyte-free liquid media and gaseous atmospheres. The sensors were characterised by high sensitivity, low detection limits, short response times and wide dynamic ranges. In 1999 Opekar & Štulík wrote another review of electrochemical sensors with solid polymer electrolytes. Until recently the sensors operating at ambient temperature have been based almost exclusively on Nafion®. Few examples of anion-exchange membranes that have been used in sensors included poly(dimethyldiallylammonium chloride) and poly(ethylene oxide)complex with silver trifluoromethane sulphonate. Their survey of applications for solid-state polymer-based sensors included O_2, CO_2, NO_2, NH_3, HCl and methanol.

1.4.4 Nafion®

The first perfluorinated, ion permeable membranes were developed by DuPont and they began to market these membranes in the early 1970s. They created a copolymer of poly(tetrafluoroethylene) with poly(sulfonylfluoride vinylether) and gave it the trade name of Nafion®. At present, it is still the most common solid polymer electrolyte in electrochemical sensors.

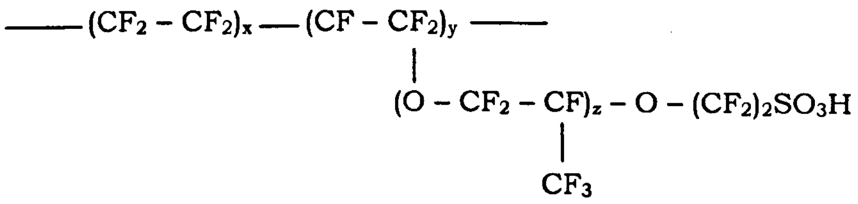

$$-(CF_2-CF_2)_x-(CF-CF_2)_y- \quad \text{with } CF \text{ bearing } (O-CF_2-CF(CF_3))_z-O-(CF_2)_2SO_3H$$

Figure 1.4 The chemical structure of Nafion® - membrane where x = 6-10 and y, z = 1. (Inzelt et al. 2000)

Perfluorosulphonate polymers typically have ordered structures where hydrophilic end groups aggregate within a hydrophobic matrix composed of the fluorocarbon backbone (see Figure 1.4). It is generally envisaged that the hydrophilic ionic groups attract further water during hydration forming pores and channels. This substructure must be three-dimensional as the membrane properties are essentially isotropic, e.g. the conductivity of Nafion® along the surface of the membrane is the same as if it was measured across the thickness of the membrane (Davis et al. 1997). The structure of the membrane has been extensively studied by a number of researchers. Methods used include x-ray scattering (James et al. 2000), IR (Laporta et al. 1999), NMR (Wintersgill & Fontanella 1998) and measurement of thermodynamic properties (Reucroft et al. 2002). On a larger scale the structure still remains controversial and the suggested models diverge. The general structure of a three-dimensional network of channels and pores is accepted, but as yet there is no agreement on their shape or dimensions. Gierke (1977) has proposed a "cluster-network" model, with the cluster diameter varying between 3 and 5 nm. Later Hsu and Gierke (1983) considered that the clusters are interconnected with short narrow channels.

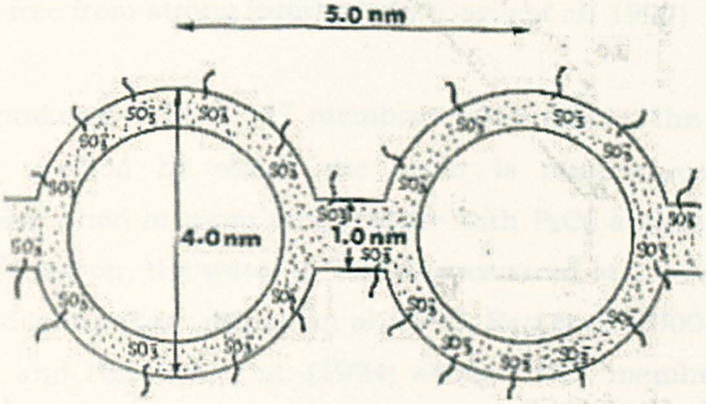

Figure 1.5 Cluster network model of Nafion® membrane (Pourcelly & Gavach 1992)

Nafion® membranes have been utilised in electrochemical processes, fuel cell membranes, coatings for ion selective electrodes, catalysis and pervaporative separators. Their relatively high cost and technical problems such as high methanol permeability and slow reaction kinetics in low operating temperatures needed for the membrane have led to development of new composites. Dimitrova et al. (2002) prepared recast Nafion® membranes by modifying them with silicon dioxide particles (Aerosil®) and molybdophosphoric acid. They found increased conductivity and reduced methanol permeability when compared to as-received Nafion® membranes. Another paper by Jung et al. (2003) describes the preparation of Nafion®/montmorillonite nanocomposite membranes. Their results also showed improved performance at high operating temperatures.

1.4.4.1 Nafion® conductivity as a function of water content

The electrical properties of Nafion® are strongly dependent on the amount of water contained in the membrane. The effect of humidity on conductivity and the uptake of water from surrounding media have interested several researchers, although sometimes with conflicting results. Studying the structure of water on membrane using differential scanning calorimetry (DSC) have revealed that the membranes contain at least three types of water; water that is bound tightly to the ions, weakly bound water and water that is free from strong interactions (Davis et al. 1997)

The water uptake of Nafion® 117 membrane depends on the pre-treatment and on the method by which the water is reintroduced. When the membranes are dried in room temperature with P_2O_5 and re-humidified in contact with solution, the water uptake is measured at 21 water molecules per sulphonic group (Zawodzinski et al. 1993, Ren et al. 2000). Zawodzinski et al. (1993) and Hinatsu et al. (1994) showed that membranes dried in room temperature can imbibe nearly twice as much water as those dried at elevated temperatures when immersed in liquid water. As polymer is partly dried, the ionic clusters in the membrane shrink in size, but remain aggregated. Further heating changes the structure of the membrane and when final traces of the water are removed disintegration of the cluster is possible (Zawodzinski et al. 1993). In 1996 Sone et al. came to the same conclusion. Zawodzinski et al. (1993) also showed, that the final water content of the heated membranes is dependent of the water temperature increasing from 11 to 16 water molecules per sulphonic group with increasing temperature. With the same pre-treatment Divisek et al. (1998) found the value to be slightly higher at 18.3 water molecules per sulphonic group, but they saturated the membranes in vacuum. The liquid water uptake depends on the structure of the membrane indicating strong interaction between the solvent and the polymer (Futerko & Hsing 1999).

When exposed to a humidified gas phase the membrane has been measured to absorb only 14 water molecules per sulphonic group. However the uptake was found to be independent from the pre-treatment (Futerko & Hsing 1999) in that case. This difference in water uptake by polymers exposed to liquid vs. saturated vapour phases is known as 'Schroeder's paradox' (Zawodzinski et al. 1993). It has been explained with the difficulty in condensing water vapour within the pores and the strongly hydrophobic surface of the polymer, which is less favourable than the imbibition of liquid water (Broka & Ekdunge 1997, Hinatsu et al. 1994, Zawodzinski et al.1993). Measurement of water content in various relative humidities has shown that there are two clear regions in water vapour activity. At 14-75 %

relative humidity there is relatively little increase in water content and the uptake of water results in solvation of the ions in the membrane. At relative humidities above 75 % there is a significantly greater increase of water content as the water is filling the pores and swelling the polymer.

Conductivity of the membranes is determined by measuring membrane resistance. As with water uptake, this data can vary, depending on whether the membrane is in contact with liquid electrolyte or gas, for electrical conductivity is a function of both temperature and the water content. Experimental values for perfluorinated membranes are reported to be within the range of 6 – 13 S m^{-1}, which at room temperature is comparable to the conductivity of 0.1M aqueous sulphuric acid at the same temperature (Davis et al. 1997).

The amount of water present in Nafion® membrane has been found to be more important for good ionic conductivity than earlier believed. So far all researchers, who have studied the conductivity (Anantaraman & Gardner 1996, Sone et al. 1996 to mentione a few), have agreed that in dry state Nafion® is a poor ionic conductor. In fact at low humidities, the membrane behaves more like an insulator. This is a result of drying out causing the channels to collapse and proton transport to become more difficult (Sumner et al. 1998). The conductivity increases with the increasing water content. It is believed that ions and water move along the same hydrophilic paths in the membrane (Okada et al. 1998). The proton drags 1-3 water molecules during migration and 4 water molecules are needed for the best proton migration in the membrane (Sone et al. 1996).

When relating the water content to conductivity, the majority of researchers have agreed that the membrane conductivity does not change linearly with regard to humidity (Anantaraman and Gardner 1996, Pourcelly et al. 1990) as can be seen in Table 1.1. However Zawodzinski et al. 1993 compared three different perfluorosulphonic membranes and reported that for Nafion® the conductivity depends roughly linearly on membrane water content. The research by Fontanella et al. in 1995 has also supported this idea.

RH%	**Conductivity S cm^{-1}**		
0			4.70E-07
20		5.00E-04	
31			4.40E-03
34	1.40E-04		
41	2.45E-04		
53	7.67E-04		
55	8.19E-04		
60	1.40E-03		
68	2.56E-03		
73	3.47E-03		
80	6.18E-03		
81			2.80E-02
93	1.36E-02		
100	6.61E-02	7.80E-02	5.50E-02
	Anantaraman & Gardner 1996	Sone et al. 1996	Sumner et al. 1998

Table 1.1 Conductivities of Nafion® membrane measured by several researchers at varying humidity levels.

1.4.4.2 Oxygen electrochemistry at the metal/Nafion® interface

A well-hydrated ionomer is a prerequisite not only for high electrolytic conductivity, but also for fast oxygen reduction reaction kinetics in polymer electrolyte fuel cells. The oxygen reduction reaction is studied extensively, as its slow reaction rate at fuel cell operation can cause large cell voltage losses. That can create a major problem for practical use of polymers as electrolytes. Most studies are with platinum electrodes as it is the favoured electrode material in fuel cell research (Paik et al. 1989, Parthasarathy et al. 1991, Uribe et al. 1992, Chu 1998). Chu studied platinum rotating ring disc electrode coated with varying thickness of Nafion®-film in 85% H_3PO_4.

He discovered that the Nafion®-coated electrodes exhibited higher kinetic currents than bare platinum electrodes and that the kinetic current increased with film thickness. This was due to higher oxygen solubility in Nafion® compared to the acid. However the advantage in dilute acid electrolyte is not as obvious as the overall oxygen concentration of those solutions is higher than in concentrated acid.

In 1989 Paik et al. studied the Pt/Nafion® interface without added electrolyte. They used platinum gauge that was either pressed directly to the Nafion®-membrane or was first coated with varying thickness of Nafion® solution. They discovered that coating the gauge with Nafion® increases the active surface area as it made the total surface area electrochemically active whereas for uncoated wire only the platinum/membrane contact area is active. In these samples mass transport and ohmic potentials were predominant, requiring modelling for kinetic parameters.

In 1991 and 1992 Parthasarathy et al. did a detailed study of oxygen reduction kinetics at Pt/Nafion® electrodes and at carbon supported and unsupported Pt microcrystallite/Nafion® electrodes. They criticised previous studies using rotating ring disc electrodes in acidic solutions, as these were not actually characterising the Pt/Nafion® interface. With no contacting liquid electrolyte phase they found two well-defined linear regions in Tafel-plots with slopes very similar to those obtained with aqueous acid electrolytes. They also agreed that Nafion® impregnation increases the active surface area.

In 1992 Uribe et al. used 10 and 100 μm platinum disks covered with Nafion® without added electrolyte at various levels of humidification and temperatures. They discovered that partial drying of Nafion® affected the kinetics of oxygen reduction reducing it sharply with the lowering of the water content. They speculated that at very low interfacial water levels there is ionomer surface restructuring and the hydrophobic domains of the ionomer may become predominant at the surface. Measurements by Divisek et al (1998) of the contact angles at the outer surface supports the theory that the surface is hydrophobic and the hydrophobicity increases with a decrease in water content.

In 2002 Mitsushima et al. studied oxygen reduction on platinum microelectrodes with various proton exchange membranes and again saw two distinct slopes of –60 mV/decade in the high concentration and -200 mV/decade in the low concentration region. They interpreted this as the number of electrons in the rate-determining step: a two-electron step in the high and a one-electron step in the low concentration region.

Gold has much less catalytic activity for oxygen reduction than platinum making subtle effects of Nafion® that could not be detected at platinum more easily observable. In 1992 Amadelli et al. studied gold-Nafion® electrodes where the gold layers faced either solution or gas phase. The free side was always in contact with an electrolytic solution. They discovered that oxygen reduction on Au-Nafion® electrodes show the same mechanism as on a conventional gold electrode. The Tafel-values close to –120 V/dec. indicate that the rate-determining step is the first electron-transfer reaction:

$$O_2 + H^+ + e^- \rightarrow {}^{\cdot}O_2H$$

In previous studies by Gottesfeld et al. 1987 and Lawson et al. 1988 it was found that Nafion® enhances the kinetic current for oxygen reduction at platinum electrodes. In 1998 Maruyama et al. studied the influence of Nafion® films on oxygen reduction using electropolished gold discs and found no significant effect on the kinetics or reaction mechanisms. They speculated that this could be due to pH levels of the membrane. Štrbac and Adžić (1996) had shown that the catalytic activity of gold for oxygen reduction is pH dependent and that the activity increases as the pH increases. As Nafion® is a superacid, the activity of Nafion® coated Au may be lower than bare Au. Another possible reason suggested was the structure of the interface between Nafion® and the Au-electrode.

1.4.4.3 Nafion® in fuel cell and sensor research

Perfluorinated proton conductors are characterised by high mechanical stability, chemical inertness and thermal stability that gives them advantages when used in applications involving high temperatures and corrosive environment. Nafion® has been widely studied for use in industrial electrolysers and fuel cells and until recently it has been the only polymer used in solid polymer electrolyte fuel cell research.

The first use of Nafion® membranes was in 1960s as fuel cells for space applications (Gavach & Pourcelly 1992) and by 1990s the use of Nafion® had been frequently studied for both methanol and H_2/O_2 fuel cells. In fuel cells the polymer is used as a proton conductor between the cathode and the anode. Most of the recent studies have concentrated on specific issues in fuel cell operations such as studying water uptake and transport in the membrane, the reaction kinetics or methanol cross over through the membrane, but few researchers are still using the membrane in actual fuel cells. In 1996 Samms et al. studied the thermal stability of Nafion® membranes in fuel cell conditions and found the membrane to be thermally stable up to 280°C, at which temperature the sulphonic acid groups began to decompose. In 1998 Scott et al. studied the performance of direct methanol fuel cell based on Nafion® and in 2003 Cao and Bergens suggested using 2-propanol as the fuel instead of methanol to reduce the cathode poisoning.

The sensor research using Nafion® as electrolyte does not start until the 1980s, when Miura et al. (1984) reported a voltammetric oxygen sensor using Nafion® as the electrolyte. The response of their sensor was reported to be too slow (>30 min for 90% response) and it did not present a practical system. In 1989 Yan & Lu reported studies with a solid polymer based oxygen sensor and they claimed to have written the first report on a successful solid-state electrochemical oxygen sensor. The sensor had a hydrophobic Teflon-bonded Pt black layer pressed on a piece of Nafion® membrane as a sensing electrode, with a diffusion-controlling capillary in front. It featured fast response reaching a 95% response in less than 5 s, low temperature coefficient and long-term stability with satisfactory linearity for oxygen contents in the range of 0-23%.

One of the first extensive studies for using Nafion® membranes in sensors was done by Schiavon et al. in 1989 when they investigated the use of Nafion® 417 in gases and low conductivity solvents. As electrode materials they tested platinum, gold, carbon and mercury. The vapour phase components varied from hydrogen and oxygen to ammonia, bromine and triethylamine. In each case they achieved satisfactory results and deemed electrodes supported on ion-exchange membrane to be very promising, especially since they are effective for both anodic and cathodic processes.

In the same year Opekar reported on a new development on solid polymer electrode sensor development (Opekar 1989). In all previous cases of metal/solid polymer electrolyte cells at least one side of the electrode was in contact with an electrolyte solution. In his case Nafion® 117 membrane with platinum electrodes with both sides in gaseous phase was used for detecting hydrogen. He found the sensor to have similar sensitivity to existing solid detectors. However the sensor was only useful in cases of low hydrogen concentration levels. For the higher ones the sensor required a reference gas. He continued the studies and in 1994 reported an improved design using platinum wire as an indicator and chemically deposited platinum as a reference electrode (Opekar et al. 1994).

The interest in using Nafion® as the electrolyte, in sensor research, remains strong for various analytes with Yan & Lu 1997, Hwang et al. 1998 and Liu et al. 2001 using it for O_2 sensors, Liu et al. 2002 for H_2 sensors and Yu et al. 2002 for H_2S just to mention a few.

1.4.5 Polybenzimidazole

Apart from Nafion®, another material that has gained interest in the fuel cell industry is sulphonated polybenzimidazole (PBI).

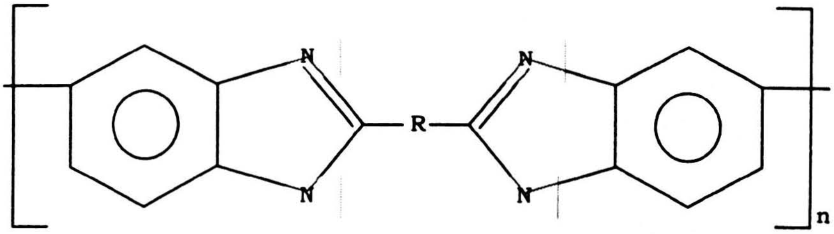

Figure 1.6 The chemical structure of PBI-membrane (Qingfeng et al. 2001)

PBI (poly(2,2'-(m-phenylene)-5,5'-bibenzimidazole)) is a rigid, highly aromatic polymer known for its excellent thermal and mechanical properties. Hoechst Celanese commercialised PBI fibre for thermal property clothing and fire blocking applications in 1983 (Chung 1997). Complexation of the basic polymer with a strong acid created a relatively inexpensive material that is reported to be conductive even when the activity of water is low (Bouchet et al. 1997, Kawahara et al. 2000).

1.4.5.1 Properties

Although the blends of PBI with monoprotic acids are reported to be poorly conducting, the immersion of PBI film in aqueous phosphoric acid is reported to lead to an increase in its conductivity (Wainright et al. 1995). PBI films that have been doped in acid form a single-phase polymer electrolyte with the acid dissolved in the polymer. Wang [1] et al. 1996 found the acid sorbed inside the membrane to be relatively immobile as compared to free acid. The studies on FT-IR have shown that phosphoric acid used for doping the films does not protonate the imidazole groups, but interacts with them by hydrogen bonding interactions of OH and NH groups (Kawahara et al. 2000).

In 1998 Fontanella et al. studied the conductivity of phosphoric acid doped polybenzimidazole at high pressures and temperatures. They observed that acid doped PBI behaved like a true polymer electrolyte where the ion transport is mediated by segmental motions in the polymer.

In 1999 Xing and Savadogo did a more systematic study of PBI conductivity using various acids for doping. They discovered that the conductivity depended on the type of acid used and on its concentration. The highest conductivities were measured with membranes that were doped with H_2SO_4, H_3PO_4 or $HClO_4$. In the same year Glipa et al. (Glipa et al. 1999) reported a systematic study on the conduction properties of PBI doped with phosphoric or sulphuric acid. They discovered that the conductivity of the membrane was independent of the concentration of the acid bath and depended only on the duration of the immersion. However the uptake of acid by the membrane depended on both the acid concentration and on time. Equilibration at 11-M phosphoric acid for 16 hours was found to yield a doping level of ~ 5 H_3PO_4 molecules / repeat unit.

Bouchet & Siebert (1999) and Bouchet [1] et al. (2001) studied structural characteristics and electrical properties of PBI that were doped with H_2SO_4 and H_3PO_4. They found the conductivity to follow Arrhenius behaviour and contrary to Fontanella et al. (1998) they suggested the proton transport to be by hopping mechanism (Grotthus mechanism) with which Qingfeng et al (2001) agreed. Qingfeng et al. also agreed that the electrical conductivity was dependent on the acid doping levels but they found it to be insensitive to moisture. That has been seen as a great improvement when comparing polybenzimidazole membranes to Nafion®.

For polymer electrolyte fuel cells it is critical to manage the water content of the membrane for sufficient proton conductivity (and to avoid electrode flooding). PBI is known to be hydrophilic and it can absorb 15 wt-% of water when at equilibrium with 100% RH atmosphere. The water molecules interact with imidazole groups increasing ionic conductivity by two orders of magnitude. The water not only form additional proton transport channels, but also significantly boosts proton mobility (Trichachev et al.

1989) However PBI has been reported to have relative insensitivity to humidification conditions by Wainwright et al. 1995 and Wang [1] et al. 1996. The study by Brooks et al. 1993 showed that the majority of the water in PBI is effectively mobile and not bonded to the polymer. In addition PBI has almost zero electro-osmotic drag compared to 0.6 – 2 for Nafion® (Phillips et al. 1993, Weng et al. 1996, Spry et al. 1997) so when protons transport through the membrane, they do not carry water and should lessen the problems with water redistribution. With the known problems of humidity on Nafion®, it makes PBI more interesting a material for sensor studies.

1.4.5.2 PBI in fuel cell and sensor research

After PBI was introduced as a new polymer electrolyte several researches have used it in fuel cells with various types of fuels. Wainright et al. 1995 performed preliminary tests with laboratory H_2/O_2 and methanol/O_2 fuel cells. Wang [1] et al. continued studies for H_2/O_2 fuel cell in 1996. Although their system had not been optimised, the system worked reasonably well and they could see potential benefits in the simplification of the cell design and cell maintenance. In the same year Wang [2] et al. also studied acid-doped PBI for methanol fuel cells.

In 1999 Pivovar et al. investigated several pervaporation membranes including PBI to reduce the cross-over in methanol fuel cells compared to Nafion®. Most of the other membranes offered no significant improvements when compared to Nafion®, but the characteristics of PBI suggested up to 15-fold improvement. They suggested that the improvements are due not only to limiting methanol crossover but also due to proton conduction via a Grotthus mechanism.

In 2000 Savadogo & Xing continued work on H_2/O_2 fuel cell and studied the potential-current characteristics of an acid-doped PBI fuel cell. They found that the cell exhibited high performances even when the cell was fuelled with hydrogen containing 3% CO, that would normally poison the electrodes.

The sensor research on PBI has concentrated on hydrogen sensors. Bouchet started his research in 1997 (Bouchet et al.) with preliminary experiments that showed linear dependence vs. hydrogen partial pressure. By 2001 (Bouchet [2] et al. 2001) they had improved the sensor structure and were concentrating on the sensing characteristics of the system.

1.5 All-planar amperometric sensors

The most common designs for commercially available amperometric sensors are sandwich-type sensors where the gas to be determined diffuses through a barrier to the sensing electrode that is separated from the reference/counter electrode by liquid or solid electrolyte. The counter electrode is usually embedded deep into the cell where no atmospheric gasses can enter. When designing these devices the resistivity of the electrolyte becomes an important factor. With the invention of solid electrolytes planar designs, where all the electrodes are on the same side of the electrolyte became possible. In these sensors the gas can either pass through the solid electrolyte or the electrodes are on the atmospheric side of the electrolyte. When the electrodes are in direct contact with the gas sample, faster response times and higher sensitivities are expected due to high mass-transport rates. Also as the labour-intensive stacking steps of sandwich-sensors can be avoided, the sensors are easier and cheaper to manufacture.

In the early experiments Brina et al. (1988) and Fleischmann and Pons (1991) used a planar design for a gas sensor, which consisted of two metal layers separated by a short path of glass serving as the ionic conductor. They proposed that the gas-phase electrochemistry would be occurring at the edge of the metallic sensing electrode. The sensor was used as alternative gas chromatography detector and required elevated temperatures due to the low conductivity of the glass. However, the sensors exhibited excellent performance when compared to a thermal conductivity detector and were even able to analyse complex mixtures.

In 1994 Sotiropoulos presented preliminary experiments in development of an all-solid planar amperometric sensor for oxygen determination in gas samples using Nafion® as the ionic conductor. He considered two different configurations: film-covered microelectrodes, where the Nafion® layer served both as a solid electrolyte and a diffusion barrier, and line electrode/solid ionic conductor/line electrode-devices. The electrodes exhibited a linear response to oxygen concentration changes with high diffusion rates in the line electrode case. A main disadvantage of the film-covered electrode was found to be the polymer dependence on hydration levels that restricted any practical use to well-humidified atmospheres, which could be avoided, by using the second configuration. The line electrode/solid ionic conductor/line electrode-devices offer the possibility of keeping the Nafion®-membrane wet by placing the backside of the membrane on to of a small reservoir.

Hodgson et al. (1998) continued experiments on devices where all of the electrodes are placed on the atmosphere side of the electrolyte to demonstrate the cell concept for the oxidation of SO_2. The proton-conducting medium in these investigations was phosphoric acid that was absorbed onto a silicon carbide matrix. Again fast response times were reported and the response was proportional to the SO_2 content in the analyte gas. Since then various planar designs have also been used for other gases e.g. CO (Yasuda & Shimidzu 1999) and NO_2 (Hrncirova et al. 2000).

1.6 Aims and objectives of the research program

The aim of the research program presented in this thesis was dual:

a. Further establishing the feasibility of using all-planar solid polymer electrolyte amperometric sensors in gas detection.

b. Investigating the mechanism of operation of all-planar solid polymer electrolyte sensors.

The specific objectives of the project have been:

- Using all-planar amperometric sensors, based on Au and Pt layer electrodes and Nafion® and PBI polymer electrolytes, for the detection of gaseous oxygen and methanol.

- Investigating the effect of sensor configuration (electrode arrangement and dimensions, inter-electrode gap, presence of capillary etc) on the amperometric response and clarifying the processes involved in the electrochemical detection.

- Studying the electrochemistry of gaseous oxygen at the Au (or Pt)/Nafion® and Au/PBI interface, particularly as a function of sample humidity and corresponding polymer water content.

- Studying the electrochemistry of gaseous methanol at the Pt/Nafion® interface.

1.7 Thesis structure

This thesis consists of six main chapters including this introduction. The introduction (Chapter 1) contains a literature review on electrochemical gas sensors in general and oxygen and methanol sensors in particular. The use of solid electrolytes in sensor research is also covered.

Chapter 2 describes the arrangement and fabrication of solid state sensors as well as the materials and equipment used in the experimental investigations.

Chapter 3 describes the use of Nafion® polymer electrolyte in all-solid planar oxygen sensors detailing experiments in gas streams of controlled humidity. The effect of humidity on sensor response and the mechanism of oxygen reduction are studied in a systematic way at both gold and platinum electrodes. The location of oxygen reduction at the planar sensors is also investigated.

Chapter 4 describes alternative sensor configurations to the all-planar sensor and details preliminary experiments of planar sensors using other than Nafion® solid electrolytes (PBI polymer and alumina).

Chapter 5 describes a method of determining dissolved methanol in acidic solutions either directly, using platinum microelectrodes or indirectly by the oxidation of methanol vapours at all-planar three-electrode Nafion®-based platinum sensors.

Chapter 6 summarises the main conclusions drawn from the thesis.

CHAPTER 2

Experimental

2.1 Planar sensor fabrication

2.1.1 Polymer electrolyte substrates

Nafion® membranes (Nafion® 117 protonic form, approximately 180 µm thick, Aldrich) were washed thoroughly with distilled water before it was stored in distilled water. A piece of membrane, of typical dimensions of 40 by 40 mm, was cut when required and dried using lint-free tissue paper prior to use.

PBI (Polybenzimidazole) films were prepared by dissolving 10 % w/w of PBI (Aldrich) in DMAc (Dimethyl-acetamide, Aldrich). 2% w/w LiCl (Aldrich) was added to the solution to prevent stretching of the final membrane. The mixture was stirred at 60°C for 5 days to increase PBI solubility and then centrifuged for any undissolved material to settle. The homogeneous upper part of the solution was used to cast films, which were cured in an oven at 50° C for two days. This produced flexible films of approximately 200 µm thickness. The films were boiled in distilled water for 4 h to remove any remaining solvents and then treated in 11-M phosphoric acid for 2 days. The films remained under ambient conditions overnight before metal sputtering took place.

2.1.2 Electrode layers

The metal layers of the working and counter electrodes (WE and CE) were vacuum-deposited onto the polymer substrates using varying numbers of deposition cycles with a PS3 E500C Series 3 Polaron sputter-coater. One second of coating gave about 3 nm thick gold layer or about 1.5 nm thick platinum layer. The thickness of layers was varied from 360 nm to 1140 nm in all planar samples to 1600 nm in sandwich-type samples.

A 0.5 mm thick stainless steel sheet with machined openings was used as a mask during vacuum metal deposition of the electrode layers. A piece of the membrane with the mask was attached tightly to a 40 mm square stainless steel slide before being placed in the sputtering chamber.

Electrical contacts between commercial insulated wires and the metal deposits were made either with the help of Ag-loaded epoxy resin (RS) with Araldite epoxy resin (RS) providing mechanical strength to the contact or with crocodile clips in contact with small pieces of aluminium foil pressed onto the electrode surfaces. In the last case the aluminium foil was acting as a current collector.

2.1.3 Electrode arrangement

Picture 2.1 shows an example of a typical two-electrode all-planar sensor, where contacts were made using Ag-loaded epoxy resin (RS) and Araldite epoxy resin (RS).

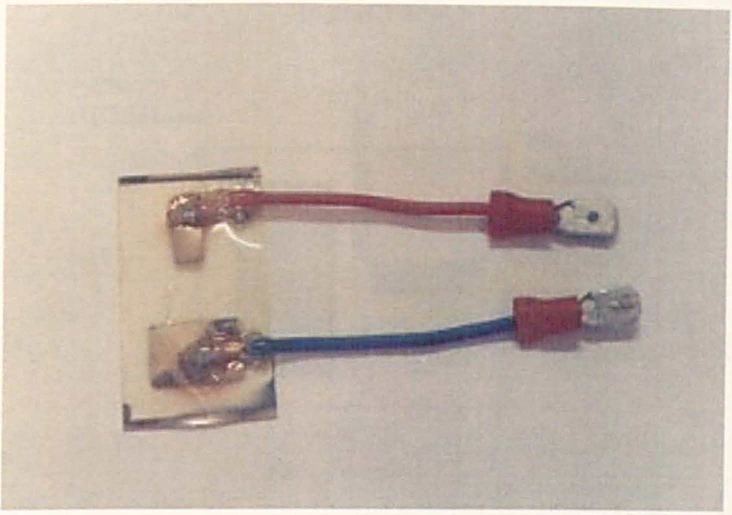

Picture 2.1 Photograph showing a typical two-electrode Nafion® sensor with working electrode length of 5 mm, Nafion® path of 10 mm and counter electrode length of 15 mm. The connections (red for sensing electrode, blue for counter electrode) were made with Ag-loaded epoxy resin (RS) and Araldite epoxy resin (RS).

For three electrode experiments (majority of experiments) a strip of Ag/AgCl electrode was placed between the working and counter electrode layers and pressed onto the membrane at c.a. 1 mm distance from the working electrode with a crocodile clip. A top- and side-view drawings of the device used for three-electrode experiments is given in Figures 2.1 and 2.2.

For most experiments, both the top/front of the sensor and the back/membrane side of the sensor were fully exposed to the reactant gases in the reaction cell.

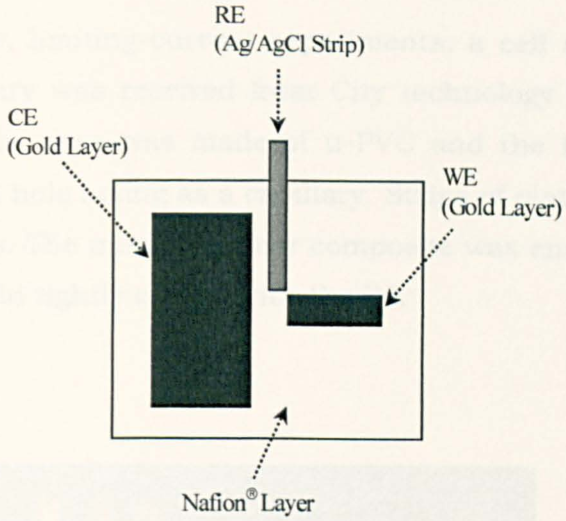

Figure 2.1 Schematic representation of the three-electrode device with working electrode length of 5 mm, Nafion® path of 5 mm and counter electrode length of 30 mm. Overall mask dimension 40 mm square.

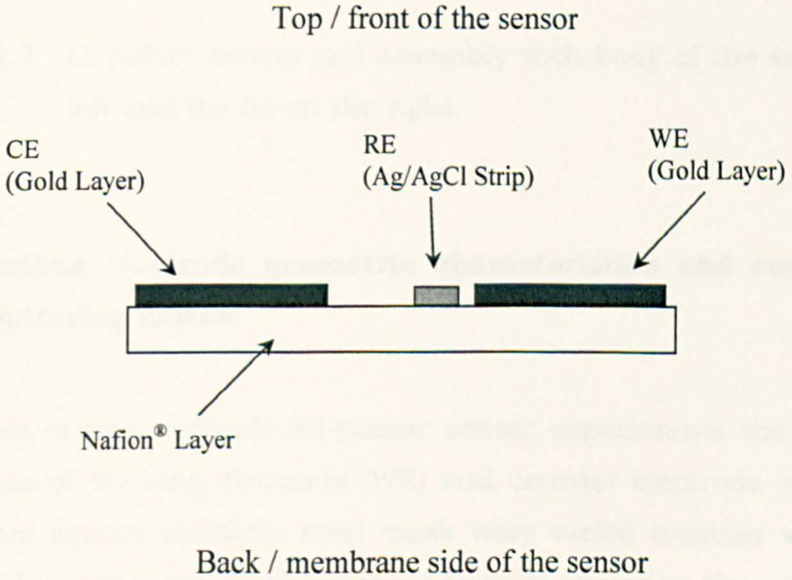

Figure 2.2 Side view of the three-electrode device

For capillary sensor, limiting-current experiments, a cell assembly with a lid bearing a capillary was received from City technology Ltd (see Picture 2.2). The body of the case was made of u-PVC and the lid was made of Nylon with a 1.5mm hole acting as a capillary. Strips of platinum were used as current collectors. The metal/polymer composite was encased in the cell bottom plate and held tightly onto it with the lid.

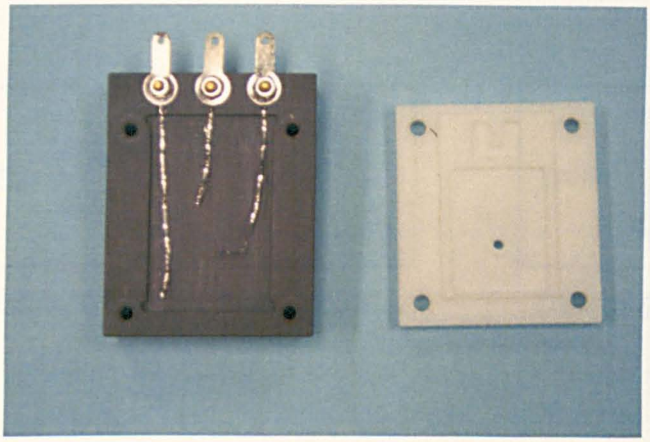

Picture 2.2 Capillary sensor cell assembly with body of the sensor on the left and the lid on the right.

2.1.4 Various electrode geometric characteristics and corresponding sputtering masks

In a series of two-electrode all-planar sensor experiments the sizes of the open areas of working electrode (WE) and counter electrode (CE) cut into the 40 mm square stainless steel mask were varied together with the gap between the electrodes to study the effects of changing the configuration. The following configurations were used in two-electrode open sensor experiments:

Device A: WE length = 5 mm, Nafion® path = 10 mm , CE length = 15 mm
Device B: WE length = 5 mm, Nafion® path = 5 mm , CE length = 30 mm
Device C: WE length = 1.6 mm, Nafion® path = 1 mm , CE length = 30 mm

A diagram of the masks can be seen in Figure 2.3. As was stated also before, for three-electrode open sensor experiments, mask for device type B was used exclusively.

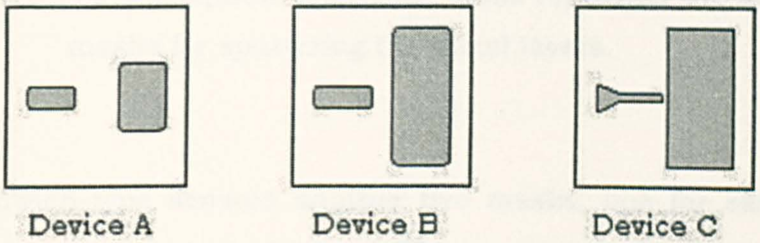

Figure 2.3 40 mm square stainless steel masks used for sensor configuration of devices A, B and C. Darkened areas represent the openings on the masks for sputtering the metal layers.

The usual assembly used in three-electrode open-type sensors was too large to fit within the cell assembly so a new mask of a smaller size, but same electrode proportions to configuration B, was prepared for these experiments.

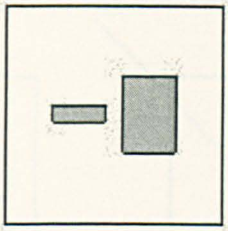

Figure 2.4 Mask used for capillary sensor configuration with working electrode length of 1.6 mm, Nafion® path of 1.6 mm and counter electrode length of 10 mm. Overall mask dimension 40 mm square. Darkened areas represent the openings on the masks for sputtering the metal layers.

For sandwich-type sensors another two masks, one for each face of the polymer membrane, were prepared. The sensing electrode was a circle of 15 mm diameter with another strip connected to the end of the circle, opposite to the reference electrode. During experiments this strip was covered with thick aluminium foil. The counter electrode was then deposited on the other side of the membrane, covering most of the sensing electrode. The reference electrode was positioned on the counter electrode side of the sensor opposite to the covered strip of the working electrode.

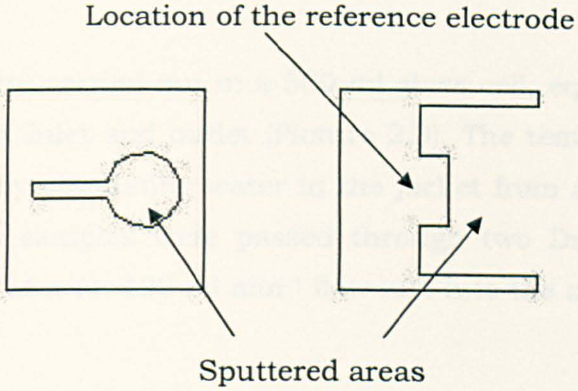

Figure 2.5 Masks used for sandwich-type sensor configuration. The left mask was used to cover the front/sensing electrode side and the right back/counter electrode side of the membrane during sputtering.

For all platinum sensing electrodes, the sensor was first scanned at fast rate to extreme potentials to clean the surfaces from impurities. For gold sensing electrodes no pre-treatment was required. All scans used in the result chapters are from stable voltammograms.

2.2 Electrochemical and analytical equipment

Two-electrode experiments were carried out with a purpose built waveform generator and current amplifier. A Duo 18, 2-channel 18-bit A/D converter (World Precision Instrument) was connected to a 486 PC and used for data acquisition.

For three-electrode experiments two different potentiostats were used. For preliminary cyclic voltammetry and oxygen concentration step experiments, a Radiometer Voltamaster 21® potentiostat, interfaced to a 486 PC by a Duo 18 A/D converter, was used. The majority of experiments were performed with an Autolab PGSTAT30 potentiostat controlled by GPES software version 4.5 for Windows 95.

2.3 Cell and Gas Mixtures

Experiments were carried out in a 500 ml glass cell, equipped with a wall-jacket and a gas inlet and outlet (Picture 2.3). The temperature of the cell was controlled by circulating water in the jacket from a thermostatic bath (25°C). The gas samples were passed through two Dreschler-type flasks before being fed at a ca. 100 ml min^{-1} flow rate into the cell.

Picture 2.3 Reaction cell used in experiments

The gas streams were laboratory compressed air (21% Oxygen), Pure Nitrogen (Air Products Ltd, 99.998%) and gas mixtures of 4%, 8%, 12% and 16% v/v Oxygen in Nitrogen (Air Products Ltd, White Grade, 2% accuracy).

For controlled humidity experiments, KOH (Aldrich, 85+%) solutions with distilled water were prepared to concentrations of 16, 10.5, 7.5 and 4M equivalent to 20%, 40%, 60% and 80% relative humidity (data from international critical tables, National Research Council (US) 1926-1930) and divided evenly to both Dreschler-flasks. For 100% relative humidity pure distilled water was used. The humidities were confirmed with TESTO6400 hygrometer. Also LiCl (Aldrich, 99%) solutions of 8, 4 and 2M concentrations, which are equivalent of 50%, 65% and 80% relative humidity (National Research Council (US) 1926-1930), were prepared to exclude the possible effects of alkalinity on obtained results.

For methanol vapour determination experiments one of the Dreschler-flasks was always filled with distilled water for initial humidification of the gas sample. A second flask contained 1%, 2%, 3%, 4%, 6% and 8.5% w/w methanol in water solutions, to achieve different methanol partial pressure values in the gas stream.

2.4 Chemicals

The chemicals used in this work are listed in a table 2.1 below, together with their supplier and grade.

Chemical	Supplier	Grade / Purity
Ag-loaded epoxy resin	RS	
Araldite epoxy resin	RS	
N,N-Dimethyl-acetamide	Aldrich	99%
Lithium chloride	Aldrich	99%
Methanol	Fisher chemicals	SLR / >99.5%
10% Platinum in activated carbon	Alfa (Johnson Matthey)	HiSPEC™2000
Orthophosphoric acid	Fisher chemicals	SLR / >85%
Polybenzimidazole	Aldrich	
Potassium hydroxide	Aldrich	ACS / 85%+
Nafion® membrane	Aldrich	
Nafion® perfluorinated ion-exchange resin	Aldrich	
β/β"-alumina	Ionotec Ltd.	
Gold disc	Agar Scientific	
Platinum disc	Agar Scientific	
Distilled water		
Compressed air		
Nitrogen	Air products	99.998%
4%, 8%, 12% & 16% Oxygen in Nitrogen	Air products	White grade, 2% accuracy

Table 2.1 Chemicals used in this work.

CHAPTER 3

All-solid planar oxygen sensors based on Nafion® polymer electrolyte

3.1 Introduction

Commercially available amperometric gas sensors usually involve a metallised gas-permeable porous material in contact with an internal electrolyte (Bergman 1970, Evans et al.1989). This type of design has been found to lead to slow response times due to gas diffusion through the porous medium and to limited lifetime, due to occasional drying out of the liquid film. The use of a solid ionic conductor as an electrode substrate allows the active electrode material to be directly exposed to the gas sample, improving the response time and sensitivity of the device (Hobbs et al. 1991, Schiavon et al. 1989 and 1990). All-solid electrochemical gas sensors, where the solid ionic conductor (e.g. Nafion® (Opekar 1992, Millet et al. 1996), antimonic acid (Miura et al. 1984, Chviruk et al. 1997) or Zr phosphates and phosphonates (Alberti & Palombari 1989, Alberti et al. 1995)) is sandwiched between the working and counter electrodes, have also been tested.

An alternative design for all-solid amperometric gas sensors where all the electrodes are deposited or attached on the same face of the ionic conductor, separated by an uncovered strip of the electrolyte, and in direct contact with the gas sample (Hodgson et al. 1998, Sotiropoulos et al. 1999) has been tested. It was suggested that due to the non-porous nature of the electrodes and the arrangement used in that design, the gas is reacting at the line formed between the working electrode metal layer, the solid electrolyte and the gas sample. Potential advantages of the design include faster response times and higher sensitivities per useful electrode area. The mass-transport rates of the gas to the sensing electrode are higher since no significant membrane or liquid film barrier are expected at the locus of the electrode reaction. Furthermore, smaller quantities of precious metal catalyst could be used for the working electrode as the reaction is occurring at the edge of the deposit and hence a thin line of catalyst should suffice. Finally, the labour-intensive stacking steps required for the fabrication of sandwich-type designs could be avoided. The use of Nafion® as the ionic substrate in the new sensor design is a convenient first choice for a material since there is extensive literature regarding oxygen reduction at the Pt/Nafion® interface (Gottesfeld et al. 1987, Lawson et al. 1988, Parthasarathy et al. 1992 and Uribe et al. 1992, to mention a few).

In this chapter the behaviour of three-electrode oxygen sensors based on the arrangement described above is investigated, in water-saturated and ambient gas samples. The dependence of oxygen electrochemistry, gold surface electrochemistry and uncompensated resistance on humidity levels is studied to determine whether it is merely an IR drop effect or whether it is related to changes in electrode activity as the polymer water content is varied. We also investigate the possibility of using a two-electrode device based on the new design concept, a modification, which could further simplify the manufacturing and operation of the sensor.

3.2 Sensor response in water-saturated gas streams

3.2.1 Voltammetry at three-electrode Au (vs. Ag/AgCl)/Nafion®/ Au planar sensors

Figure 3.1 shows a cyclic voltammogram recorded at 50 mV/s at a three-electrode assembly with all electrodes on the same face of the membrane (sometimes termed simply as "planar arrangement" hereafter) in a water-saturated air stream.

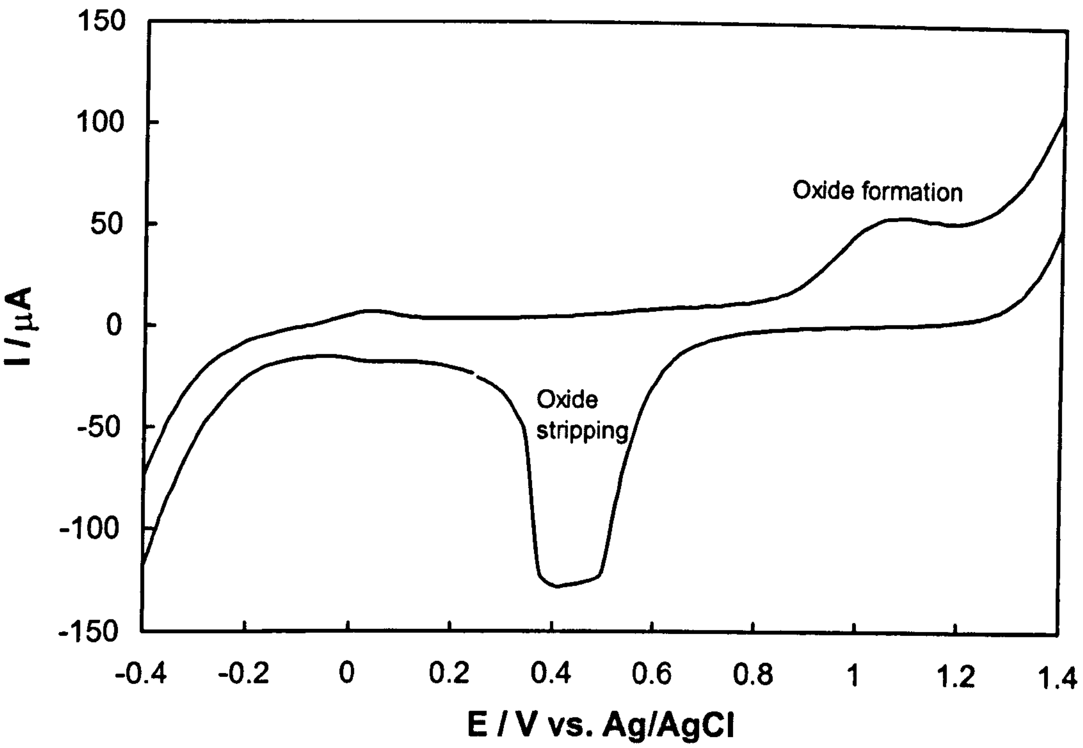

Figure 3.1 Voltammogram recorded at 50 mV/s in a water-saturated air stream at a three-electrode Au (vs. Ag/AgCl)/Nafion®/Au planar device

A well-defined voltammogram, typical of aqueous gold electrochemistry reported by Capon and Parsons (1972), was recorded with a Type B (WE:CE length ratio = 5:30 mm, see also Experimental 2.1.4) solid-state device. The three-electrode operation mode ensures that the features can safely be attributed to the working electrode layer that is in contact with the hydrated Nafion® environment. These features are the oxide formation plateau in the +0.85 to +1.25 V vs. Ag/AgCl range, and its stripping-reduction peak at +0.45 V vs. Ag/AgCl, which is slightly broader than those reported by Capon and Parsons (1972). A crude estimation of the area below this cathodic peak gives an approximate charge of 606 µC. Since the charge corresponding to the formation/stripping of a gold monolayer on a smooth gold electrode is known from the literature to be 420 µC/cm^2 (Capon and Parsons 1972), the true active electrode area of the working electrode is estimated to be as high as 1.4 cm^2. Using the roughness factor of similar gold deposits on Nafion®, reported to be anywhere in the 10-100 range (Kita & Nakajima 1986, Schiavon et al. 1989, Amadelli et al. 1992), and the length of the working electrode edge parallel to the counter electrode layer (0.5 cm), the effective width of the electrode layer in the direction away from the counter electrode layer that undergoes gold surface reactions can be estimated, at the given current range of 100 μA. The uneven current distribution encountered at this type of planar electrode arrangement (i.e. the electric field focusing between the two opposing edges of the coplanar working and counter electrode layers) results in the current passing through an apparent working electrode area of 0.28 cm wide x 0.5 cm long (0.14 cm^2) or 0.028 cm wide x 0.5 cm long (0.014 cm^2), depending on whether a roughness factor of 10 or 100 is assumed. Note that the nominal planar geometric area of the entire working electrode layer is 1.25 cm long x 0.5 cm long = 0.625 cm^2 and hence, the electroactive area is only a fraction of the nominal area. The calculations hold for the given current range (100 μA) and conductivity conditions (water-saturated polymer substrate), which determine the current and potential distribution in the planar electrode arrangement.

Figure 3.2 presents voltammograms recorded at 5 mV/s in water-saturated air and nitrogen streams with the same device. At the moderate polarisations shown here, there is a clear exponential rise of the current in the presence of oxygen. The difference between forward and reverse scans at higher negative potentials could be due to partial proton depletion of the electrolyte as oxygen reduction proceeds on gold.

$$O_2 + 2H^+ + 2e^- \rightarrow H_2O_2$$

$$H_2O_2 + 2H^+ + 2e^- \rightarrow 2H_2O$$

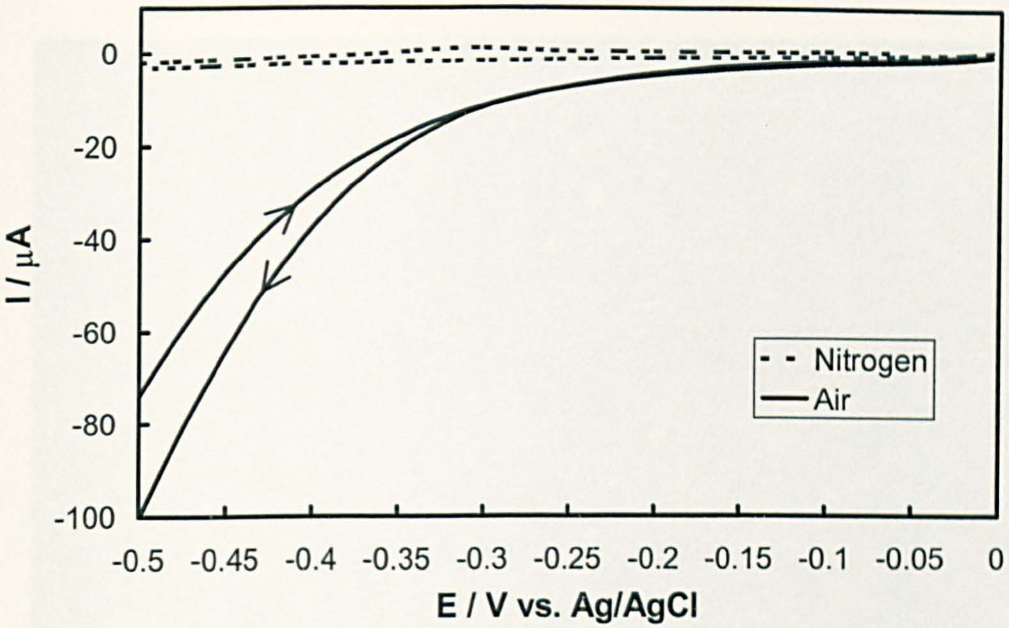

Figure 3.2 Voltammograms recorded at 5 mV/s in water saturated air and nitrogen streams at a three-electrode Au (vs. Ag/AgCl)/Nafion®/Au planar device

The current keeps rising exponentially up to moderate polarisations, with no signs of a limiting current even at extreme negative potentials up to −1.0 V (not shown here). Note that in aqueous acid solutions, oxygen reduction on gold electrodes does show limiting current (see for example El-Deab and Ohsaka [1] 2002). This indicates that oxygen reduction is never under mass transfer control at least in the 4-25 % concentration range studied in this set of experiments. Such lack of limiting current would be expected for a fuel-cell type porous electrode but in the case of a uniform non-porous gold layer, as confirmed by SEM micrographs (Picture 3.1), the scans seen in Figure 3.2 could be possible if oxygen reduction occurs primarily at the metal/Nafion®/gas line formed at the edge of the gold deposit or/and through the permeable 175 μm thick Nafion® membrane, i.e. in the absence of a significant mass transfer barrier (compared to the very slow kinetics of oxygen reduction on gold).

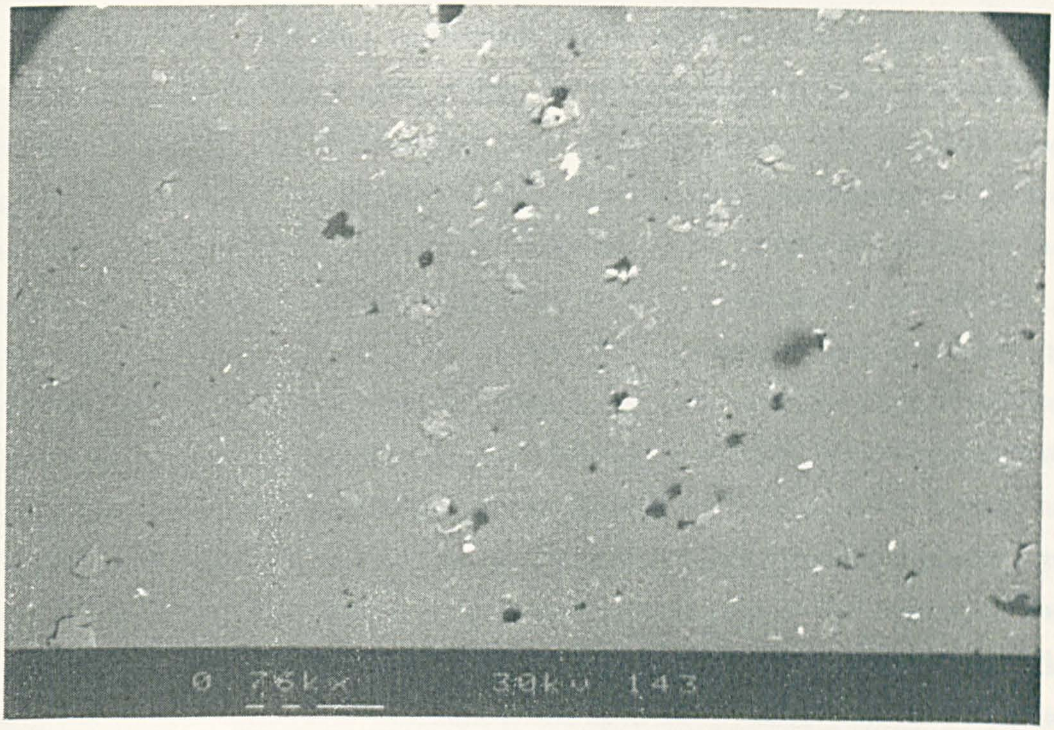

Picture 3.1 SEM micrograph of gold coating on Nafion® film. The pinholes observed are already present in the membrane.

The possibility of oxygen diffusing through the thin (0.36 μm thick) gold layer can be dismissed at this stage on the following grounds. In experiments where the gas flow rate was varied in the 50-600 ml/min range, no flow dependence of the current was found even at extreme potentials where, in the presence of a thin mass transport barrier, the current should be at least under a mixed mass transport and kinetic control. Schiavon et al. (1989) used gold layers on Nafion®, with the latter in contact with the electrolyte where the counter electrode was positioned. In such an arrangement oxygen had to diffuse through their 0.1 μm metal layer, and they did indeed find an increase of the signal with increasing flow rate until the former stabilised at flow rates higher than 100 ml/min. The same authors also observed a clear limiting current plateau for oxygen reduction on their devices, using alkaline internal electrolytes (Schiavon et al. 1989).

The oxygen reduction current in air at –0.1 V vs. Ag/AgCl (ca. 4.8 μA after background correction, for the particular device of Figure 3.2) corresponds to 4.8 μA/1.4 cm^2 =3.4 μA / active cm^2, if it is assumed that oxygen diffuses through the metal layer and reacts at a large part of the Au/Nafion® interface beneath. The true surface area of the metal at this interface was estimated as above by means of gold surface electrochemistry. Careful examination of results obtained by Schiavon et al. (1989) shows that the results correspond to oxygen reduction current densities of ca. 40 μA / active cm^2 at –0.15 V vs. SCE in air. This indicates that the current densities observed are an order of magnitude lower from those that should have been observed if oxygen had been diffusing through the gold layer and reacted at a Au/Nafion® interface of a significant width (e.g. 2.8-0.28 mm as was estimated from Figure 3.1 above). Therefore, either the three-phase line interface on top of the device, or a limited area of gold at the bottom of the layer and in contact with Nafion® (but always close to the counter electrode and also under mixed control) seem to be the most probable locations of the reaction.

It should also be noted that the absence of a limiting current plateau for oxygen reduction at the Au/Nafion®-planar device is in contrast with previous results by Hodgson et al. (1998) for SO_2 detection on a similar Au/SiC-H_3PO_4 planar sensor. The difference may arise from the much lower gas levels used in their work (100-1000 ppm), the difference in the kinetics of oxygen and sulphur dioxide reactions, as well as the possibility of a thin hymen of H_3PO_4 solution covering the edge of the gold layer when phosphoric-acid-impregnated SiC was used.

The three-electrode device was also used in some streams of varied humidity, namely in "dry" air (laboratory compressed air of 20% RH) and in ambient air (40% RH during the experiments reported here). Figure 3.3 presents the surface electrochemistry of the gold working electrode, recorded at 50 mV/s in the dry (20% RH) and ambient air (40% RH) samples. These voltammograms, together with that of Figure 3.1 for water-saturated air, show that it is mainly the size, and not the position or shape, of the oxide formation and stripping peaks that changes with humidity. It seems that the decrease in Nafion® conductivity as the humidity decreases from 100% to 20% RH, does not result in significant IR distortion for currents up to ca. 100 μA.

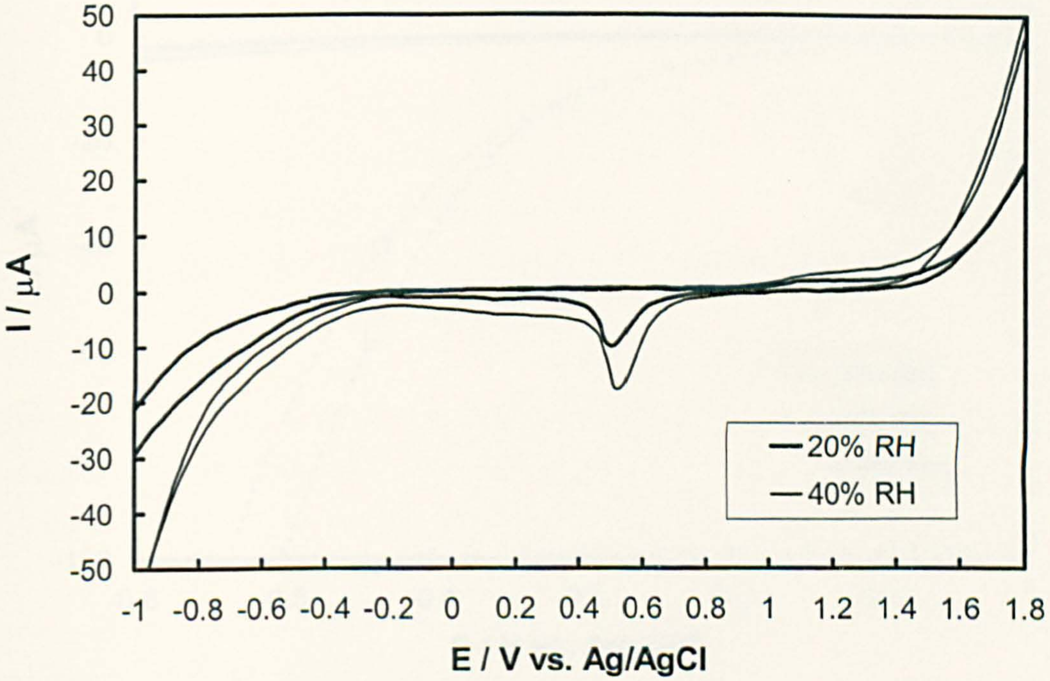

Figure 3.3 Voltammograms recorded at 50 mV/s in 20% and 40%RH air streams at a three-electrode Au (vs. Ag/AgCl)/Nafion®/Au planar device

Figure 3.4 presents the oxygen reduction voltammograms in streams of different humidity and there is a dramatic fall of the oxygen signal when one passes from a water-saturated to an ambient stream. Hence, both the gold surface electrochemistry and oxygen reduction show the same trend with changing humidity of the gas sample as Table 3.1 presents. This dependence is unlikely to be due to the effect of humidity on conductivity alone. In fact, the uncompensated resistance between working and reference electrodes in these devices as measured by the current interrupt technique and presented in Table 3.1, does not justify such an effect. For example, based on the resistance values, a current of 100 μA, which was the maximum current recorded with this device, due to oxide formation or oxygen reduction, would give rise to 19 mV and 34 mV ohmic losses in water-saturated and 40% RH gas streams respectively.

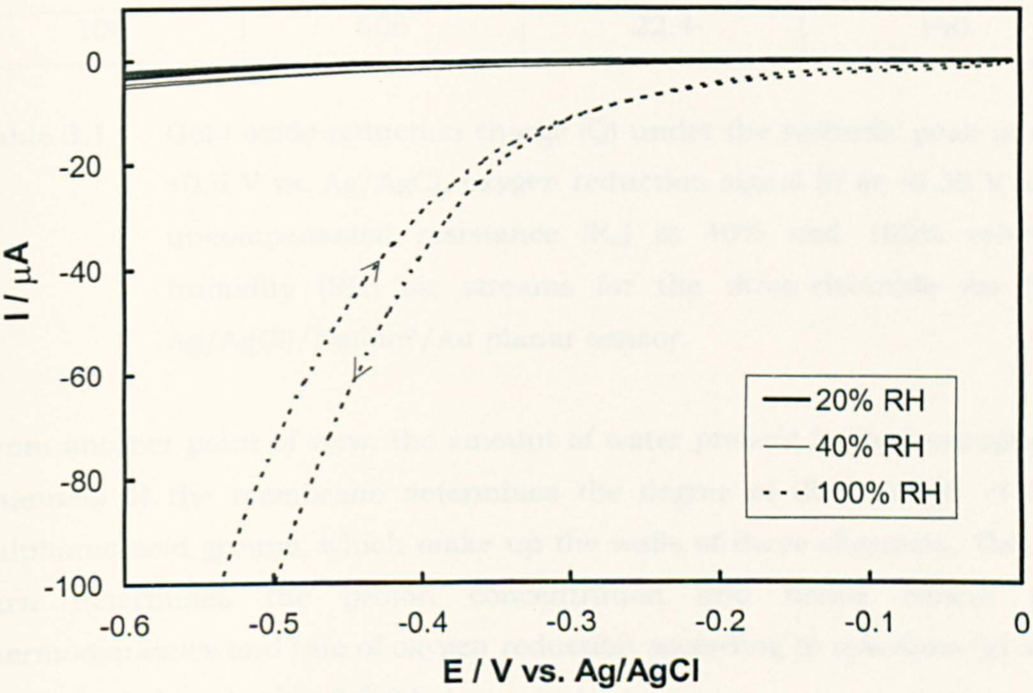

Figure 3.4 Voltammograms recorded at 5 mv/s in water saturated air streams of different humidity at a three-electrode Au (vs. Ag/AgCl)/Nafion®/Au planar device

A possible explanation of humidity effects on the oxygen reduction reaction is based on the work of Zawodzinski et al. (1991) who found that when the RH (and hence water activity) falls below ca. 50% there is a sharp decrease in the number of water molecules per sulphonic group (from12 to 6 or less) in the ionic regions of the Nafion® polymer. These ionic-aqueous regions are known to be the active sites for both gold oxide formation/stripping and oxygen reduction since gold oxide formation requires water as a reactant and both gold oxide stripping and oxygen reduction require a mobile-solvated proton as a reactant and an aqueous environment for solubilization of the produced water. A decrease in the number of water molecules present in these sites is expected to decrease the active area of the metal/ Nafion® interface and might also decrease the catalytic properties of the sites too (Parthasarathy et al. 1991, Uribe et al. 1992).

RH (%)	**Q (µC)**	**I (µA)**	**R_u (Ω)**
40	46	2.0	340
100	606	22.4	190

Table 3.1 Gold oxide reduction charge (Q) under the cathodic peak at ca. +0.5 V vs. Ag/AgCl, oxygen reduction signal (I) at –0.35 V and uncompensated resistance (R_u) in 40% and 100% relative humidity (RH) air streams for the three-electrode Au (vs. Ag/AgCl)/Nafion®/Au planar sensor.

From another point of view, the amount of water present in the hydrophilic channels of the membrane determines the degree of dissociation of the sulphonic acid groups, which make up the walls of these channels. This in turn determines the proton concentration and hence affects the thermodynamics and rate of oxygen reduction according to reactions (2) and (3) presented in chapter 3.2.2 below.

3.2.2 Voltammetry at two-electrode Au/Nafion®/Au sensors and Au/Nafion®/Pt sensors

The current flowing through a two-electrode system can be determined by either one or both of the processes occurring at the working and counter electrodes, if these are of comparable dimensions. Negative currents reflect reduction processes at the working electrode i.e. gold oxide stripping:

$$Au_2O_3 + 6H^+ + 6e^- \rightarrow 2Au + 3H_2O \qquad (1)$$

or oxygen reduction on gold in oxygen containing samples, which is realised in two steps at first to hydrogen peroxide:

$$O_2 + 2H^+ + 2e^- \rightarrow H_2O_2 \qquad (2)$$

and finally to water.

$$H_2O_2 + 2H^+ + 2e^- \rightarrow 2H_2O \qquad (3)$$

In the absence of oxygen the reaction at the sensing electrode is hydrogen evolution:

$$2H^+ + 2e^- \rightarrow H_2 \qquad (4)$$

The reactions on sensing electrode are supported by the oxidation processes at the counter electrode i.e. gold oxide formation:

$$2Au + 3H_2O \rightarrow Au_2O_3 + 6H^+ + 6e^- \qquad (5)$$

and oxygen evolution:

$$2H_2O \rightarrow O_2 + 4H^+ + 4e^- \qquad (6)$$

in order of increasing potential. The potential sweep experiments reported by Hoare (1968) show that in case of gold electrodes, only one type of oxide is formed.

Figure 3.5 presents voltammograms recorded at 50 mV/s with Au/Nafion®/Au assemblies in water saturated nitrogen streams. In the dark solid line voltammogram, which was recorded with Device A, the cathodic peak at ca. -0.5 V is likely to correspond to gold oxide stripping from the working electrode. The plateau in the -1.0 to -1.5 V region corresponds to gold oxide formation at the counter electrode, and the increase of the current beyond -1.5 V to hydrogen evolution at the working electrode supported by oxygen evolution at the counter electrode. The double peak at positive potentials (0.25 to 1 V) should be attributed to surface processes on both gold electrodes, supporting each other. To attribute with certainty each peak recorded at intermediate polarisations to a specific process occurring at one of the two electrodes, the dimensions of both the working and counter electrodes were varied (see Experimental Figure 2.3).

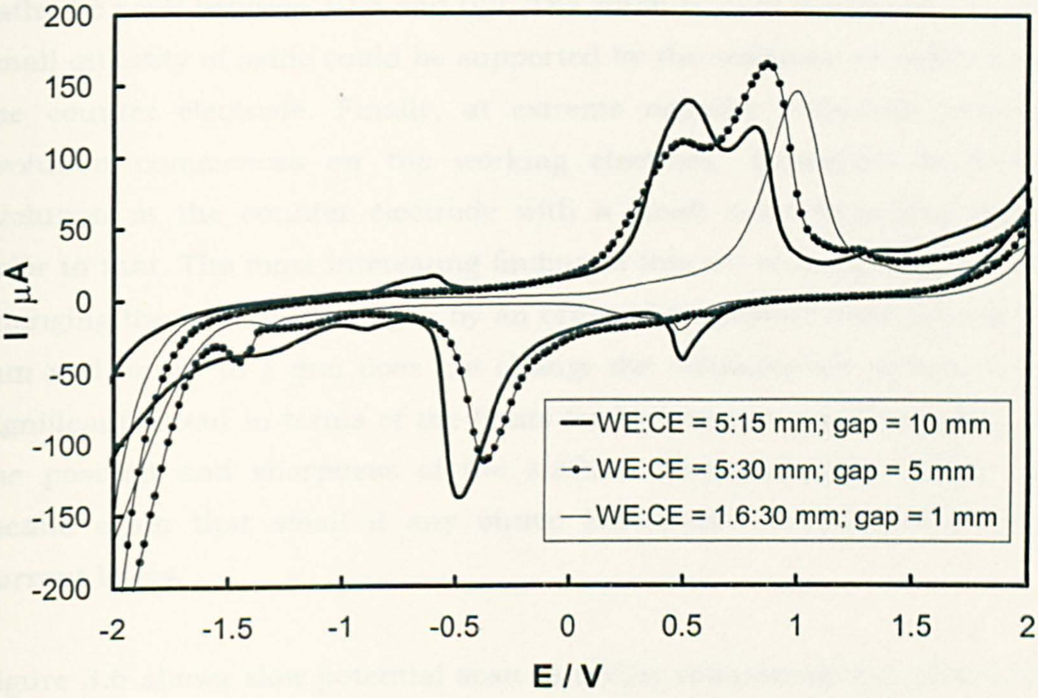

Figure 3.5 Voltammograms recorded at 50 mV/s in water saturated nitrogen streams at different two-electrode Au/Nafion®/Au planar devices. (WE = working electrode, CE = counter electrode)

From Figure 3.5 it also can be seen that the ratio of the anodic peak at ca. +0.4 V to that at ca. +0.7 - +0.9 V, decreases as the working-to-counter electrode length ratio is decreased. It is therefore reasonable to assume that the first peak corresponds to oxide formation at the working electrode supported by the onset of oxide stripping at the counter electrode, which results in the second peak. The latter process cannot be completed once the oxide from the working electrode is formed and therefore the current drops again. The size of the peaks cannot be rigorously correlated to exact electrode length because of the expected difference in roughness factors between the electrode layers used in each device. The cathodic peak at ca. –0.5 V recorded for Devices A and B is due to oxide stripping from the working electrode, supported by the onset of oxide formation at the counter electrode. However, in the case of Device C, where the smallest working electrode was used, the stripping of the small quantity of oxide produced at the working electrode during anodisation is realised as a wide small cathodic peak between +0.5 and 0 V. The small current needed to strip this small quantity of oxide could be supported by the oxidation of impurities at the counter electrode. Finally, at extreme negative potentials hydrogen evolution commences on the working electrode, supported by oxygen evolution at the counter electrode with a small oxide-formation plateau prior to that. The most interesting finding of this set of experiments is that changing the interelectrode gap by an order of magnitude from 10 mm to 5 mm and finally to 1 mm does not change the voltammetric picture to any significant extent in terms of the limits for hydrogen/oxygen evolution and the position and sharpness of the surface electrochemistry peaks. This means again that small if any ohmic losses are encountered at these current levels.

Figure 3.6 shows slow potential scan (5 mV/s) voltammograms in a water-saturated air stream (and, for Device C, in nitrogen too). Device C with the smallest working electrode length of 1.6 mm (thin curve) shows appreciably smaller cathodic currents than Devices A and B as was expected. Comparison of the response at the latter two devices which have same working electrode lengths but different counter electrode lengths supports the idea that the plateau observed between ca. -0.8 and -1.4 V is limited by a process occurring at the counter electrode, most likely the formation of a gold oxide layer on it, since the height of that plateau increases with counter electrode length. The same comparison reveals that the exponentially rising cathodic current observed at potentials more negative than -1.5 V increases too with the counter electrode length. As this current is due to oxygen reduction at the working electrode and oxygen evolution at the counter electrode, its dependence on counter electrode size implies that at least at high oxygen concentrations this current is not solely determined by oxygen reduction at the sensing electrode, but also by the extend of oxygen evolution at the counter electrode. This may result in a "current saturation" effect with increasing oxygen concentration, for a 2-electrode sensor.

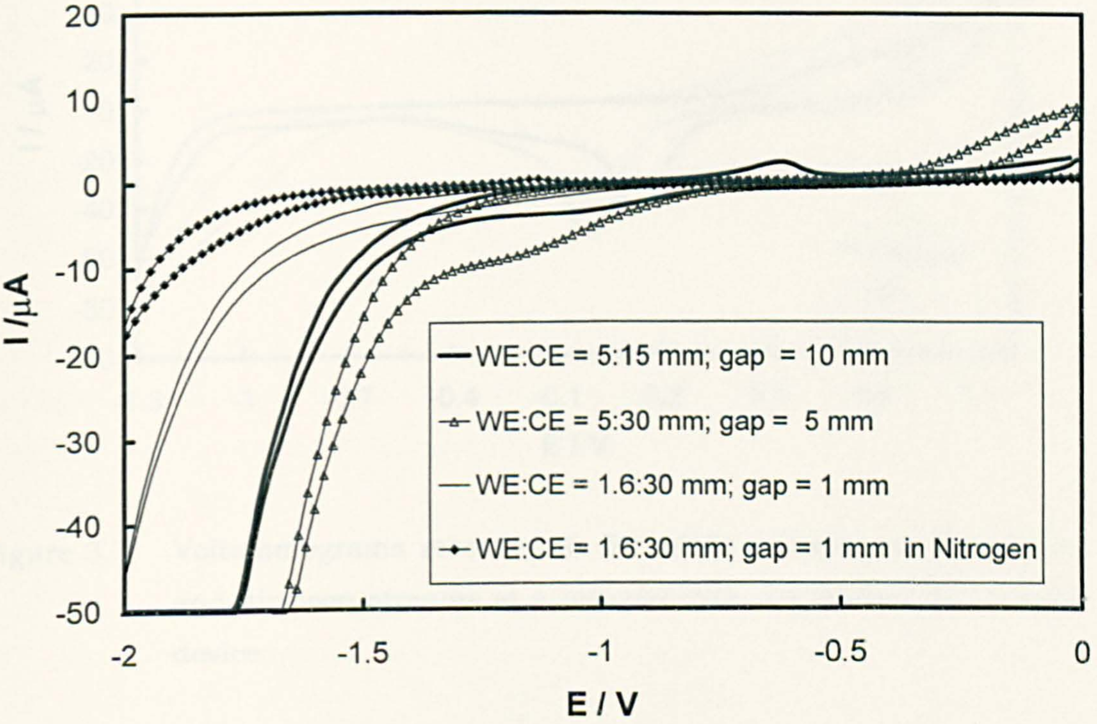

Figure 3.6 Voltammograms recorded at 5 mV/s in water saturated air and nitrogen streams at different two-electrode Au/Nafion®/Au planar devices. (WE = working electrode, CE = counter electrode)

Since platinum is known to be a much better oxygen evolution catalyst than gold, the gold counter electrode layer was replaced by a platinum one in a two-electrode Au/Nafion®/Pt device. For the preparation of different working electrode/counter electrode material planar devices Device B (WE:CE = 5:30 mm) was prepared by covering the counter electrode opening with a piece of paper while the gold working electrode was sputtered and repeating process for the platinum counter electrode.

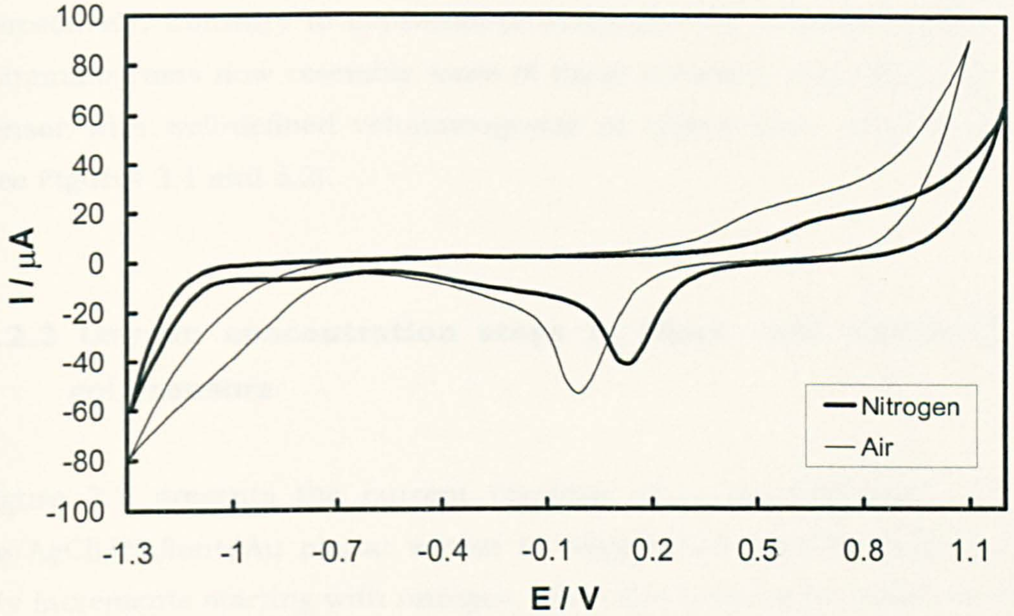

Figure 3.7 Voltammograms recorded at 50 mV/s in water saturated air and nitrogen streams at a two-electrode Au/Nafion®/Pt planar device

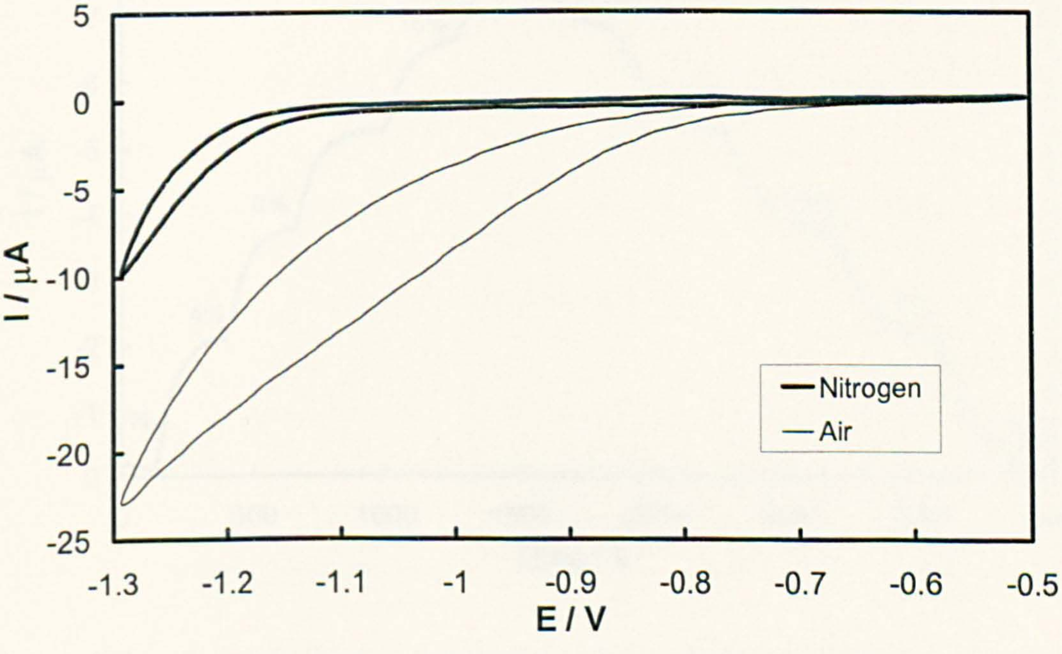

Figure 3.8 Voltammograms recorded at 5 mV/s in water saturated air and nitrogen streams at a two-electrode Au/Nafion®/Pt planar device

The fast and slow voltammograms are shown in Figures 3.7 and 3.8 respectively. Contrary to experiments using gold as counter electrode the voltammograms now resemble more of those recorded with three-electrode sensor with well-defined voltammograms of typical gold electrochemistry (see Figures 3.1 and 3.2).

3.2.3 Oxygen concentration steps at three- and two-electrode gold sensors

Figure 3.9 presents the current response of a three-electrode Au (vs. Ag/AgCl)/Nafion®/Au planar sensor to oxygen concentration steps of 4% v/v increments starting with nitrogen, when the working electrode was kept at –0.35 V vs. Ag/AgCl.

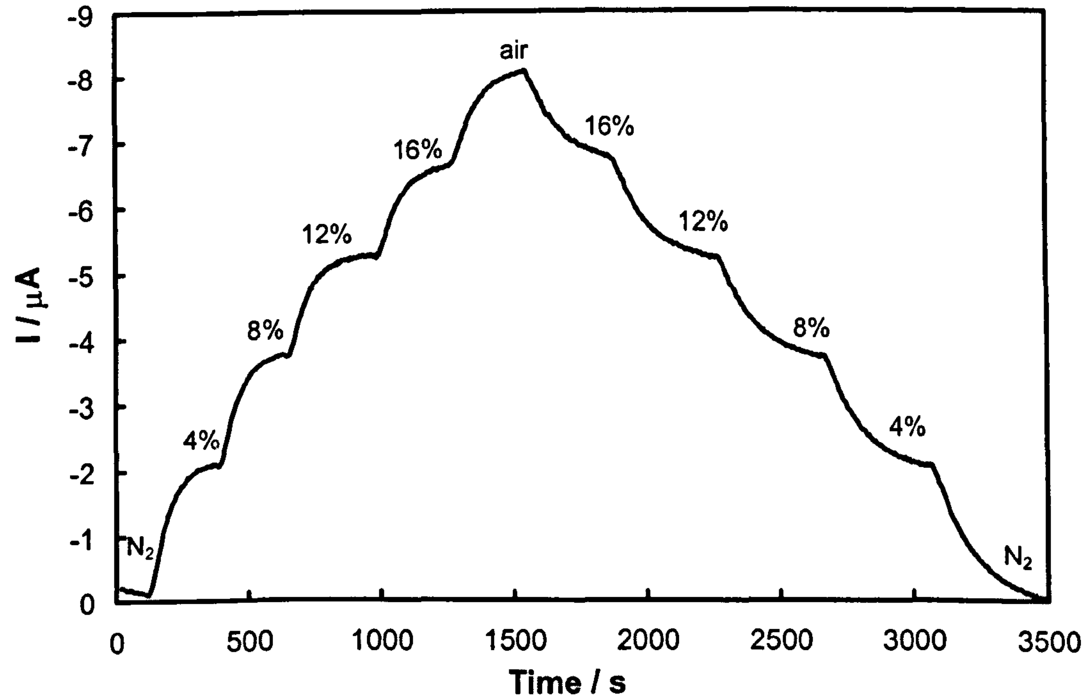

Figure 3.9 Current-time response of three-electrode Au (vs. Ag/AgCl)/Nafion®/Au planar sensor to oxygen concentration steps as indicated in the graph in water saturated samples with the working electrode held at –0.35 V vs. Ag/AgCl

The change between streams of different oxygen content was achieved with the use of a two-way valve connected to the corresponding gas cylinders. Thus, the time needed for changing the concentration at the cell inlet without taking into account the time due to the cell's dead volume was minimised and estimated to be less than a minute, mainly due to the tubing dead volumes.

A nice step-wise pattern is observed but high background currents are encountered, probably due to reduction of impurities and residual oxygen in the Nafion® membrane, since the device had not been cured-equilibrated in nitrogen for long periods.

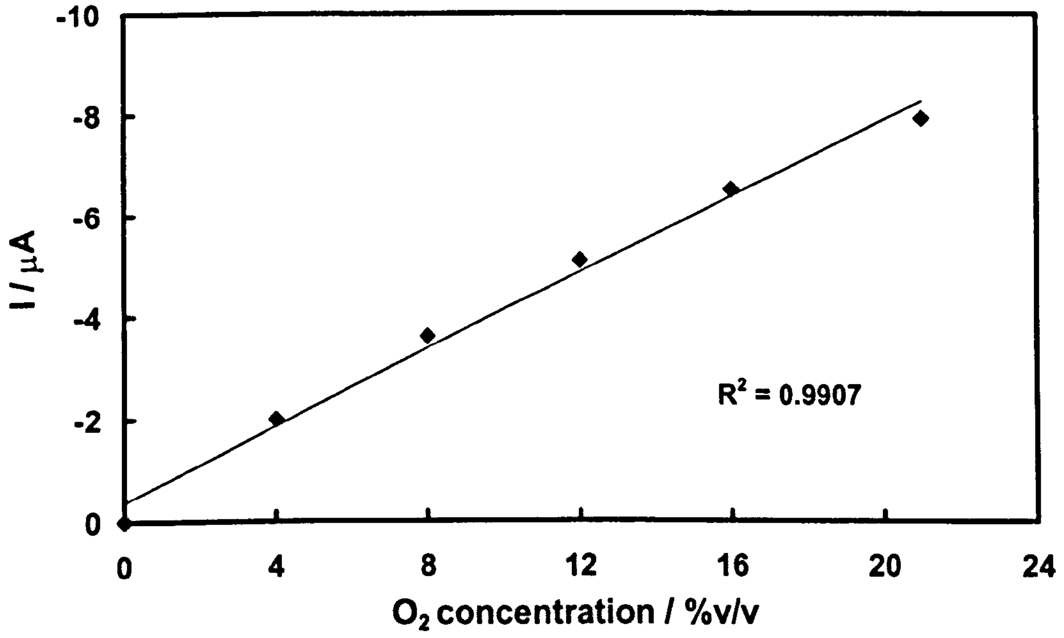

Figure 3.10 Variation of the background-corrected current of three-electrode Au (vs. Ag/AgCl)/Nafion®/Au planar sensor collected at the end of each concentration step vs. the oxygen concentration.

Figure 3.10 shows the variation of the background-corrected oxygen reduction current collected at the end of each concentration step with oxygen concentration. Good linearity is observed ($r^2 > 0.99$) with very weak signs of signal saturation, indicating that the current is determined by the oxygen concentration in the sample. The background correction approach would be valid if the background current is stable or diminishes after long period curing in nitrogen.

Since, as stated also before, gold is known to be a poorer electrocatalyst for oxygen evolution than platinum and it has been reported that oxygen does not even evolve until the surface has been covered with an oxide layer (Hoare 1968) platinum as a counter electrode was tested again in the planar devices. The samples were prepared as was mentioned in Chapter 3.2.2, but this time Ag/AgCl strip was inserted in the inter-electrode gap to serve as a reference electrode. The current vs. time response of Au (vs. Ag/AgCl)/Nafion®/Pt-device is shown in Figure 3.11. The sensor was maintained at a constant potential at –0.2 V vs. Ag/AgCl reference electrode. As with the Au (vs. Ag/AgCl)/Nafion®/Au planar device a smooth change of signal was observed with a similar magnitude of currents.

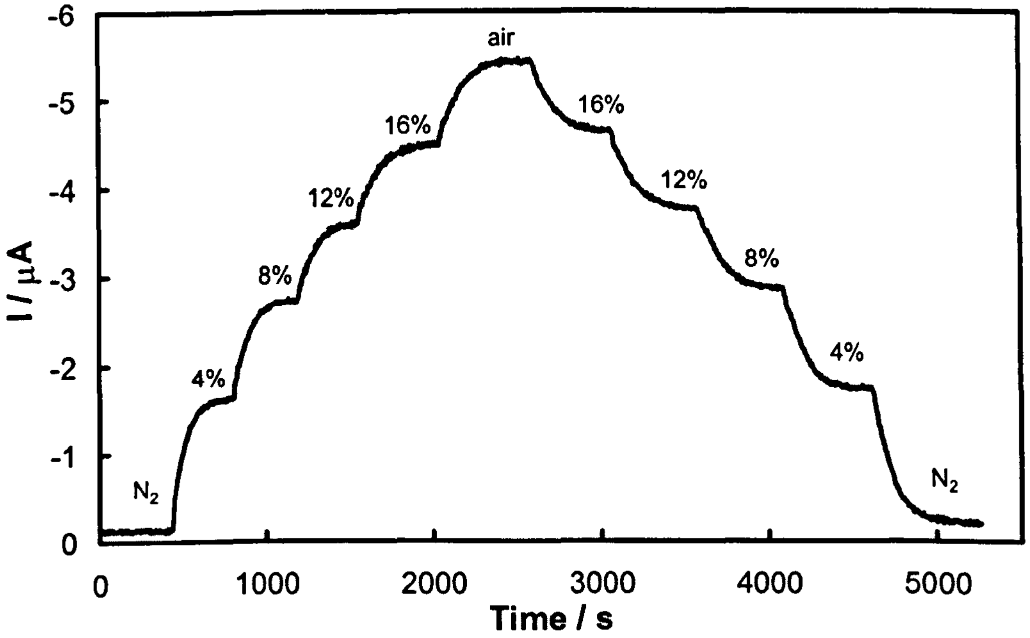

Figure 3.11 The current vs. time response of Au (vs. Ag/AgCl)/Nafion®/Pt-device to oxygen concentration steps in water-saturated gas samples. The device was held at –0.2 V vs. Ag/AgCl.

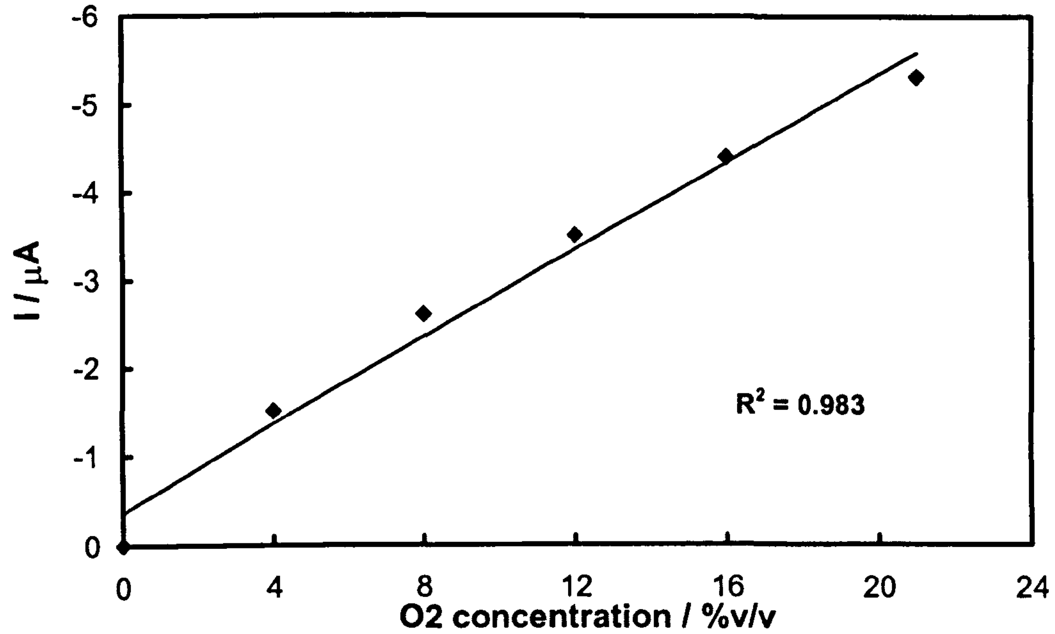

Figure 3.12 Variation of the background corrected current of Au (vs. Ag/AgCl)/Nafion®/Pt-device collected at the end of each step vs. the oxygen concentration.

Again slight saturation can be seen in the background-corrected currents on Figure 3.12, and no further linearity improvement is observed compared to the three-electrode gold device. This means that the type of the counter electrode does not significantly affect the behaviour of three-electrode sensors.

During previous experiments on planar two-electrode sensors by Sotiropoulos (1994) the possibility of operating the sensor at moderate potentials, using the difference of oxide formation at the anode as an indication of changes in oxygen concentration reacting at the cathode (see Figure 3.6), had not been considered. This time experiments in the counter electrode oxide-forming region were attempted. Thus, the most promising two-electrode device (Device B from Figure 3.5) was operated at moderate voltages.

Figures 3.13 and 3.14 show the current-time response of B-type device (WE:CE = 5:30 mm) with gold electrodes to oxygen changes in water saturated gas streams. In the experiment the working electrode was held at −1.0V and −1.6 V respectively vs. the counter electrode. It can be seen that although there is a clear increase in the current with oxygen concentration, the response is very sluggish. This is most likely due to slow kinetics of oxide formation at the counter electrode surface, as that reaction is known to be kinetically slower process than oxygen reduction.

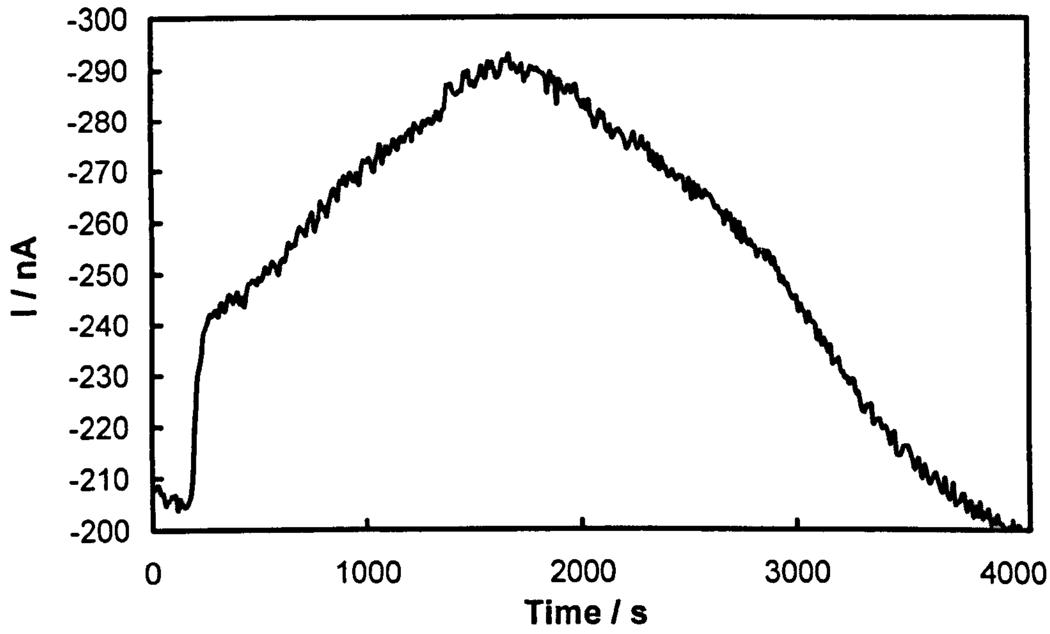

Figure 3.13 Current-time response of the two-electrode B-type Au/Nafion®/Au sensor to oxygen concentration steps in water saturated samples with the working electrode held at −1.0 V vs. the Au counter electrode.

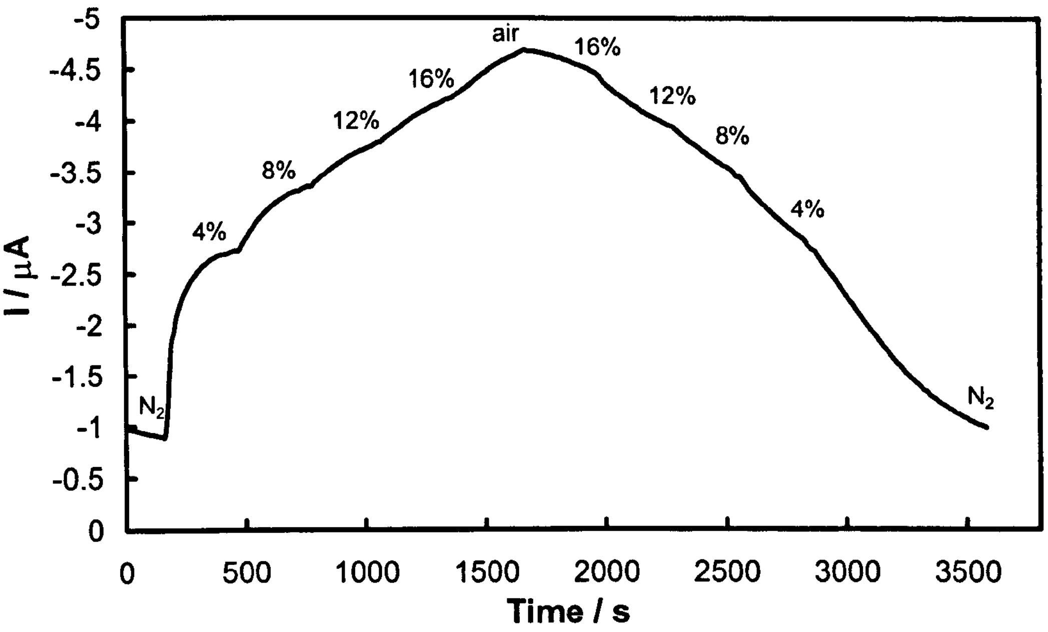

Figure 3.14 Current-time response of the two-electrode B-type Au/Nafion®/Au sensor to oxygen concentration steps in water saturated samples with the working electrode held at –1.6 V vs. the Au counter electrode.

Changing the counter electrode from Au to Pt and operating the two-electrode sensor at the moderate potential of –0.9 V (with respect to Figure 3.8 above) certainly improves the sharpness of the response as can be seen in Figure 3.15 below, but still significant signal saturation is observed. To improve the response time and step clarity, the measurement potential of the Au/Nafion®/Au sensor was increased to a region where oxygen reduction at the working electrode would be mainly supported by the oxygen evolution at the counter electrode (see Figure 3.6 and its discussion above).

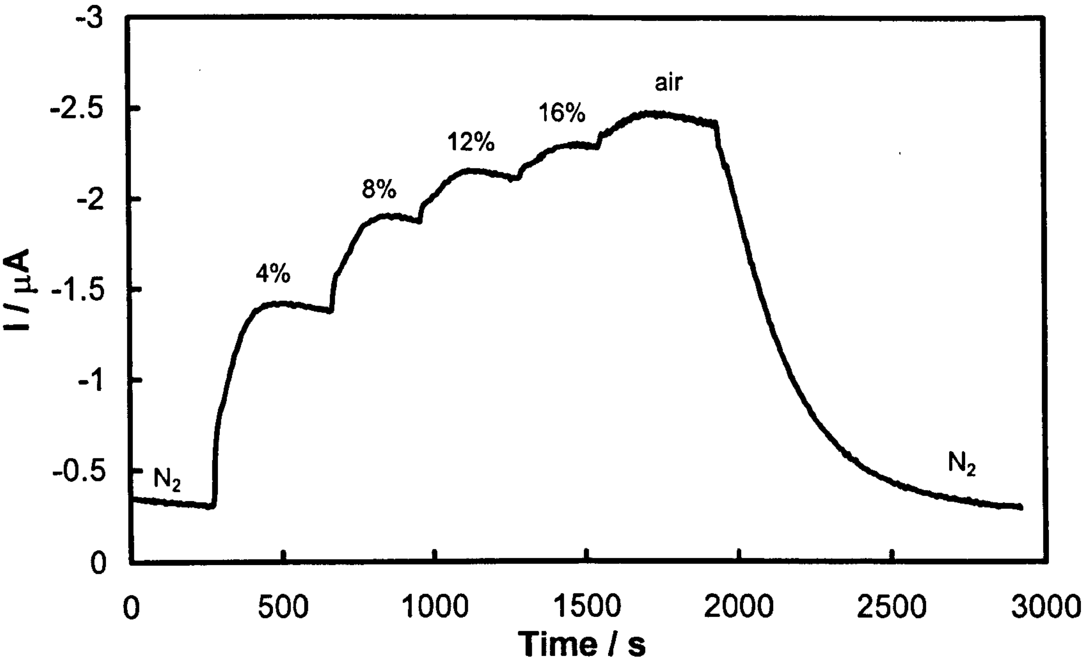

Figure 3.15 Current-time response of the two-electrode B-type Au/Nafion®/Pt sensor to oxygen concentration steps in water saturated samples with the working electrode held at –0.9 V vs. the Pt counter electrode

Figure 3.16 shows the response of Device C (WE:CE = 1.6:30 mm) to oxygen concentration steps when the working electrode was held at –1.9 V vs. the counter electrode. The experiment started with a nitrogen stream passed to a 4% oxygen stream and back to nitrogen again before continuing with a complete series of oxygen steps in increments of 4%. For comparison, a commercial fuel-cell type CiTiceL® sensor (City Technology Ltd) was placed in the test cell and its response was simultaneously recorded. The CiTiceL® sensor has nominal range of 0-25% oxygen, temperature range of -20°C to +50°C, response time $T_{95} \leq 10$ seconds and long term output drift of < 2% signal/month (typically < 5% over operating life).

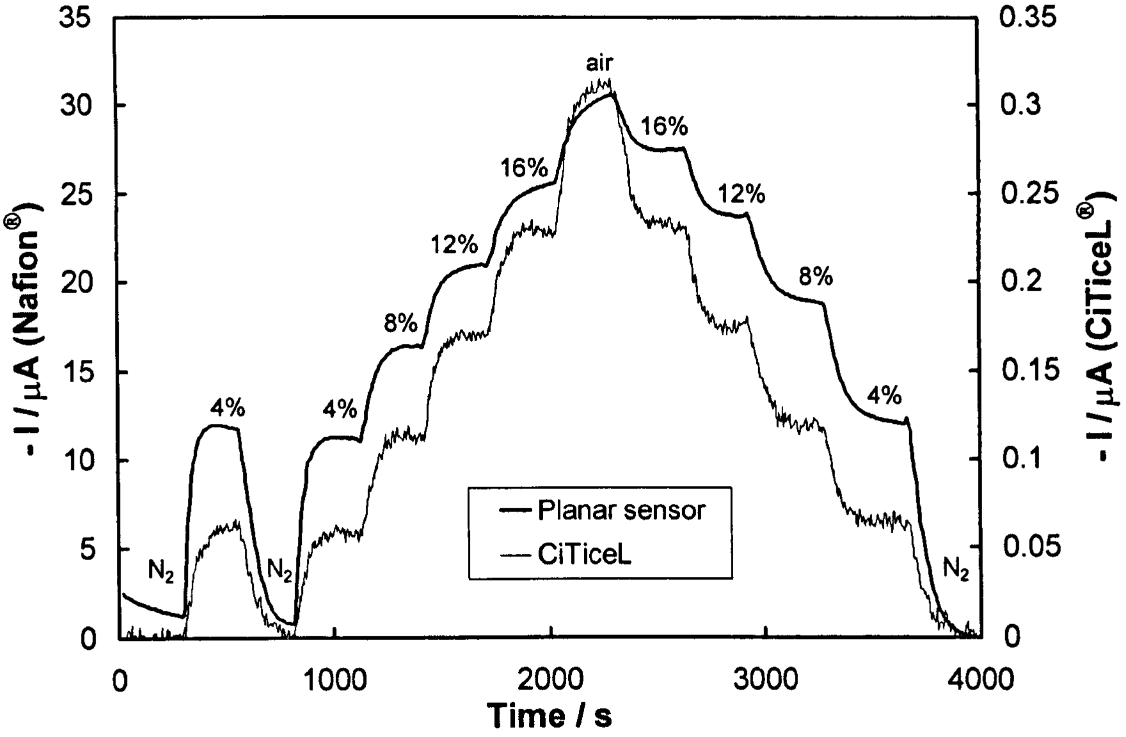

Figure 3.16 Current-time response of the C-type Au/Nafion®/Au sensor together with CiTiceL® (City Technology Ltd.) sensor to oxygen concentration steps in water saturated samples. The working electrode was held at –1.9 V vs. the Au counter electrode.

It can be seen that Device C follows a similar stepwise pattern with that of the CiTiceL® but exhibits a higher background current. This might be due to residual impurities and oxygen in the Nafion® membrane as the planar device has not been cured-equilibrated in nitrogen for long periods. This could also originate from the continuous occurrence of hydrogen evolution at the extreme negative potentials. The rather high response times obtained with both devices (ca. 100 s) should be due to the dead volumes of our gas tubing, humidification vessel and test cell.

Figure 3.17 presents current-concentration curves based on the current recorded at the end of each concentration step after background current subtraction.

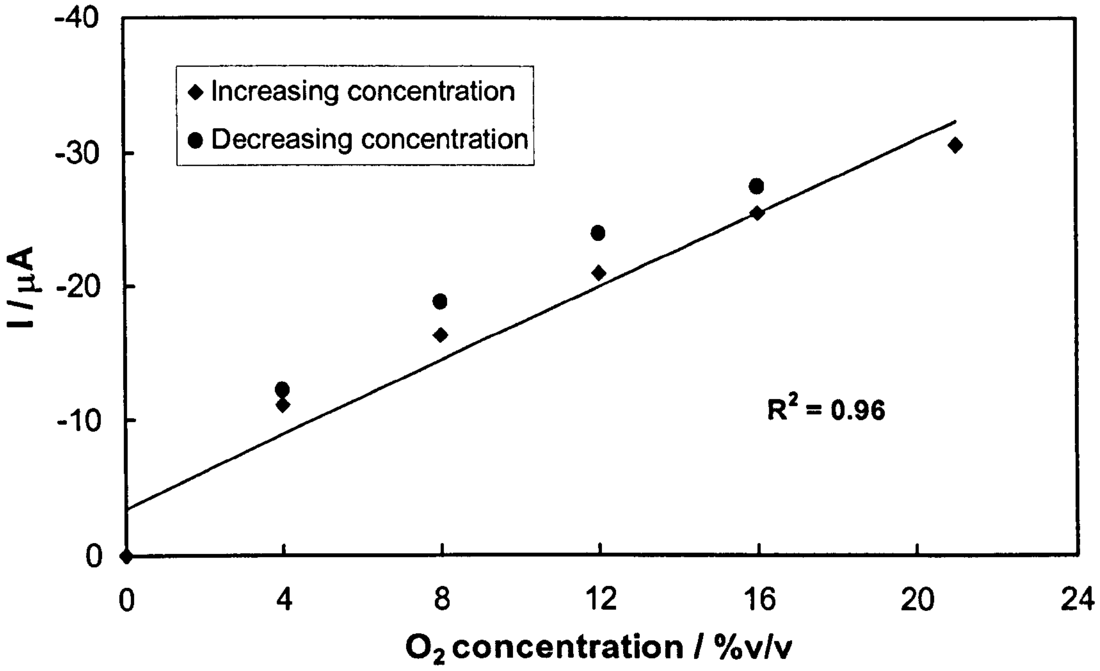

Figure 3.17 Variation of the background-corrected current of the two-electrode C-type Au/Nafion®/Au sensor collected at the end of each concentration step vs. the oxygen concentration.

From this figure it can be seen that there is a smooth change of the signal with oxygen concentration, but some saturation is observed in the higher concentration range. The possibility that this effect is due to IR drop at higher currents is, as in the case of the three-electrode device (Figures 3.9 and 3.10 above), unlikely since clear voltammetry was observed in Figure 3.6 in the 100 µA range. In addition, the voltammetry was not affected by the interelectrode gap as discussed above. It seems that, as also mentioned in the discussion of Figure 3.6 above, this saturation is due to limitations imposed by the reaction occurring at the counter electrode, namely oxygen evolution, which cannot sustain the high oxygen reduction currents expected at high oxygen concentrations. Attempts to operate the device at lower potentials were also proven unsuccessful, limited in that case by gold oxide formation at the counter electrode.

The signal saturation of the two-electrode sensors poses a serious inherent limitation on the use of such a version of the planar oxygen sensor proposed. The linearity of the sensors is markedly improved when the three-electrode version of the sensor is used with gold as the sensing electrode and either gold or platinum as the counter electrode.

The detection limit of these (two- or three-electrode) sensors is estimated to be ca. 2% v/v. That would mean that the sensor is suitable for crude environmental monitoring of relatively high oxygen levels.

3.2.4 Voltammetry and oxygen concentration steps at three-electrode Pt (vs. Ag/AgCl)/Nafion®/Pt sensors

Platinum is the most commonly used material as a sensing electrode in commercial oxygen sensors, although the mechanism of oxygen reduction on it is very complicated. In acidic media platinum is by far the best catalyst for oxygen and H_2O_2 reduction with other noble metals exhibiting lower activity. In order to maximise the sites at which electrochemical reactions occur porous gas diffusion electrodes were introduced. Unfortunately, sintered platinum powder electrodes that were first used, are excessively expensive and still do not have high enough surface area. The optimum use of the precious metal catalyst is by mixing the metal in a finely divided form on high surface area substrate such as carbon (Hoare 1968). However, if the electrochemical reaction takes place at the electrode/electrolyte/gas interface restricted at the edge of the metal layer electrode, then a sputtered line electrode could be used.

Figure 3.18 presents a fast potential sweep voltammogram (50 mV/s) recorded at a Pt (vs. Ag/AgCl)/Nafion®/Pt-device in a water-saturated nitrogen atmosphere. The general features of hydrogen adsorption/desorption and oxide formation/stripping that are characteristic of platinum surface electrochemistry can be seen. Compared to typical voltammogram recorded in sulfuric acid, the peaks for hydrogen adsorption/desorption however are not clear (but this is a common finding of the enormous Pt/Nafion® literature). For example, Mitsushima et al. (2002) who studied oxygen reduction on platinum microelectrodes with various polymer electrolytes reported similar features when using polymer electrolytes. They attributed this to partial polymer blocking of the hydrogen adsorption sites.

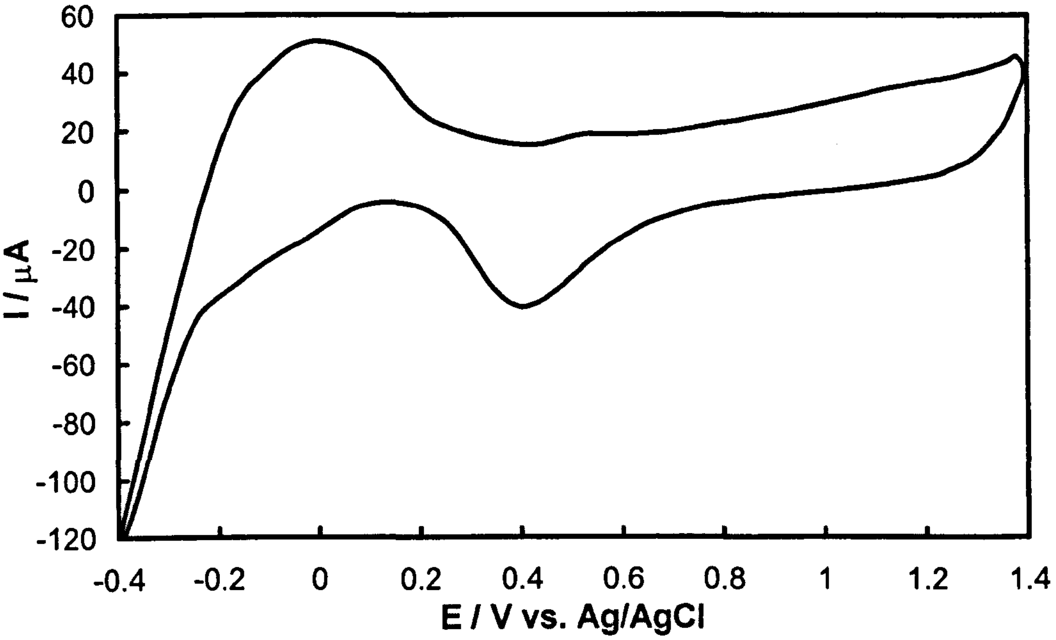

Figure 3.18 Voltammogram recorded at 50 mV/s in water saturated nitrogen stream at Pt (vs. Ag/AgCl)/Nafion®/Pt planar device.

From the cathodic charge corresponding to hydrogen-adsorption between +0.2 V and –0.2 V vs. Ag/AgCl, which is calculated from Figure 3.18 to be 160 µC, and the charge reported to correspond to a monolayer of hydrogen-adsorption on 1 cm^2 of platinum (210 µC/cm^2, Capon and Parsons 1972) it follows that the effective electrode area is 0.761 cm^2. The fact that this value is similar to the nominal working electrode area of 0.625 cm^2 together with the higher than 1 roughness factors reported for such platinum deposits in the literature, indicate that only a part of the working electrode layer (the one closer to the reference and counter electrodes) is effective at these current levels, due to current distribution limitations of the planar electrode arrangement.

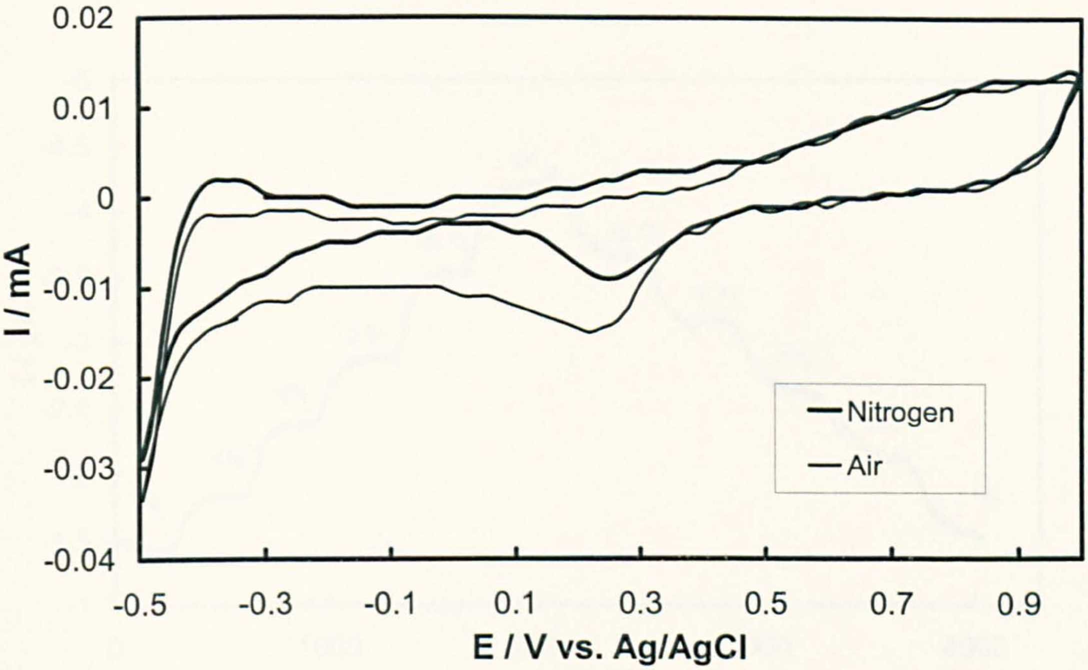

Figure 3.19 Voltammograms recorded at 5 mV/s in water saturated nitrogen and air streams at Pt (vs. Ag/AgCl)/Nafion®/Pt planar device.

Figure 3.19 presents voltammograms recorded at 5 mV/s in water saturated nitrogen and air streams. In these experiments a well-defined current plateau for potentials between 0.1 and –0.3 V vs. Ag/AgCl can be observed for oxygen containing streams. It seems therefore that, unlike gold devices, for platinum electrodes there is an oxygen reduction limiting current region. Given the fact that both gold and platinum working electrode devices are fabricated in an identical manner, this means that there is a mass transport barrier in both devices but it is thin enough to only determine the current in the case of platinum, where the oxygen reduction kinetics are much faster than on gold. Whether this thin mass transfer barrier is located on top of the working electrode layer or beneath and through the Nafion® membrane, will be investigated in more detail in chapter 3.5.

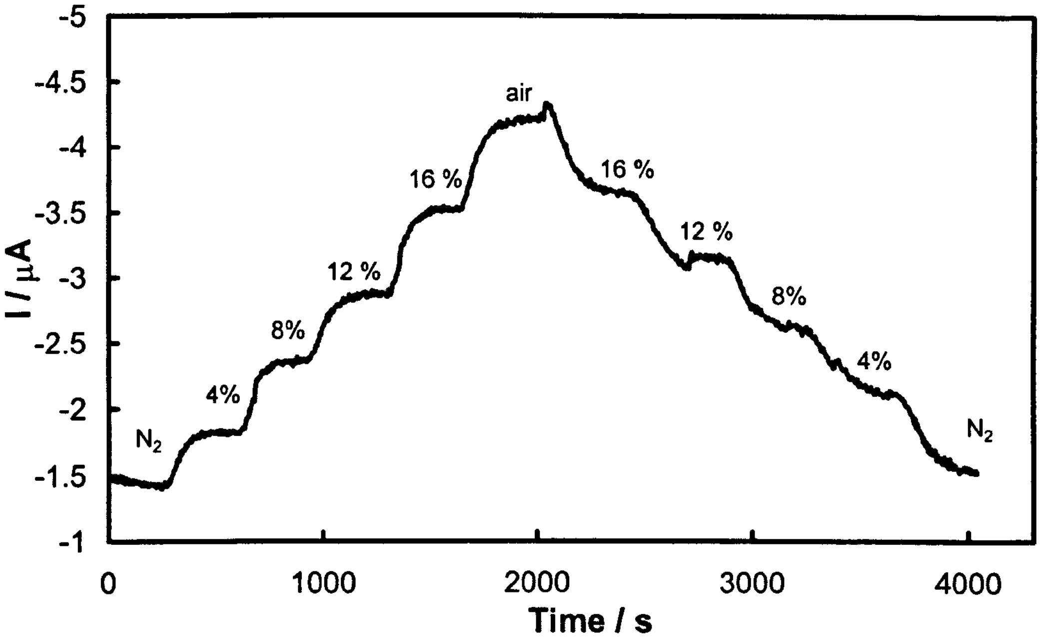

Figure 3.20 The current vs. time response of Pt (vs. Ag/AgCl)/Nafion®/Pt-device to oxygen concentration steps in water-saturated gas samples. The device was held at –0.4 V vs. Ag/AgCl.

Figure 3.20 shows the current vs. time response of a Pt (vs. Ag/AgCl)/Nafion®/Pt-device to oxygen concentration steps in water-saturated gas samples while Figure 3.21 shows the variation of the background-corrected oxygen reduction current with oxygen concentration. A smooth change of the signal with oxygen concentration was observed with no signal saturation, as opposed to Au/Nafion®/Au-device. Oxygen evolution is known to occur at higher rates at platinum than at gold and thus no significant counter electrode reaction limitations are imposed on the operation of the sensor.

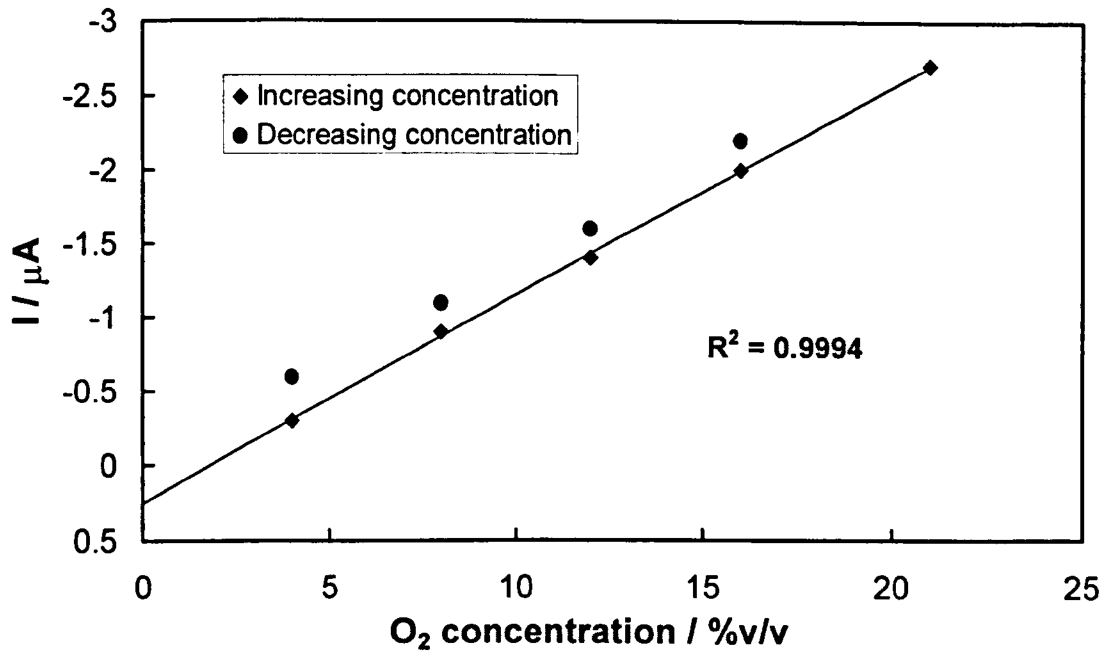

Figure 3.21 Variation of the background corrected current of Pt (vs. Ag/AgCl)/Nafion®/Pt-device collected at the end of each step vs. the oxygen concentration.

3.3 Humidity effects on the response of planar Nafion® sensors

The behaviour of the Au/Nafion®/Au device was studied with respect to both gold surface electrochemistry and oxygen reduction in water-saturated samples of varied relative humidity (RH) in the 15-85 % RH range. Figure 3.22 shows cyclic voltammograms at a 50 mV/s sweep rate in nitrogen samples of 36.5%, 77% and 83% RH. It can be seen, that it is mainly the size, and not so much the position or shape, of the oxide formation and stripping peaks that changes with humidity. Therefore, it seems that the well known decrease in Nafion® conductivity with decreasing humidity (Zawodzinski et al. 1991, Sone et al. 1996, Sumner et al. 1998) does not result in significant IR-distortion of the voltammetric picture. This can only be understood if there is a simultaneous inherent decrease in the currents associated with gold surface electrochemistry as the water content of the membrane decreases.

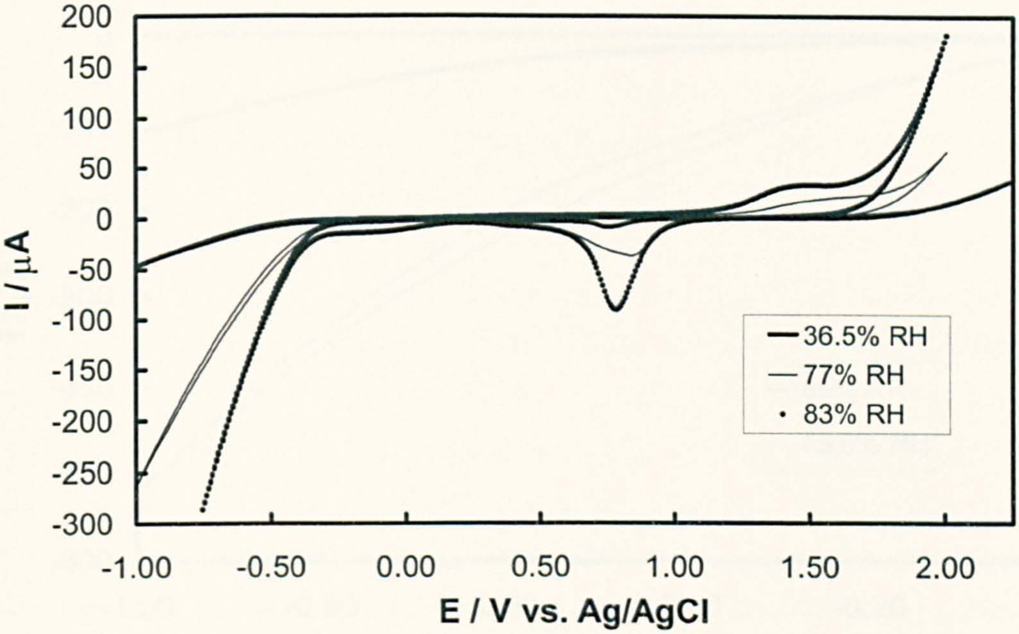

Figure 3.22 Voltammograms recorded at 50 mV/s in water saturated nitrogen streams of 36.5, 77 and 83% RH at a three-electrode Au (vs. Ag/AgCl)/Nafion®/Au-planar device

Figure 3.23 (A) shows slow-potential-sweep (5 mV/s) voltammograms for oxygen reduction from air streams of 83.6% and 55% RH, while Figure 3.23 (B) depicts similar voltammograms from 36% and 23% RH streams. It is seen that a similar (but much more pronounced) effect of humidity on the oxygen reduction signal is observed. The results of a systematic study of the effect of gas relative humidity on uncompensated membrane resistance, the charge corresponding to gold oxide stripping and the oxygen reduction current at a given potential taken from the slow voltammograms, are all shown in Table 3.2.

The continuous variation of both the gold surface oxide quantity-charge and of the oxygen signal (to a different extent each) can be clearly seen.

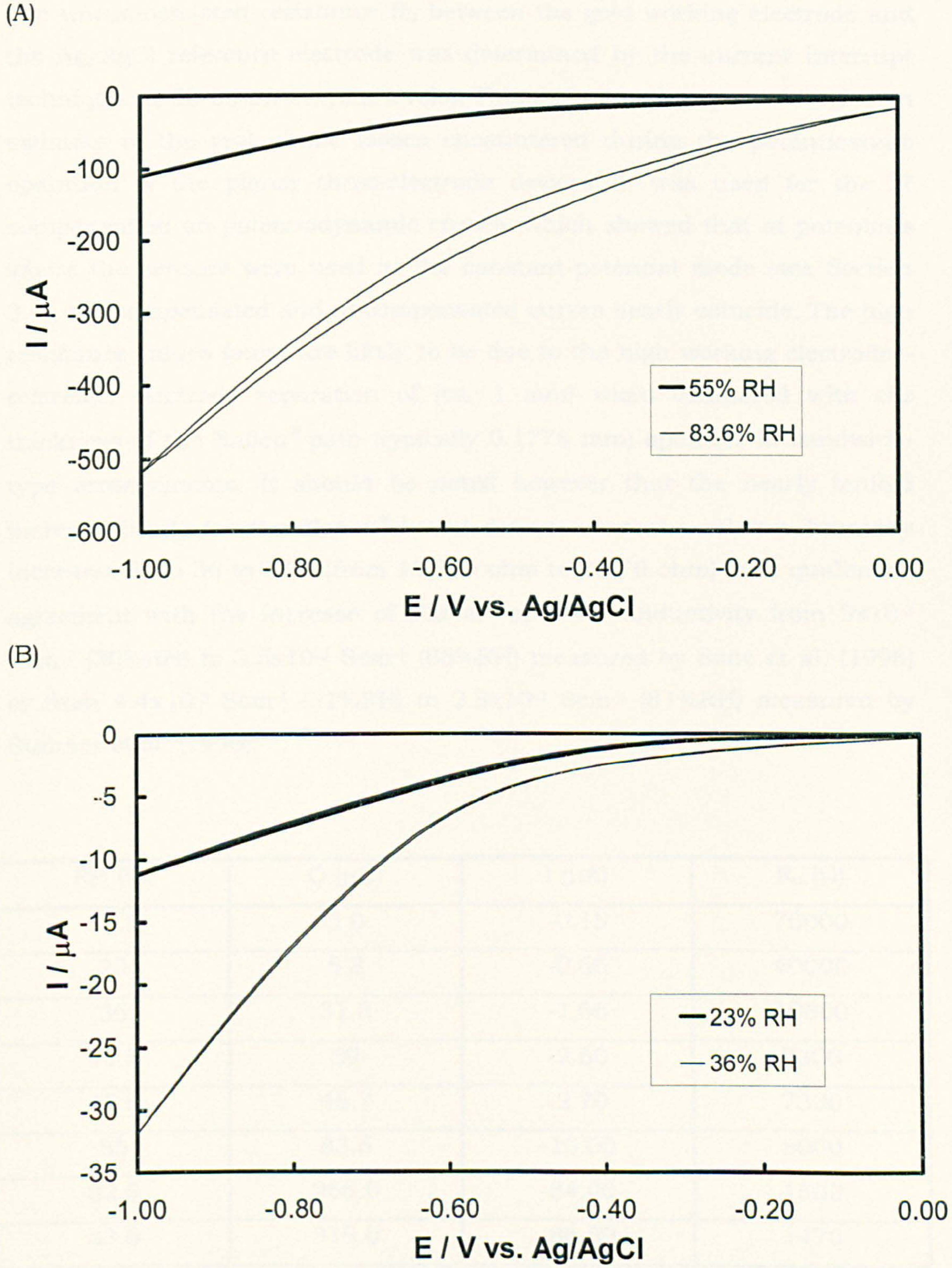

Figure 3.23 (A) Voltammogram recorded at 5 mV/s in air streams of 55 and 83.6% RH at a three-electrode Au (vs. Ag/AgCl)/Nafion®/Au-planar device. (B) Same as (A), but for air streams of 23 and 36% RH

The uncompensated resistance R_u between the gold working electrode and the Ag/AgCl reference electrode was determined by the current interrupt technique (at 50-60 µA current levels). This technique is expected to give an estimate of the real ohmic losses encountered during the potentiostatic operation of the planar three-electrode devices. It was used for the IR compensation on potentiodynamic curves, which showed that at potentials where the sensors were used in the constant-potential mode (see Section 3.4), the compensated and uncompensated curves nearly coincide. The high resistance values found are likely to be due to the high working electrode – reference electrode separation of (ca. 1 mm) when compared with the thickness of the Nafion® path (typically 0.1778 mm) operable in sandwich-type arrangements. It should be noted however that the nearly tenfold increase in R_u for the Nafion®-based device when the relative humidity increases from 36 to 83.6 (from 10,800 ohm to 1,470 ohm) is in qualitative agreement with the increase of Nafion® specific conductivity from 5×10^{-3} Scm^{-1} (30%RH) to 3.5×10^{-2} Scm^{-1} (85%RH) measured by Sone et al. (1996) or from 4.4×10^{-3} Scm^{-1} (31%RH) to 2.8×10^{-2} Scm^{-1} (81%RH) measured by Sumner et al. (1998).

RH (%)	Q (µC)	I (µA)	R_u (Ω)
17.5	3.0	-0.15	70000
23	5.8	-0.66	40000
36	31.8	-1.66	10800
40.5	39	-2.60	9300
45.5	46.7	-2.70	7300
55	83.6	-10.00	5000
82.5	266.0	-84.00	1500
83.6	319.0	-86.50	1470

Table 3.2 Gold oxide reduction charge (Q), oxygen reduction signal (I) at –0.3V vs. Ag/AgCl and uncompensated resistance (R_u) in varied humidity

As argued previously, the well-defined voltammetry of Figure 3.22 indicates that the current decrease observed in both gold surface electrochemistry and oxygen reduction is unlikely to be due to the effect of humidity on conductivity alone. The number of water molecules per sulphonic group of the Nafion® polymer electrolyte is known to vary from 2 to 14 in the 20-100 %RH range and up to 21 in water-equilibrated membranes (Zawodzinski et al. 1991). The ionic-aqueous regions within the polymer are expected to be the active sites for both gold oxide formation/stripping and oxygen reduction (see reactions (1) and (2) above) since gold oxide formation requires water as a reactant and both gold oxide stripping and oxygen reduction require a mobile-solvated proton as a reactant. Also, the amount of water present in the polymer determines the degree of dissociation of the sulphonic acid groups, which in turn determines the proton activity and hence affects both the thermodynamics and the rate of oxygen reduction and gold oxide formation/reduction. The latter follow reactions (1) and (5) presented in chapter 3.2.2 above:

Au oxide reduction-stripping

$$Au_2O_3 + 6H^+ + 6e^- \rightarrow 2Au + 3H_2O \qquad (1)$$

Au oxide formation

$$2Au + 3H_2O \rightarrow Au_2O_3 + 6H^+ + 6e^- \qquad (5)$$

In an attempt to clarify whether there is the same humidity effect on both gold surface electrochemistry and oxygen reduction reaction (e.g. a simple active site variation effect) we normalized the oxygen reduction currents with respect to the corresponding gold oxide stripping charges. Most of the values used are those given in Table 3.2. This was done by first translating the charge values into gold electroactive surface areas (based on the 420 $\mu C/cm^2$ reported for a AuO monolayer on smooth gold (Capon & Parsons 1972, Kita & Nakajima 1986, Amadelli et al. 1992)) and then converting the currents into current densities (current per electroactive surface area). Hence, the current densities reported serve as an indicator of the water content effect on two different processes: gold surface electrochemistry and oxygen reduction.

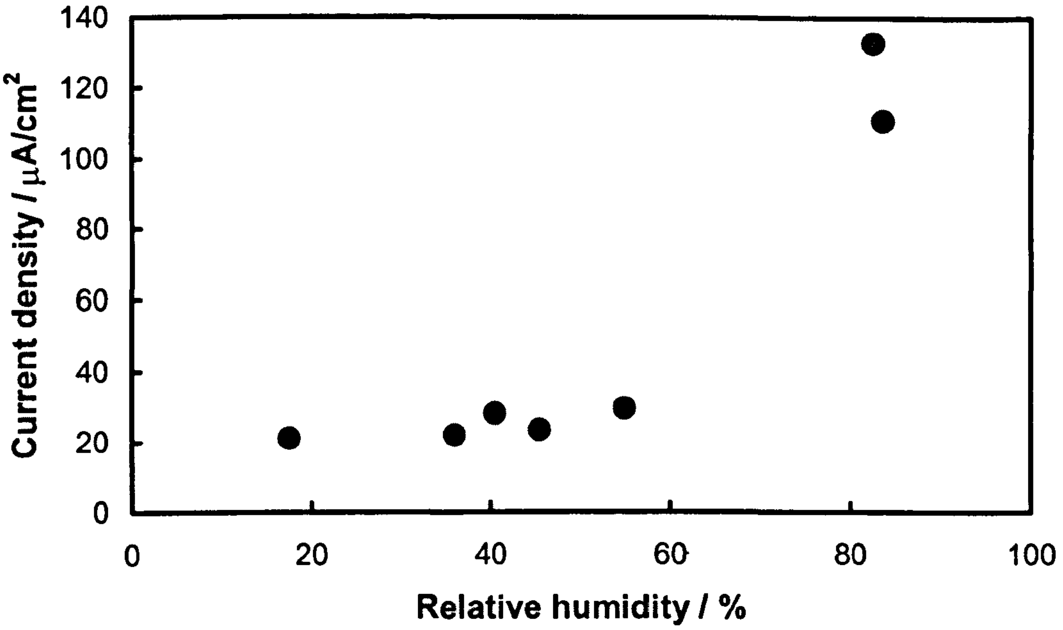

Figure 3.24 Variation of oxygen reduction current density with relative humidity of air streams for a three-electrode Au (vs. Ag/AgCl)/Nafion®/Au-planar device

Figure 3.24 presents the variation of these current densities with relative humidity. It can be seen that, within the experimental uncertainties involved in calculating electroactive surface areas from repetitive cyclic voltammetry, the current density for Nafion®-based devices varies little with humidity at RH less than ca. 60%. This indicates that a mere decrease in the number of gold sites in contact with water can explain the variation of both surface electrochemistry and oxygen reduction. However at relative humidity above ca. 70%, the increase in water content enhances significantly the reduction of oxygen. Zawodzinski et al (1991) reported that at relative humidities below 75% the water in Nafion® is bound to the ions of the polymer (solvation water) whereas at higher humidities any additional water fills the polymer channels and pinholes and swells the membrane. This water has been postulated by Zecevic et al. (1997) to form a very thin continuous layer between the electrode and the polymer and is believed to enhance the catalytic activity of the electrode with respect to oxygen reduction at the metal/Nafion® interface (Uribe et al. 1992).

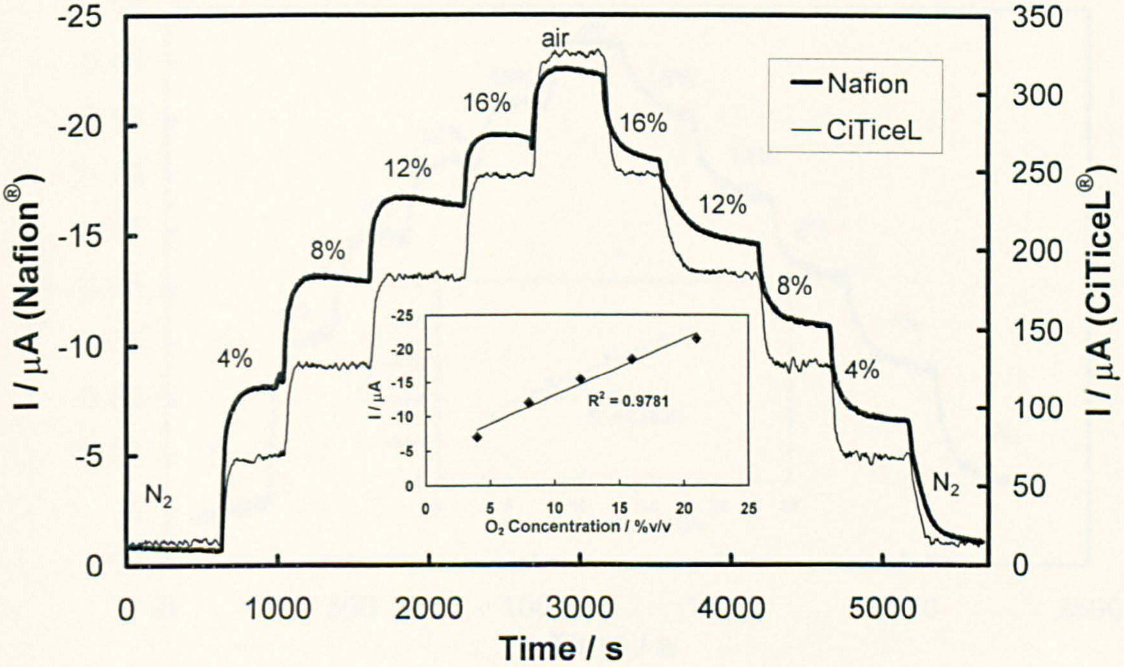

Figure 3.25 Current-time response of the Au (vs. Ag/AgCl)/Nafion®/Au and CiTiceL® (City Technology Ltd) sensor to oxygen concentration steps in water saturated (100% RH) gas samples. The working electrode was held at –0.1 V vs. Ag/AgCl. *Inset:* Variation of the background corrected current with oxygen concentration.

Figure 3.25 presents the current vs. time response of a three-electrode Au (vs. Ag/AgCl)/Nafion®/Au planar sensor to oxygen changes in a well humidified gas stream at constant potential of –0.1 V vs. Ag/AgCl with the response of the CiTiceL® (City Technology Ltd.) shown for comparison. A smooth change of the signal with oxygen concentration was observed with signs of some signal saturation in the higher concentration range as was already observed in Figure 3.9. It was speculated then together with the discussion for Figure 3.6, that the saturation was due to limitations imposed by the reaction occurring at the counter electrode, namely oxygen evolution that occurs via the oxidation of membrane water, which cannot sustain the high oxygen reduction currents expected.

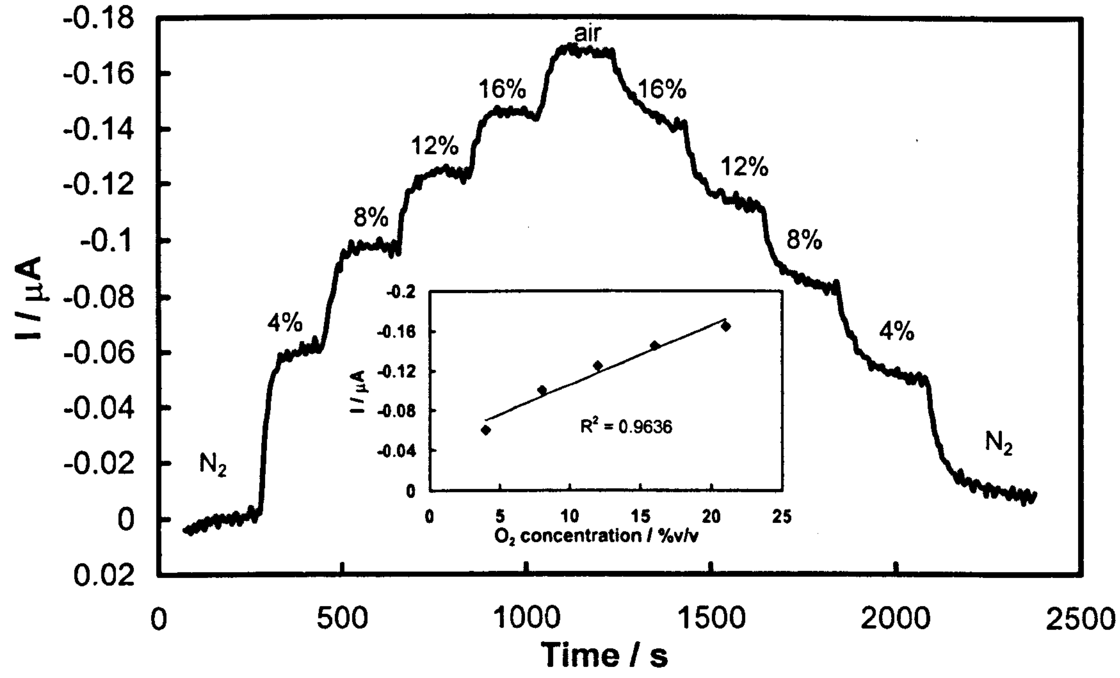

Figure 3.26 Current-time response of the Au (vs. Ag/AgCl)/Nafion®/Au sensor to oxygen concentration steps at 50% RH gas samples. The working electrode was held at –0.3 V vs. Ag/AgCl. *Inset:* Variation of the background corrected current with oxygen concentration.

To investigate if the response of the sensor to oxygen concentration steps is still nearly linear at humidity levels other than 100% RH (a point of high practical importance), the experiment was repeated in gas streams of lower relative humidity. Figures 3.26 and 3.27 present the current vs. time response of the same Au (vs. Ag/AgCl)/Nafion®/Au device to oxygen changes in gas streams of 50% and 35% respectively at constant working electrode potentials of –0.3 V and –0.5 V vs. Ag/AgCl. The insets show the variation of the background corrected oxygen reduction current with oxygen concentration in the gas streams. Again, similar step-wise patterns to that of a well-humidified sample are observed with a smooth change of the signal. It can be seen that the slight signal saturation already encountered at 100% RH (Figure 3.25) does not increase with decreasing humidity and conductivity.

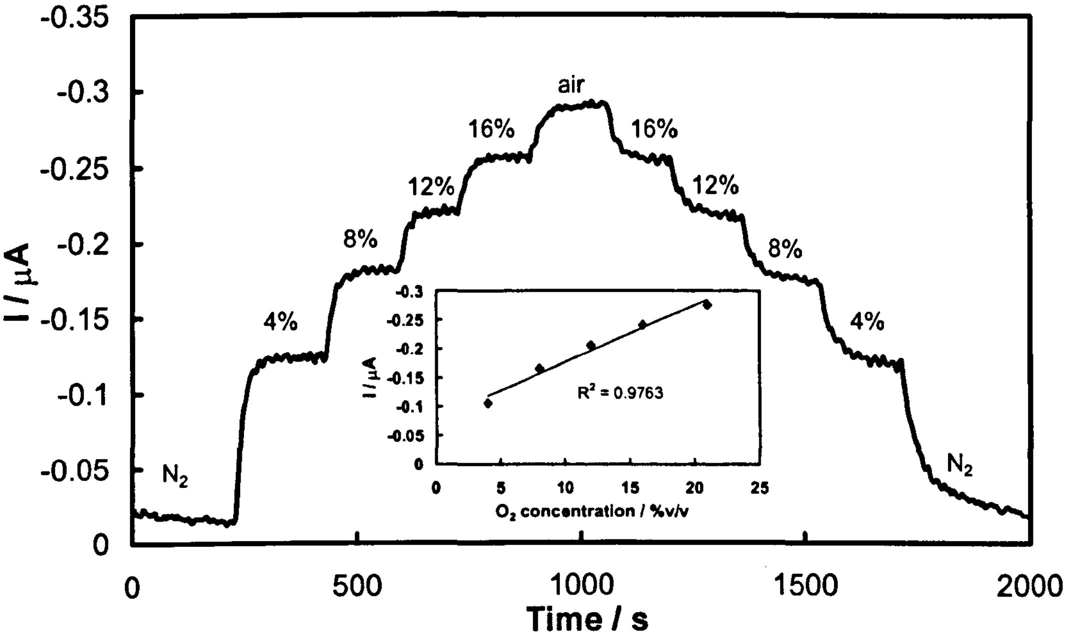

Figure 3.27 Current-time response of the Au (vs. Ag/AgCl)/Nafion®/Au sensor to oxygen concentration steps at 35% RH gas samples. The working electrode was held at -0.5 V vs. Ag/AgCl. *Inset:* Variation of the background corrected current with oxygen concentration.

3.4 Mechanism of oxygen reduction

3.4.1 Mechanism of oxygen reduction at the Au/Nafion® planar sensors

The study on gold surface electrochemistry at various humidities at the Au/Nafion® interfaces (Figure 3.22) revealed, that mainly the size and not so much the shape or position of the oxide formation and stripping changed with humidity. This could not be explained simply in terms of ohmic losses, but more likely is related to the effect of water on the number of electroactive sites and their catalytic activity.

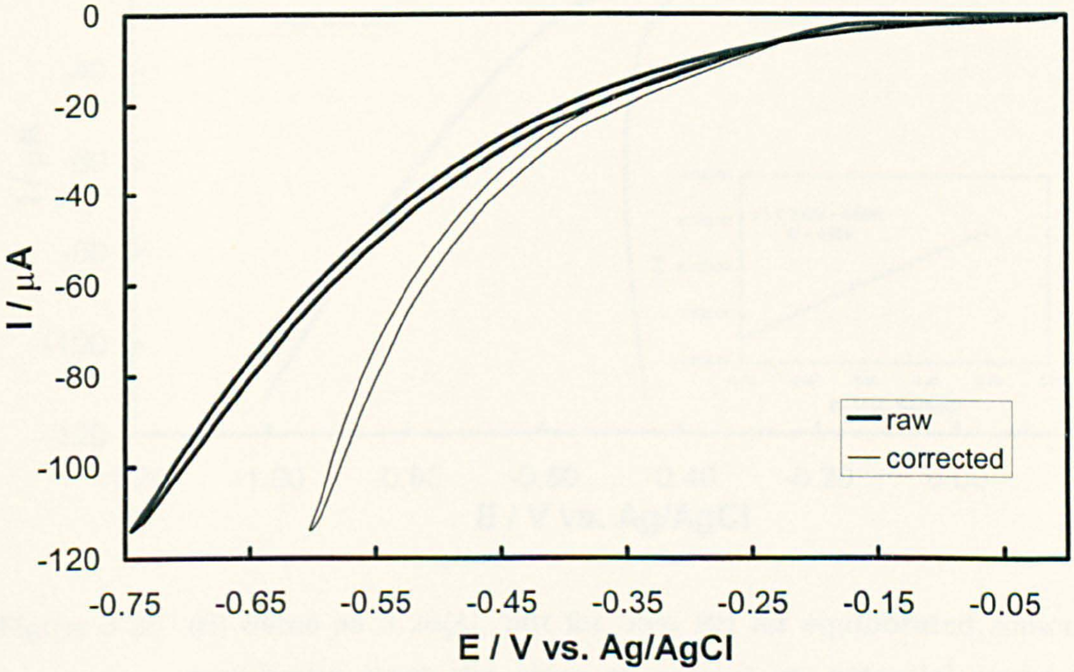

Figure 3.28 (A) Voltammograms recorded at 5 mV/s in water saturated (100% RH) air streams at a three-electrode Au (vs. Ag/AgCl)/Nafion®/Au-planar device and corrected for ohmic losses.

To study the kinetics of the oxygen reaction at the Au/Nafion® interface, the slow potential sweep cathodic scans (5 mV/s) of the varying humidity experiments were mainly used, after having been corrected for ohmic losses. Uncompensated resistance values were obtained either by the current interrupt technique (at 100 μA levels) or from the slope of current vs. potential curves at extreme negative potentials where ohmic control prevails (see for example the Inset to Figure 3.28 (B) below). Examples of these corrected curves can be seen in Figures 3.28 (A) and 3.28 (B) for a 100% RH and 55% gas-humidified samples respectively.

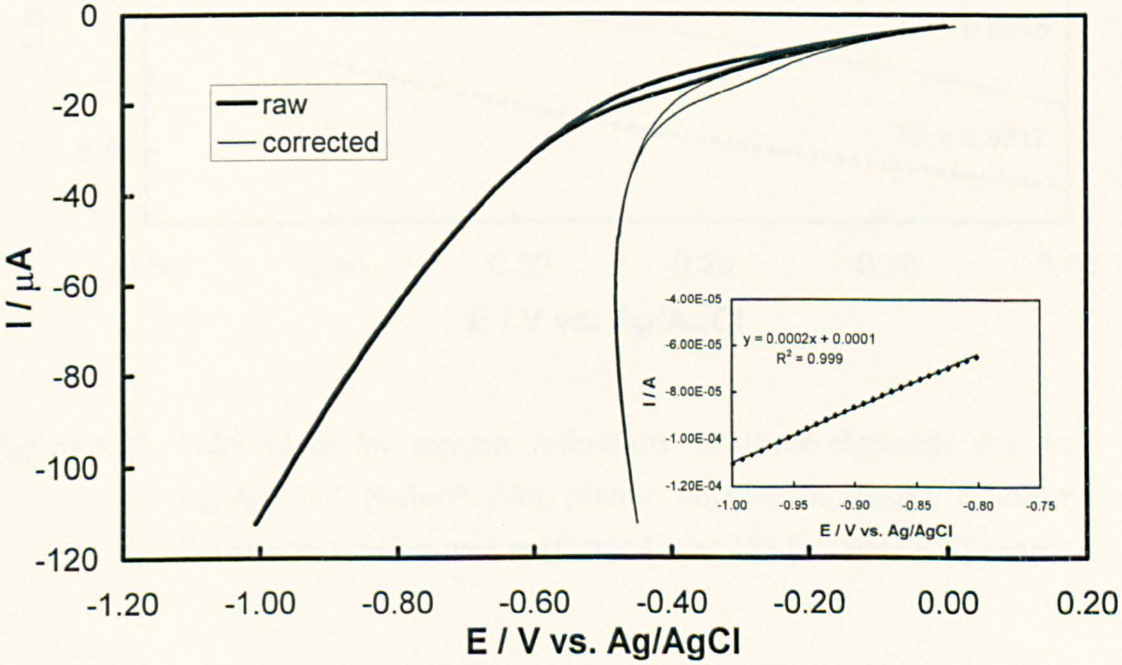

Figure 3.28 (B) Same as 3.28(A), but for 55% RH air equilibrated Nafion® membrane *Inset:* the slope of current vs. potential curve at extreme negative potentials measured from the raw curve

In most of our studies, the logI vs. $E_{(corrected)}$ plots from which Tafel slopes were estimated, has been based on these IR-corrected slow-scan potentiodynamic curves. Some indicative Tafel plots can be seen in Figure

3.29. The reasonable linearity of the plots means that no mass transfer correction is needed and that pure kinetic control of oxygen reduction at the Au/Nafion® interface prevails in the potential region shown.

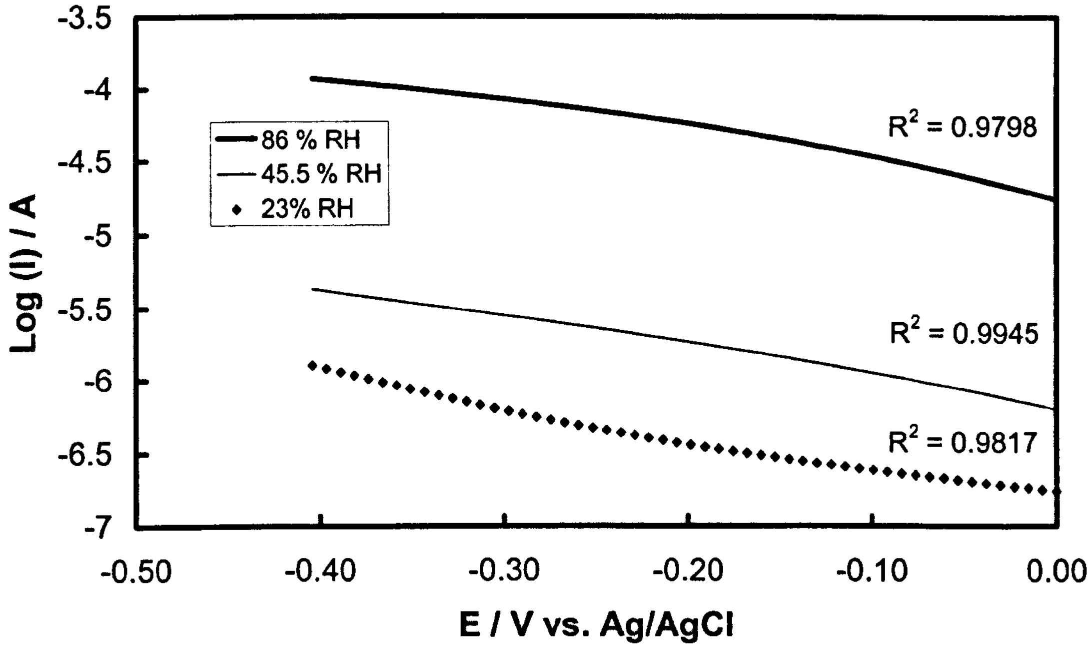

Figure 3.29 Tafel plots for oxygen reduction on three-electrode Au (vs. Ag/AgCl) / Nafion® /Au planar devices in varied humidity (Linear regression was performed over the full potential range)

In another set of experiments, raw near-steady state current data were collected at the end of a potential step to a given potential value. The potential steps were usually applied as a series of increasing potential increments (see Figure 3.30 for example) or as pulses of increasing height from an initial potential value in the region where no reaction occurs (see Figure 3.31 for example).

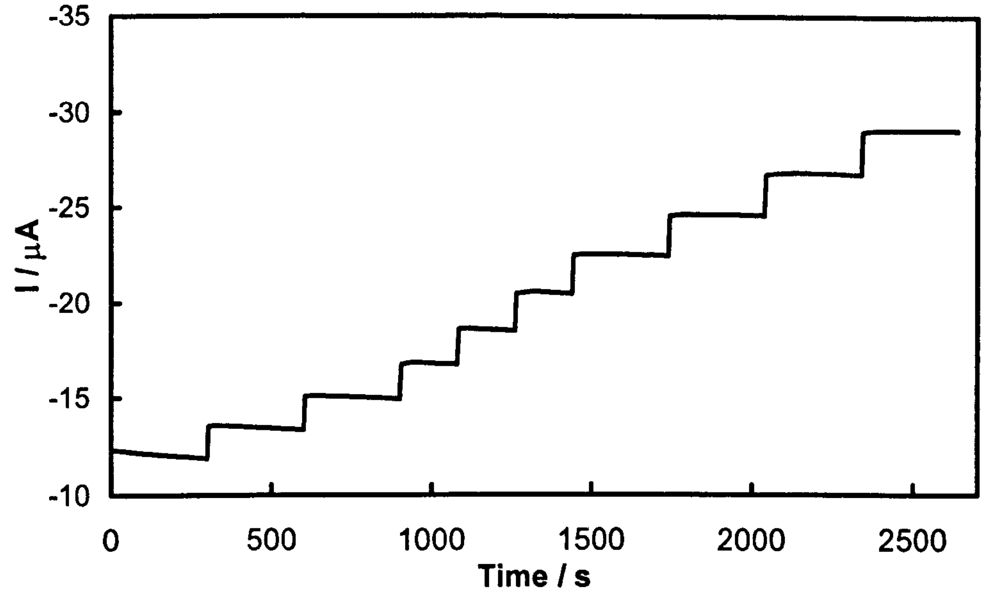

Figure 3.30 Potential steps on three-electrode Au (vs. Ag/AgCl)/Nafion®/Au planar device at 60% RH. The potential was increased by 0.025 V starting from 0 V.

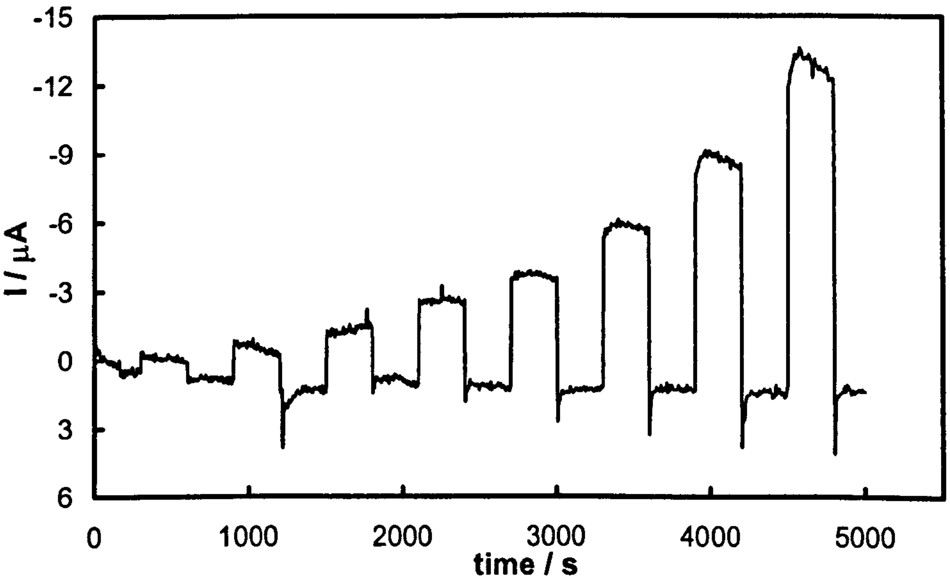

Figure 3.31 Potential pulses on three-electrode Au (vs. Ag/AgCl)/Nafion®/Au planar device at 100% RH. Starting from 0 V the potential was increased by 0.025 V for each pulse.

Table 3.3 presents results of Tafel slopes calculated at various humidities. For gold cathodes in acidic aqueous solutions, where electron transfer is the rate controlling step, the Tafel slope is reported to be around 0.110 V /dec (Hoare 1968).

RH (%)	R_u (Ω)	Tafel slope[1] V/dec	Tafel slope[2] V/dec	Tafel slope[3] V/dec
17.5	70000	0.393		
23	40000	0.524		
36	10800	0.464		
40	9000	0.408	0.428	
40.5	9300	0.45		
45.5	7300	0.463		
55	4950	0.488		
60	2500	0.464	0.467	
80	1200	0.351	0.319	
82.5	1500	0.365		
83.6	1470	0.334		
100 (gas humidified)	1250 /[4] 600	0.280 / 0.200	0.243	0.121
100 (fully hydrated)	1500 /[4] 350	0.152 / 0.135		0.110

Table 3.3 Uncompensated resistance (R_u) and calculated Tafel slopes from IR-corrected data, in air streams of varied relative humidity (RH), for three-electrode Au(vs. Ag/AgCl)/Nafion®/Au planar devices.

[1] Data from slow potentiodynamic experiments

[2] Data from staircase potential step experiments

[3] Data from potential pulse experiments (initial potential of 0 V vs. Ag/AgCl)

[4] Data from two different devices

The higher values observed here (in all but the fully-hydrated case and only in the potential pulse mode) indicate that the kinetics are not controlled by simple electron transfer, but may be affected by impurities or a chemical step that precedes charge transfer (Uribe et al. 1992) or a physicochemical process in general. The results also show that although a change in membrane water content from 21 H_2O/SO_3H for fully hydrated in contact with water to 14 H_2O/SO_3H for 100%RH gas-humidified sample (Zawodzinski et al. 1991) does not affect the membrane conductivity significantly (in effect it is the same for both cases within experimental error), it has a significant effect on the value of the Tafel slope. This implies that oxygen reduction is not merely controlled by electron transfer on these devices and that the additional limitations are water-dependent. A possible explanation is the continuous depletion of the Au/Nafion® interface from solvated protons as oxygen reaction proceeds at very high current densities at a restricted electrode area close to the deposit edge, resulting in a continuous rise of the local pH. This effect may be enhanced at low water contents, which will limit proton solvation and migration. Further evidence for the continuous proton depletion giving rise to high Tafel slopes is the fact that the only occasion when a normal Tafel slope of 110 mV/ decade is observed, is that of a fully hydrated membrane and short pulses in the oxygen reduction-proton depletion potential range. The return of the potential back to more positive values between these pulses may restore the local pH conditions. It is quite interesting that in a series of recent papers on oxygen reduction at platinum solid polymer electrolyte electrodes (Sena et al. 1999, Jaouen et al. 2002, Ihonen et al. 2002) double or even quadruple Tafel slope values have been predicted and in some cases observed at higher current densities. These values were explained by simultaneous control not only by Tafel kinetics but also by proton migration and/or water transport and/or oxygen diffusion inside the catalyst agglomerates.

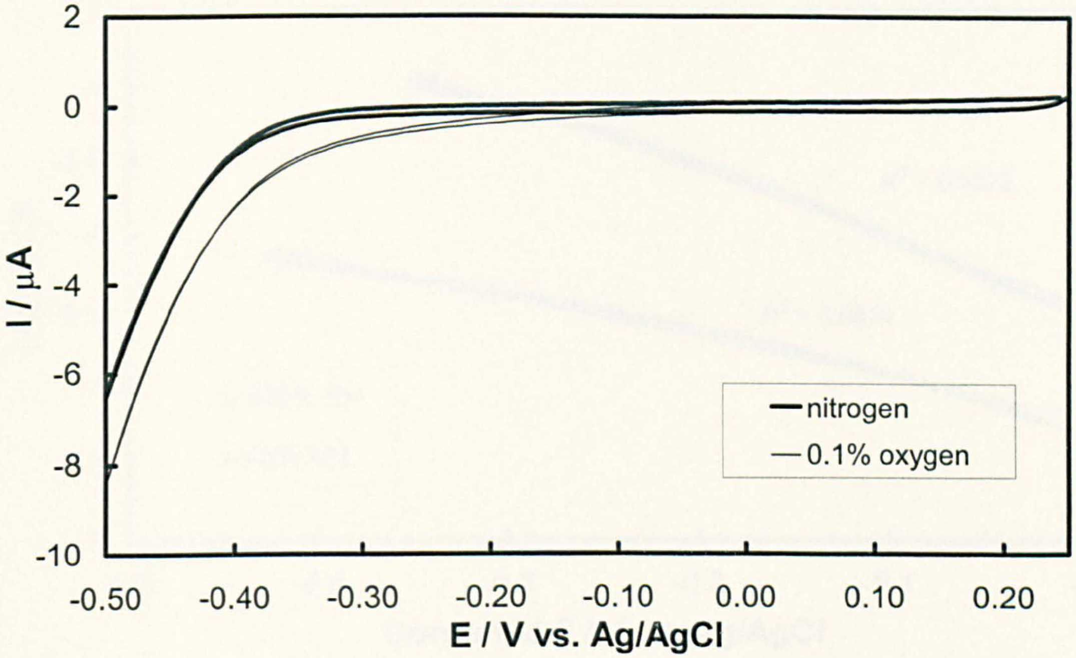

Figure 3.32 Voltammograms recorded at 5 mV/s in water saturated nitrogen and 1000 pm O_2 streams at three-electrode Au (vs. Ag/AgCl)/Nafion®/Au planar device

To further confirm that the higher slopes are not simply due to ohmic losses caused by changing conductivity with water content or to limitations imposed by water oxidation at the counter electrode, the experiments were repeated at 40% and 100% RH (gas humidified) air and 1000 ppm O_2 streams. A typical voltammogram for oxygen reduction from 1000 ppm water-saturated stream is shown in Figure 3.32. The IR corrected Tafel plots can be seen in Figure 3.33 (A) and (B). The lower currents observed at these oxygen levels should lead to smaller ohmic losses and even traces of water should support the reaction at the counter electrode.

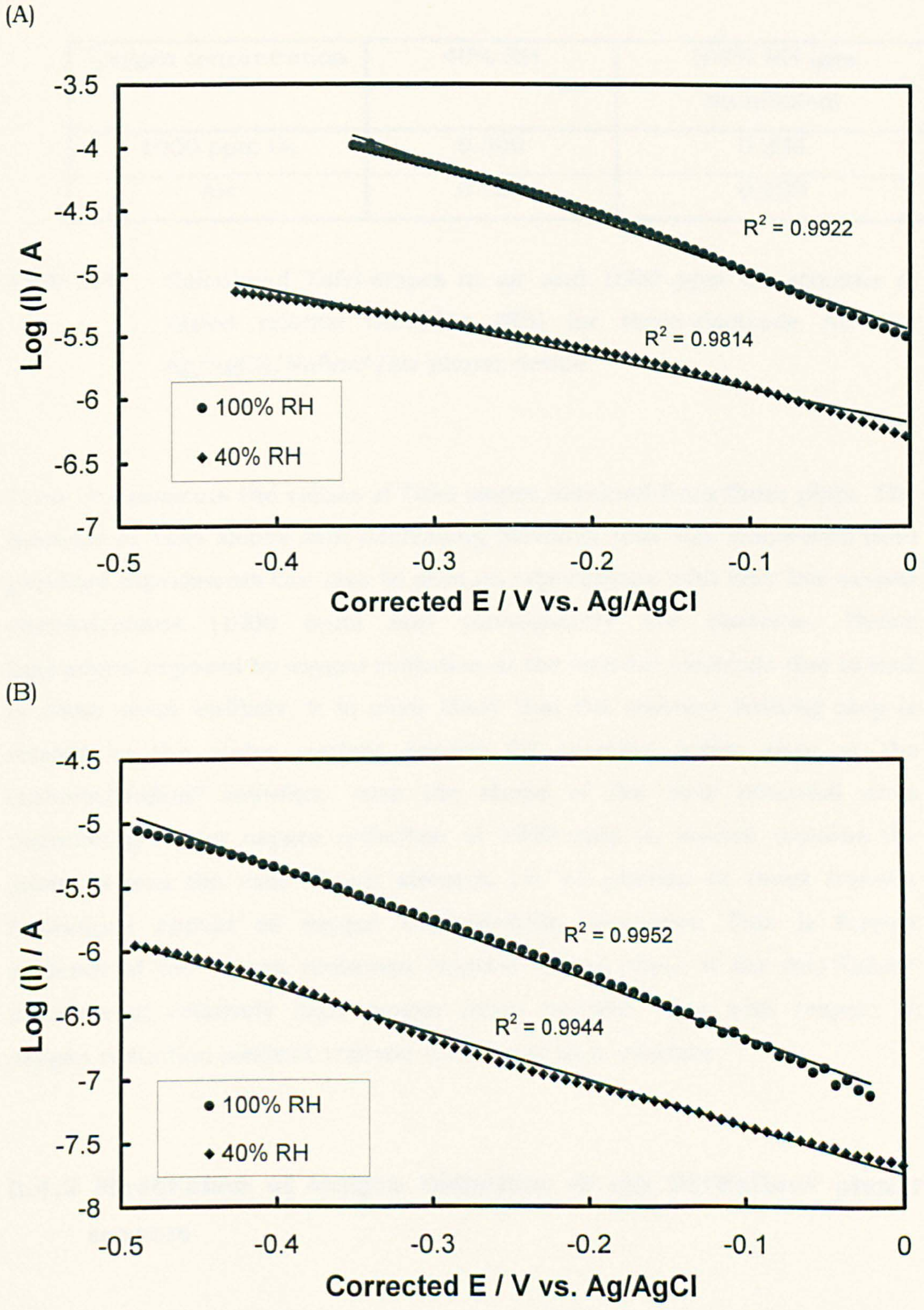

Figure 3.33 IR corrected Tafel-slopes for air (A) and 1000 ppm O_2 (B) streams of varied relative humidity (RH) for three-electrode Au (vs. Ag/AgCl)/Nafion®/Au planar device

Oxygen concentration	40% RH	100% RH (gas humidified)
1000 ppm O_2	0.300	0.226
Air	0.384	0.229

Table 3.4 Calculated Tafel-slopes in air and 1000 ppm O_2 streams of varied relative humidity (RH) for three-electrode Au (vs. Ag/AgCl)/Nafion®/Au planar device

Table 3.4 presents the values of Tafel slopes obtained from these plots. The increase in Tafel slopes with decreasing humidity that was discovered from previous experiments can also be seen on experiments with very low oxygen concentrations (1000 ppm) and consequently low currents. Hence limitations imposed by oxygen evolution at the counter electrode due to lack of water seem unlikely. It is more likely that the reaction limiting step is related to the water content needed for creating active sites at the cathode/Nafion® interface. Also the shape of the slow potential scan voltammogram for oxygen reduction at 1000 ppm O_2 stream remains the same as was the case for air streams, i.e. no plateau or mass transfer limitations appear as oxygen concentration decreases. This is further evidence of the oxygen reduction reaction taking place at the Au/Nafion® interface at relatively high oxygen mass transfer rates with respect to oxygen reduction electron transfer kinetics at that interface.

3.4.2 Mechanism of oxygen reduction at the Pt/Nafion® planar sensors

Figure 3.34 shows a slow potential sweep cyclic voltammogram for oxygen reduction from a 100%RH air stream on a three-electrode Pt (vs. Ag/AgCl)/Nafion®/Pt planar device, together with the background curve obtained in a 100%RH nitrogen stream.

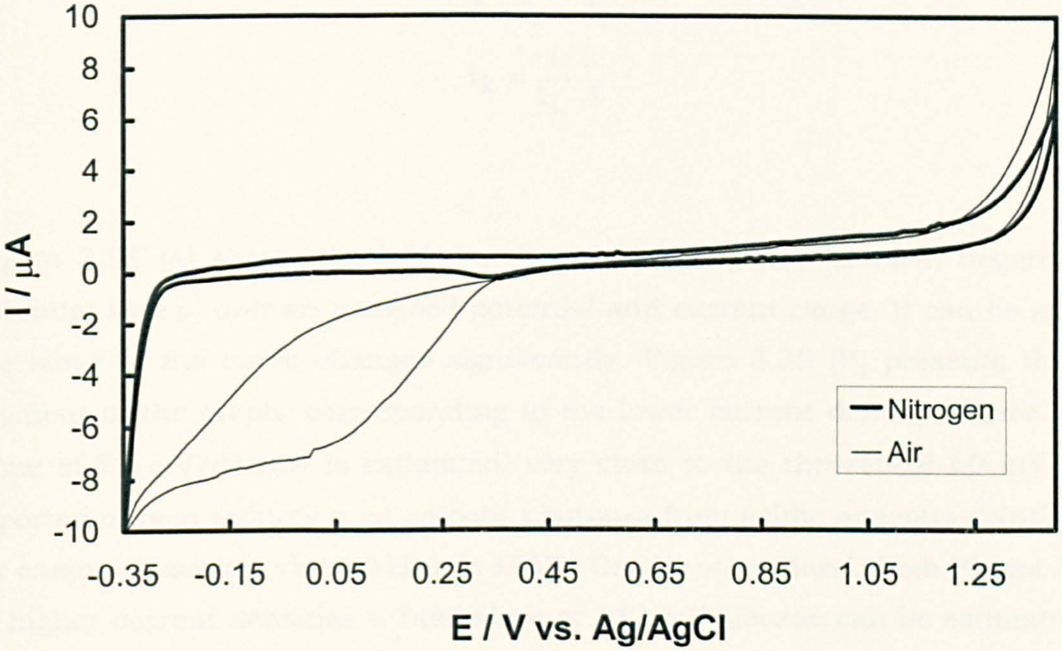

Figure 3.34 Voltammogram recorded at 5 mV/s in water saturated air and nitrogen streams at a three-electrode Pt (vs. Ag/AgCl)/Nafion®/Pt-planar device

It is seen again that, unlike gold where the oxygen reduction current in the planar sensor arrangement is never under mass transfer control, in the case of a platinum working electrode where oxygen reduction kinetics are faster a limiting current is observed, revealing the existence of a thin mass transfer barrier (either a liquid hymen at the working electrode/Nafion®/gas line interface or the Nafion® membrane underneath working electrode deposit).

The appearance of a limiting current provides the possibility to correct the currents for mass transfer limitations in a wider current range (i.e. in the mixed control potential range too) and perform a more accurate and extended Tafel analysis of the kinetic currents. The mass transfer correction of the measured currents I to give the pure kinetic currents I_k with the help of the mass transfer limiting current I_L, is based on the relationship:

$$\frac{1}{I}=\frac{1}{I_k}+\frac{1}{I_L}\Rightarrow$$
$$I_k=\frac{I_L I}{I_L-I}$$

Figure 3.35 (A) shows the logI_k vs. E curve during the forward, negative-going potential sweep, over an extended potential and current range. It can be seen that the slope of the curve changes significantly. Figure 3.35 (B) presents the linear segment of the graph, corresponding to the lower current density regime. A Tafel slope of 72 mV/decade is estimated, very close to the theoretical 60 mV/decade reported oxygen reduction on smooth platinum from acidic aqueous solutions (see for example Damjanovic and Brusic 1967). On the other hand, from Figure 3.35 (B) at higher current densities a Tafel slope of 143 mV/decade can be estimated. This is in accordance with our findings for the Au/Nafion® interface and those reported recently for the Pt/Nafion® interface (Sena et al. 1999, Jaouen et al. 2002, Ihonen et al. 2002) and discussed in more detail in the previous section. Briefly, the increase in Tafel slope at higher currents is attributed to water mass transport and/or oxygen mass transport and/or proton migration limitations. Another striking finding is that of Figure 3.35 (C) where the Tafel slope estimated from the reverse, positive going potential sweep was found as high as 518 mV/decade. This increase may be associated to the excursion of the electrode at very negative potentials where proton depletion and water flooding (dragged there by proton diffusion and migration) of the Pt/Nafion® cathode interface.

(A)

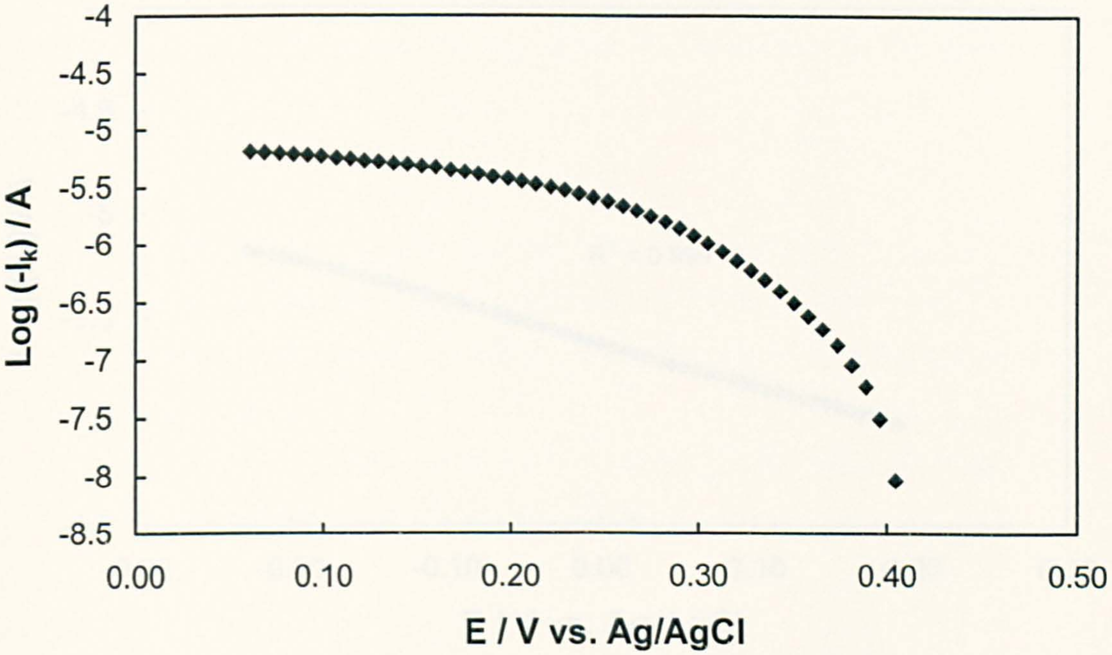
-4
-4.5
-5
-5.5
-6
-6.5
-7
-7.5
-8
-8.5
Log (-I$_k$) / A
0.00
0.10
0.20
0.30
0.40
0.50
E / V vs. Ag/AgCl

(B)

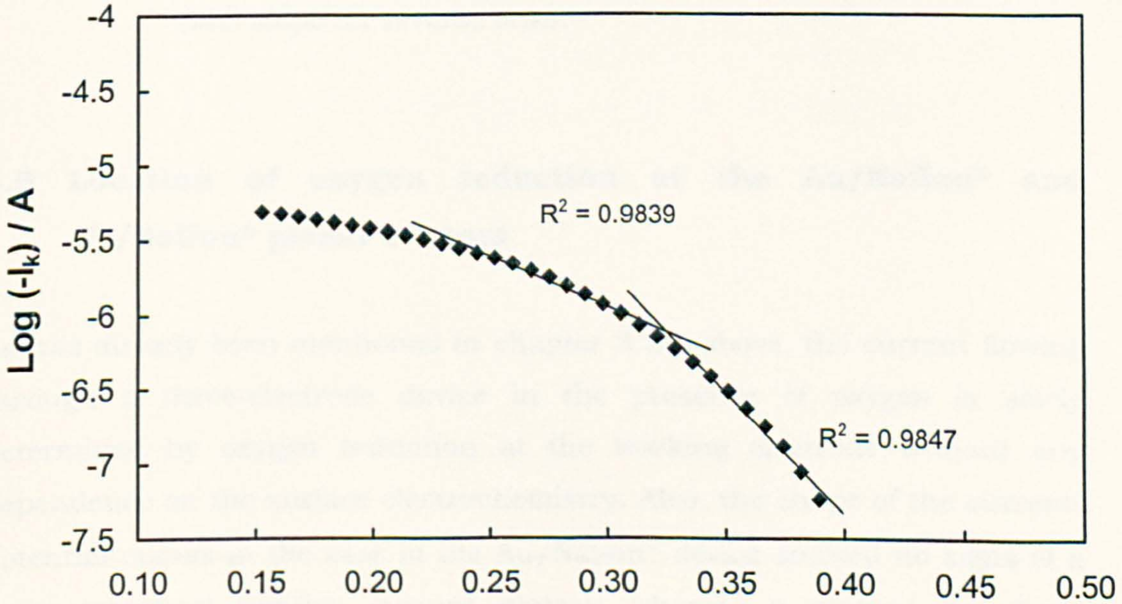
-4
-4.5
-5
-5.5
-6
-6.5
-7
-7.5
Log (-I$_k$) / A
R^2 = 0.9839
R^2 = 0.9847
0.10
0.15
0.20
0.25
0.30
0.35
0.40
0.45
0.50
E / V vs. Ag/AgCl

(C)

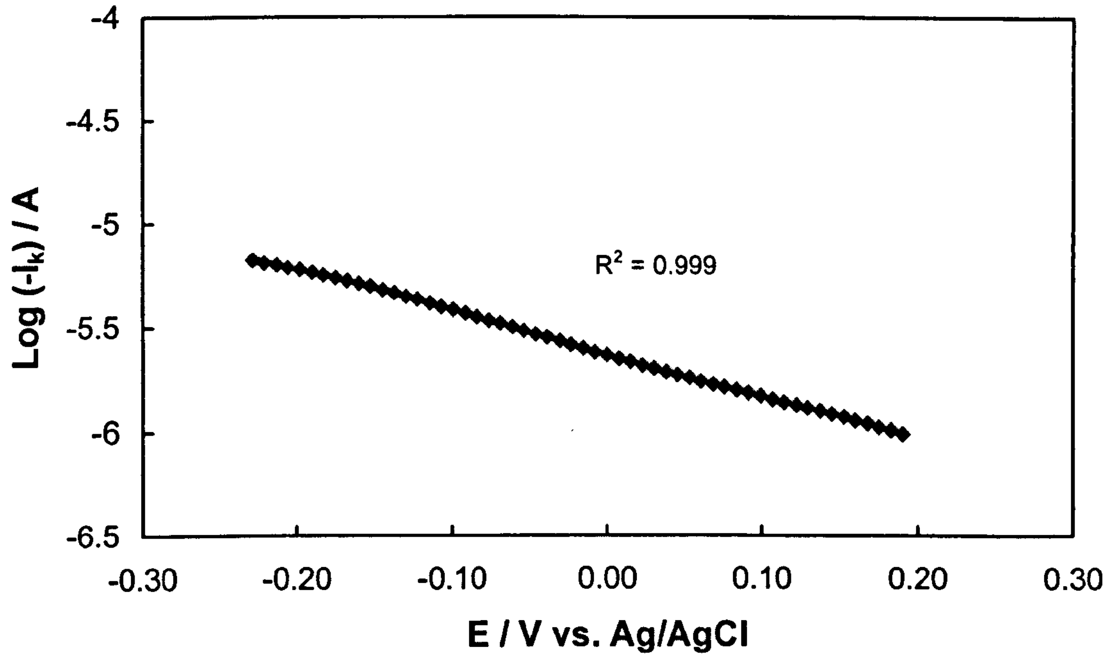

Figure 3.35 Tafel plots for oxygen reduction on three-electrode Pt (vs. Ag/AgCl) / Nafion® /Pt planar device (A) Forward potential sweep over extended current and potential range. (B) Tafel-slopes for forward scan. (C) Tafel slope for reverse scan.

3.5 Location of oxygen reduction at the Au/Nafion® and Pt/Nafion® planar sensors

As has already been mentioned in chapter 3.2.1 above, the current flowing through a three-electrode device in the presence of oxygen is solely determined by oxygen reduction at the working electrode without any dependence on the surface electrochemistry. Also, the shape of the current-potential curves in the case of the Au/Nafion® device showed no signs of a mass transport limiting current plateau whereas a plateau has been observed for Pt/Nafion® electrodes. This indicates that a thin mass transfer barrier (if any at all) exists at the location where oxygen reduction occurs. The latter, based on current distribution considerations for the co-planar arrangement and confirmed to a certain extent by the electroactive working electrode area estimated from surface electrochemistry, has been expected to be at the edge of the working electrode layer, closer to the counter and reference electrode. The question still open at this stage is whether this location lies:

i. on top of the device, at the metal/Nafion®/gas interface with oxygen diffusing through a thin aqueous film-meniscus) or
ii. at the metal/Nafion® interface, with oxygen diffusing through the metal layer or
iii. at the metal/Nafion® interface, with oxygen diffusing through the membrane underneath the metal layer.

Schiavon et al. (1989), who used sputtered gold films of similar thickness, reported S-shaped voltammograms for oxygen reduction that provided evidence of mass transport limitations to oxygen reduction. However, they used a sandwich-type arrangement where the oxygen has to diffuse through the electrode layer to reach the electrode/electrolyte interface. To study the possible diffusion through the metal layer in the three-electrode device, for Figure 3.36 the thickness of the sensing electrode was increased from 360 nm to 1440 nm.

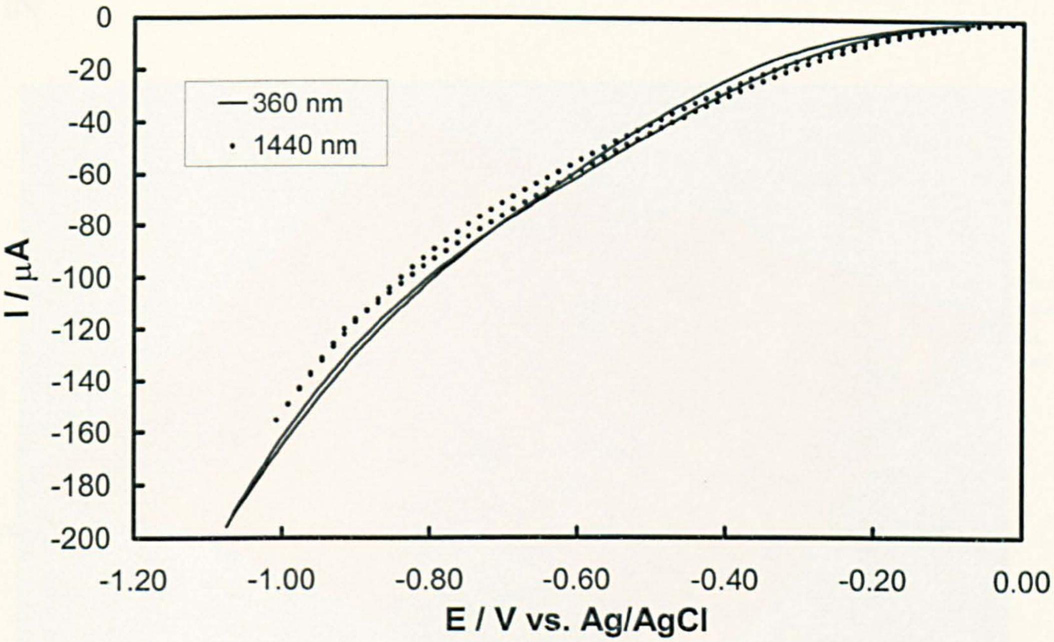

Figure 3.36 Voltammograms recorded at 5 mV/s at three-electrode Au (vs. Ag/AgCl)/Nafion®/Au planar device with varying sensing electrode thickness in water saturated air stream.

As can be seen from the voltammograms, changing the thickness of the sensing electrode by nearly five-fold had no significant effect on the oxygen reduction current. If there was diffusion through the metal layer, a limiting current plateau should be observed at higher polarisations where mixed control would be expected. This suggests that the gold layers do not impose a significant mass transport barrier to oxygen reduction.

Picture 3.2 presents surface images of uncovered and gold sputtered Nafion surface and shows that the sputtering technique gives uniform non-porous coatings.

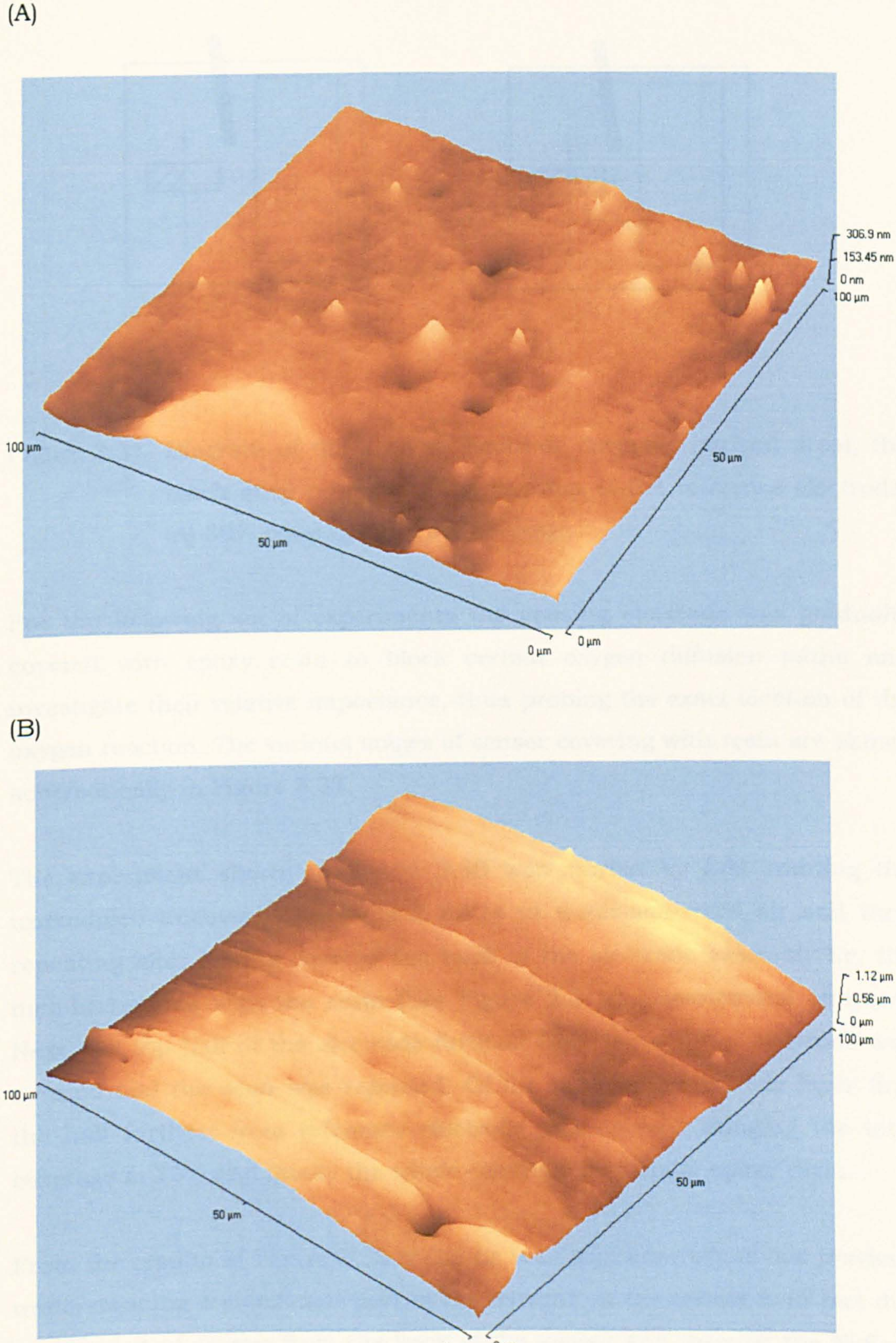

Picture 3.2 (A) Atomic microscope image (AMF) of Nafion® surface. (B) AFM image of Nafion® surface covered with 540 nm of gold.

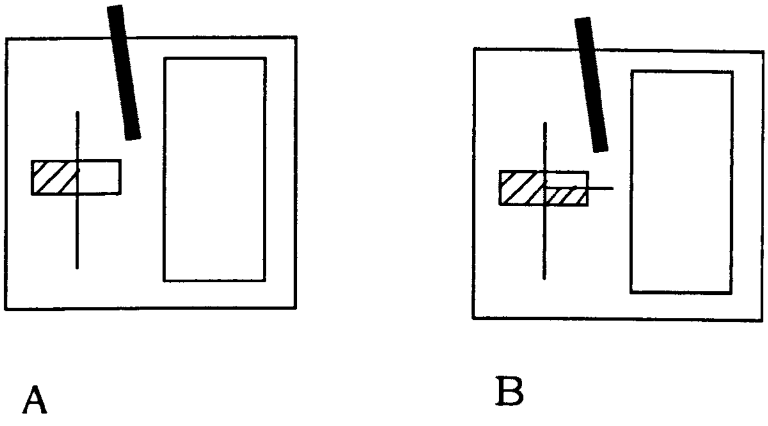

Figure 3.37 Diagram of the sensing electrode coverage (striped area), the black strip represents the position of the reference electrode. (A) 50% coverage (B) 75% coverage

For the following set of experiments the sensing electrode was gradually covered with epoxy resin to block certain oxygen diffusion paths and investigate their relative importance, thus probing the exact location of the oxygen reaction. The various stages of sensor covering with resin are shown schematically in Figure 3.37.

The experiment shown in Figure 3.38 was started by first running the unmodified uncovered sensor a 5 mV/s in water-saturated air and then repeating after having covered the back of the electrode assembly i.e. the membrane side with the resin (See Figure 2.2 on Experimental chapter). Next, the top half of the electrode furthest from the counter electrode was covered and the scan was repeated. Of the remaining electrode layer first the half furthest from reference electrode was covered bringing the total coverage to 75% and finally the whole electrode was under epoxy resin.

From the results in Figure 3.38 it can be seen that contrary to our previous understanding a significant part of the current on the sensor is in fact due to diffusion of oxygen from the back of the sensor and through the Nafion® membrane. However, given the much smaller area of the Au/Nafion®/gas line on top of the device when compared to the active electrode area of the

Au/Nafion® interface beneath the deposit, the contribution of the former to the current should still be considered to be high since, the signal does not fall to zero when the entire back of the device is blocked.

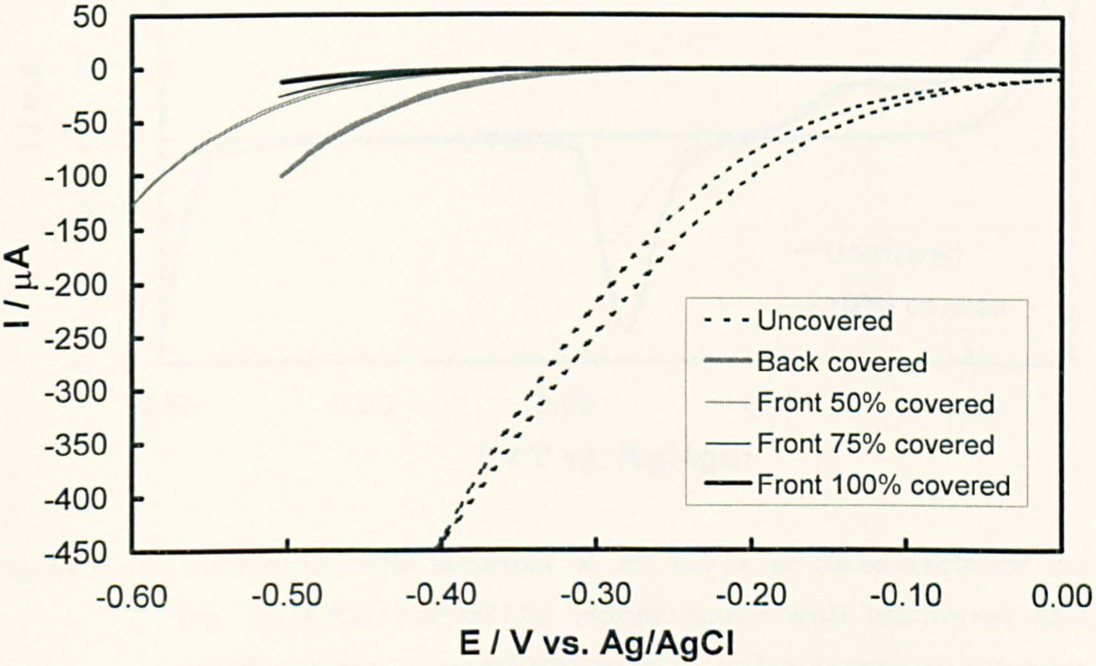

Figure 3.38 Voltammograms recorded at 5 mV/s at three-electrode Au (vs. Ag/AgCl)/Nafion®/Au planar device with varying covering of the sensing electrode in water saturated air stream.

It seems that the perimeter of the deposit on the top of the membrane exhibits increased current densities, due to very high oxygen transfer rates through a very thin barrier on those locations. The relative importance of the various parts of the perimeter is also expected to depend adversely on their distance from the reference electrode. Another interesting finding is that the surface electrochemistry of the gold working electrode remains practically unchanged (within the roughness changes expected during experimentation) as can be seen in Figure 3.39 below

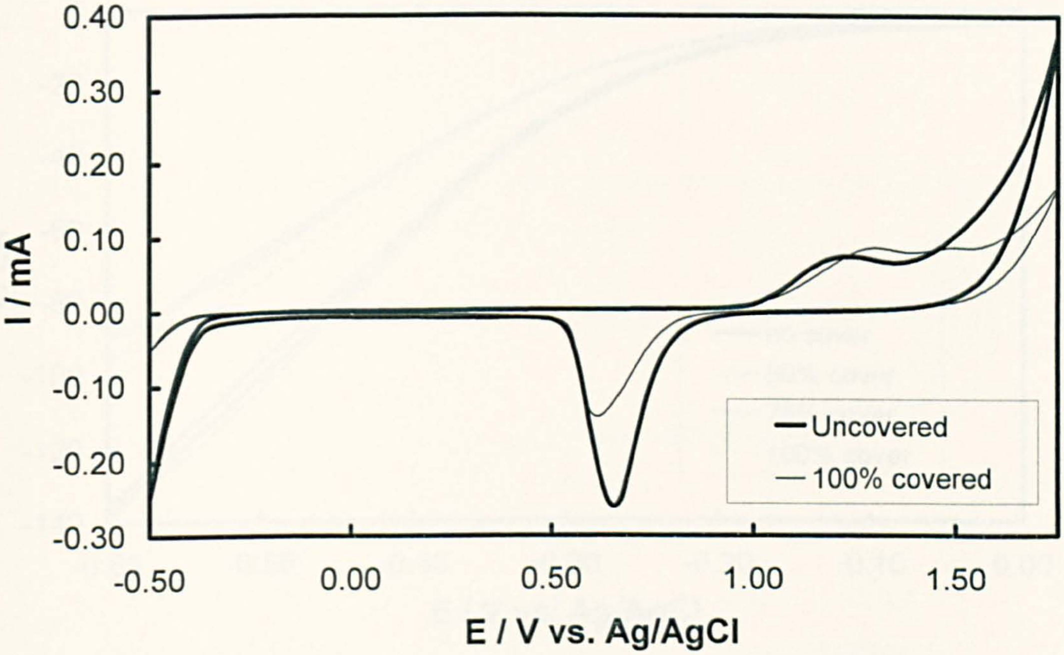

Figure 3.39 Voltammograms recorded at 50 mV/s at three-electrode Au (vs. Ag/AgCl)/Nafion®/Au planar device with uncovered and 100% covered sensing electrode in water saturated nitrogen stream.

In another set of experiments, the covering procedure for the sensing electrode was started from the front, metal face of the device as in Figure 3.37.

It follows from the difference between the un-covered and 100%- front-covered responses of the Figure 3.40(A) that the contribution of the perimeter at the top of the deposit blurs the appearance of a plateau. This is because its contribution to the total current is never under mass transfer control since no significant mass transfer barrier is expected at these locations.

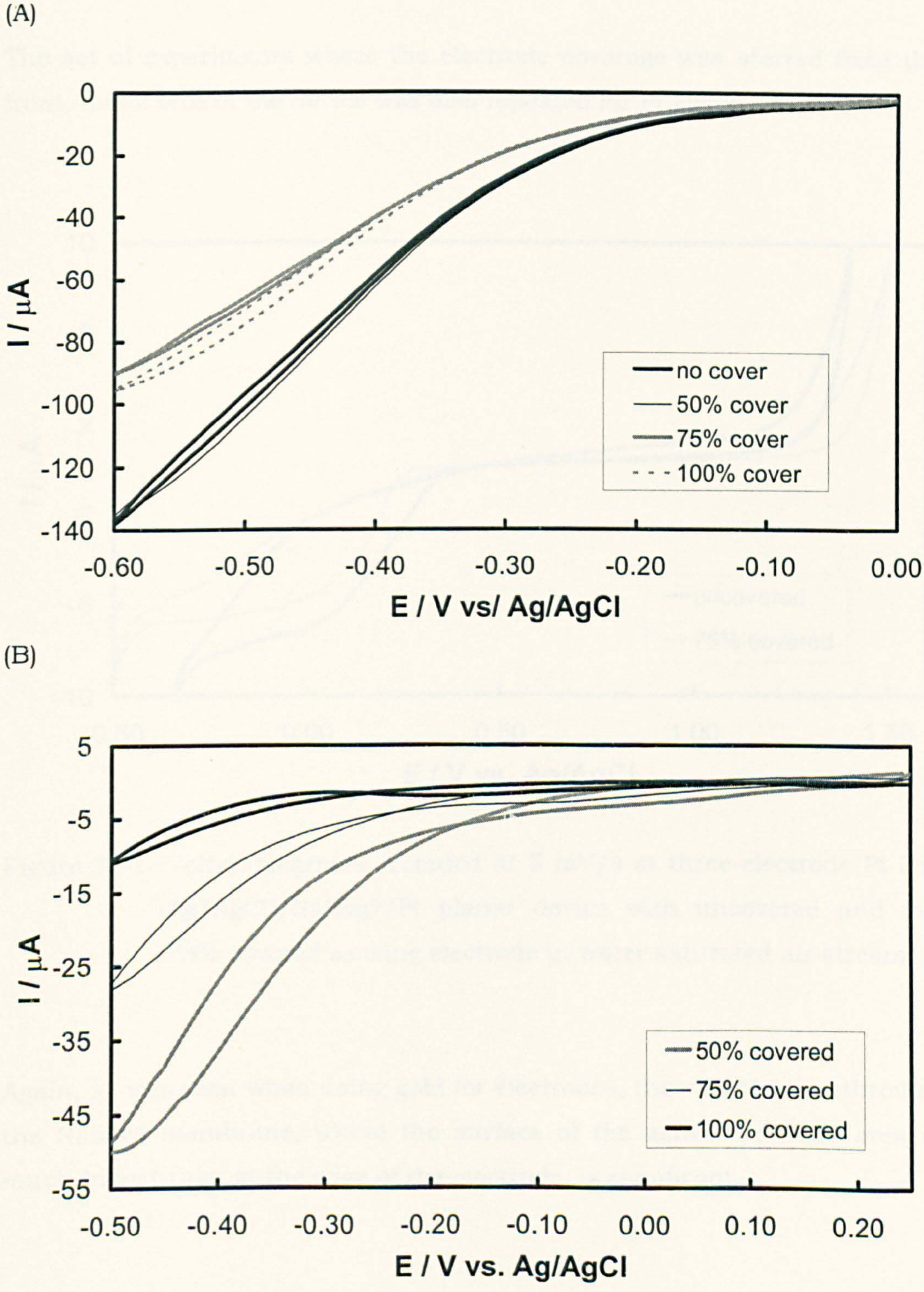

Figure 3.40 Voltammograms recorded at 5 mV/s at three-electrode Au (vs. Ag/AgCl)/Nafion®/Au planar device with varying covering of the sensing electrode in water saturated air stream. (A) Coverage of the top of the electrode. (B) Coverage of the back of the electrode

The set of experiments where the electrode coverage was started from the front, metal face of the device was also repeated for Pt electrodes.

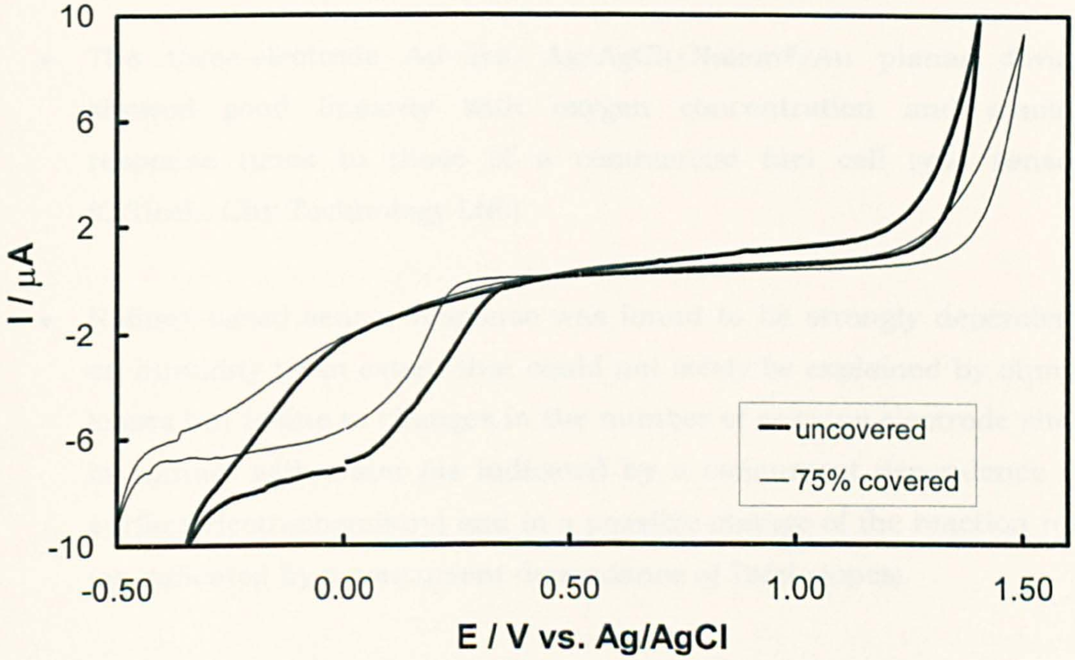

Figure 3.41 Voltammograms recorded at 5 mV/s at three-electrode Pt (vs. Ag/AgCl)/Nafion®/Pt planar device with uncovered and top 75% covered sensing electrode in water saturated air stream.

Again, as was seen when using gold for electrodes, the contribution through the Nafion® membrane, where the surface of the active electrode area is much higher than at the edge of the electrode, is significant.

3.6 Conclusions

- The "gas phase" voltammetry of all-solid three-electrode Au (vs. Ag/AgCl)/Nafion®/Au planar devices in oxygen and nitrogen gas streams was found to be well-defined and typical of aqueous gold electrochemistry. Experiments with two-electrode gold sensors showed signs that, at least at high oxygen concentrations, the oxygen reduction current is not solely determined by oxygen reduction at the sensing electrode, but also by oxygen evolution at the counter electrode.

- The three-electrode Au (vs. Ag/AgCl)/Nafion®/Au planar device showed good linearity with oxygen concentration and similar response times to those of a commercial fuel cell type sensor (CiTiceL, City Technology Ltd.)

- Nafion®-based sensor response was found to be strongly dependent on humidity to an extent that could not solely be explained by ohmic losses but is due to changes in the number of working electrode sites in contact with water (as indicated by a concurrent dependence of surface electrochemistry) and in a possible change of the reaction rds (as indicated by a concurrent dependence of Tafel slopes).

- The study of oxygen reduction at three-electrode Au/Nafion®/Au-devices showed no signs of a mass transport limiting current plateau. The voltammetry of platinum-based devices on the other hand does show a clear limiting current (due to faster oxygen reduction kinetics on platinum). For both devices however the currents were significantly higher than those reported in the literature for similar devices with a significant mass transfer barrier. Thus, the shape of the gold-device voltammogram and the current magnitude of both devices point to high mass transfer rates and a thin or very porous mass transfer barrier.

- Varying the deposit thickness and progressive masking of working electrode areas revealed that the test gas reacted both at the line formed by the gas/solid electrolyte/metal layer interface (diffusion from the gas phase) and underneath the deposit (diffusion from the back of the sensor and through the Nafion® membrane) but not through the metal layer.

CHAPTER 4

Other sensor configurations and solid electrolyte materials

4.1 Other sensor configurations

The shape of the current-potential curves at the planar electrode arrangement showed no signs of a mass transport limiting plateau, when gold was the working electrode, indicating that oxygen reduction on gold is under kinetic or at least mixed control. However, a common requirement for most amperometric sensors is that the reactant gas is reduced (or oxidised) very fast as it arrives to the sensing electrode. The sensing electrode reaction in that case is limited solely by the rate of gas diffusion, the sensing electrode current is under mass transfer control and a limiting current plateau can be observed in current-potential curves (Hobbs 1991).

The various types of diffusion control encountered in amperometric gas sensor configurations can be summarised as follows:

- Analyte gas diffusion through a condenced phase diffusion barrier:
    - Liquid phase diffusion through a liquid electrolyte film
    - Solid state diffusion through a non-porous membrane
- Analyte gas diffusion from the gas phase:
    - Gas phase diffusion through a macroporous membrane or capillary
    - Gas phase diffusion through a micro-porous membrane (Knudsen diffusion)

Each of them has differing responses to temperature and pressure that can have advantages to particular applications (Willett 1999).

In this Chapter we present results aimed to modify our solid-sate sensor design by the introduction of a diffusion barrier, so that mass transfer control is approximated. Two types of such sensor configurations were tested:

- A "sandwich-type" arrangement with the working and counter electrode layers deposited on different sides of the Nafion® membrane (see Figure 2.5 in Experimental Chapter 2). In this case diffusion through the working electrode to the working electrode/Nafion® interface may pose mass transfer limitations to oxygen reduction.

- A "capillary-type" arrangement where a cap bearing a capillary (1.5 mm) was placed on top of the planar sensor device (see Picture 2.2 and Figure 2.4 in Experimental Chapter 2). In this case diffusion through the capillary to the working electrode/Nafion® interface should introduce a mass transfer barrier to oxygen reduction.

4.1.1 Sandwich sensors

Schiavon et al. in 1989 used sputtered gold films of similar thickness to the ones used in our planar sensors, but in a sandwich-type arrangement, where the gas had to diffuse through the electrode layer to reach the electrode/polymer electrolyte interface. He thus reported S-shaped oxygen reduction voltammograms that indicate mass transfer control for oxygen reduction. To use the same method for achieving diffusion control, a sandwich-type sensor was prepared, as described in Chapter 2, with the thickness of the gold layers doubled from the typical value of ~300 nm to ~600 nm and, for the majority of experiments, increased to ~1500 nm.

Figure 4.1 presents a cyclic voltammogram recorded at 50 mV/s in 60% RH nitrogen and air streams at a three-electrode Au (vs. Ag/AgCl)/Nafion®/Au sandwich device, where the gold layer thickness was approximately 1500 nm. A sigmoidal curve is obtained in the presence of oxygen at potentials more negative than 0 V and signs of a peak or plateau are observed around –0.3 V. This suggests the existence of mass transfer limitations, in this case due to the gold layer.

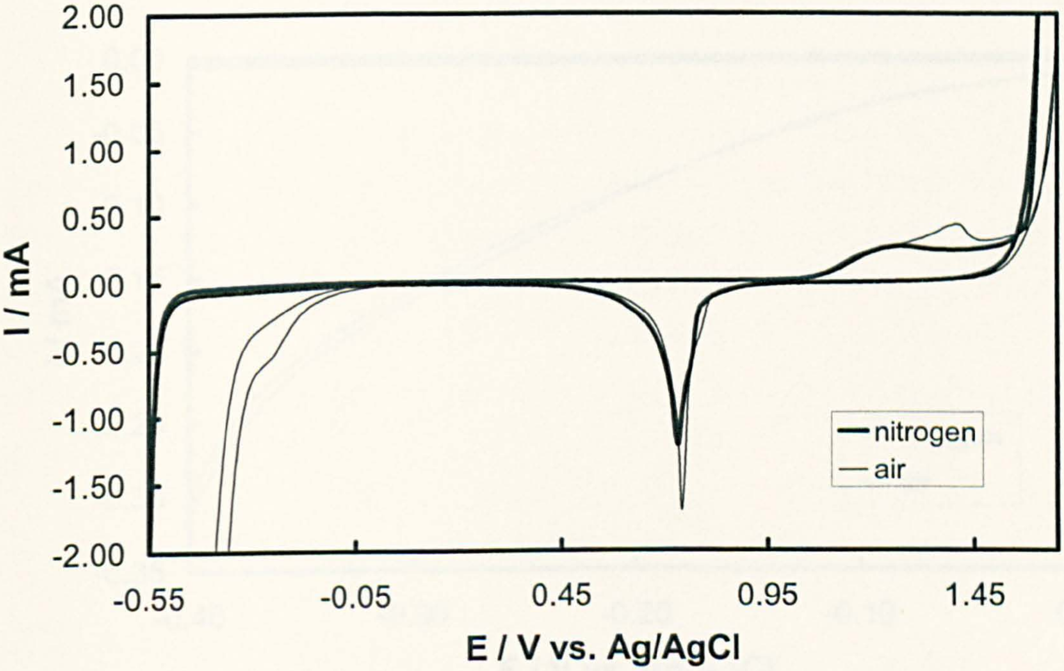

Figure 4.1 Voltammograms recorded at 50 mV/s in 60% RH nitrogen (thick line curve) and air (thin line curve) streams at a three-electrode Au (vs. Ag/AgCl)/Nafion®/Au sandwich device with a gold layer thickness of 1500 nm.

Figure 4.2 presents the slow scan voltammograms (at 5 mV/s) in air and nitrogen gas streams at 60% RH. An ill-defined plateau at ca. –0.35 V can be still seen in the oxygen reduction voltammogram. This feature is more prominent and the current corresponding to it is lower (ca. –0.20 mA at –0.35 V) than those recorded at 50 mV/s (ca. –0.70 mA at –0.30 V). This can be due to the characteristics of planar semi-infinite diffusion in the metal layers, which predict a peak-shaped voltammogram and higher currents at high scan rates and an S-shaped voltammogram and lower currents as a diffusional steady state is approached. (Note that the ratio of currents is 0.70/0.2=3.5, comparable to the square root of the ratio of the corresponding scan rates which is $(50/5)^{1/2}=10^{1/2}=3.3$).

It can also be seen that the oxygen reduction voltammograms are shifted in the sandwich-type sensor positive with respect to those obtained at the all-planar sensors of Chapter 3.

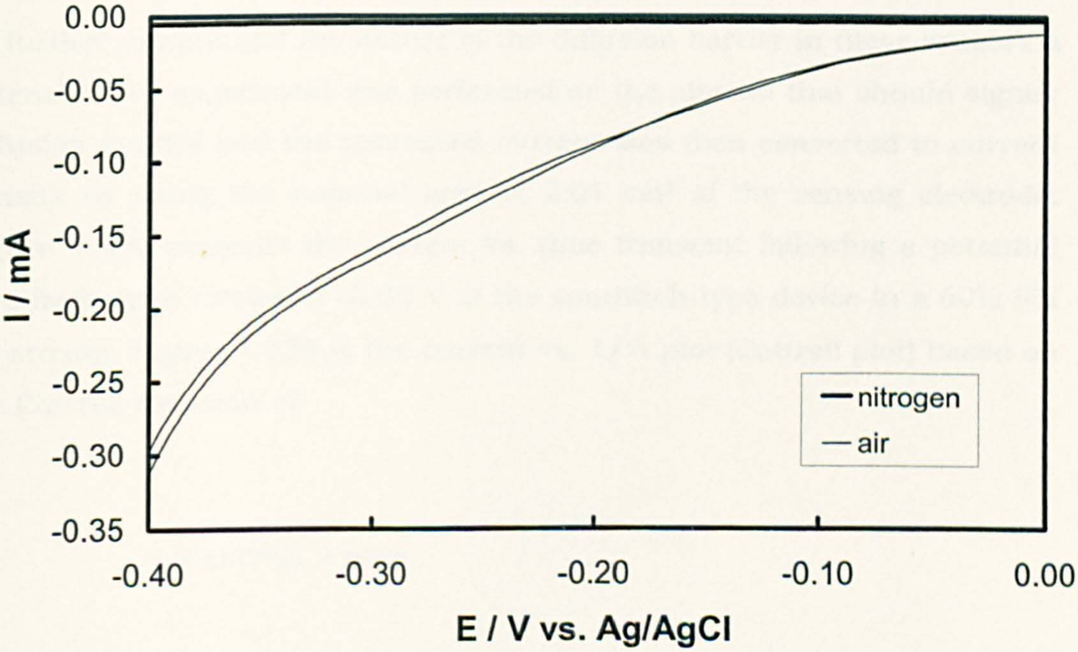

Figure 4.2 Voltammograms recorded at 5 mV/s in 60% RH nitrogen (thick line curve) and air (thin line curve) streams at a three-electrode Au (vs. Ag/AgCl)/Nafion®/Au sandwich device with a gold layer thickness of 1500 nm.

This again is expected for a highly irreversible reaction like oxygen reduction: as the mass transfer rate increases, in the absence of a significant mass transfer barrier at gold all-planar devices, the kinetic control potential range is extended and the voltammogram is shifted to more negative potentials. Finally, the fact that the observed oxygen reduction currents for the sandwich-type sensor are of similar magnitude (if not higher) than those at the open all-planar sensor, is probably due to the fact that the mass transfer limitations introduced in the former case are offset by the increase in electroactive surface area since the sandwich electrode arrangement ensures a more uniform current distribution and a complete utilisation of the entire electrode layer (see also below).

It has therefore been confirmed that with sandwich-type sensors the gas has to diffuse through the electrode layer to the electrode/electrolyte interface.

To further understand the nature of the diffusion barrier in these sensors a potential step experiment was performed on the plateau that should signify diffusion control and the measured current was then converted to current density by using the nominal area of 2.01 cm^2 of the sensing electrode. Figure 4.3(A) presents the current vs. time transient following a potential step from open circuit to –0.35 V at the sandwich-type device in a 60% RH air stream. Figure 4.3(B) is the current vs. $1/\sqrt{t}$ plot (Cottrell plot) based on the Cottrell equation of

$$j = nFD^{½}c_R \ / \ \pi^{½}t^{½}$$

from the slope of which an apparent value for the product of $D^{½}c_R$ can be estimated; a value of ca $2x10^{-8}$ mol cm^{-2} $s^{-1/2}$ has thus been calculated. For oxygen diffusion in water ($D = 2 \times 10^{-5}$ cm^2/s, $c = 2.5 \times 10^{-7}$ mol/cm^3) and air ($D = 0.14$ cm^2/s, $c = 9 \times 10^{-6}$ mol/cm^3) using data from CRC handbook of Chemistry and Physics this product is estimated as $1.1*10^{-9}$ mol cm^{-2} $s^{-1/2}$ and $3.4*10^{-6}$ mol cm^{-2} $s^{-1/2}$ respectively.

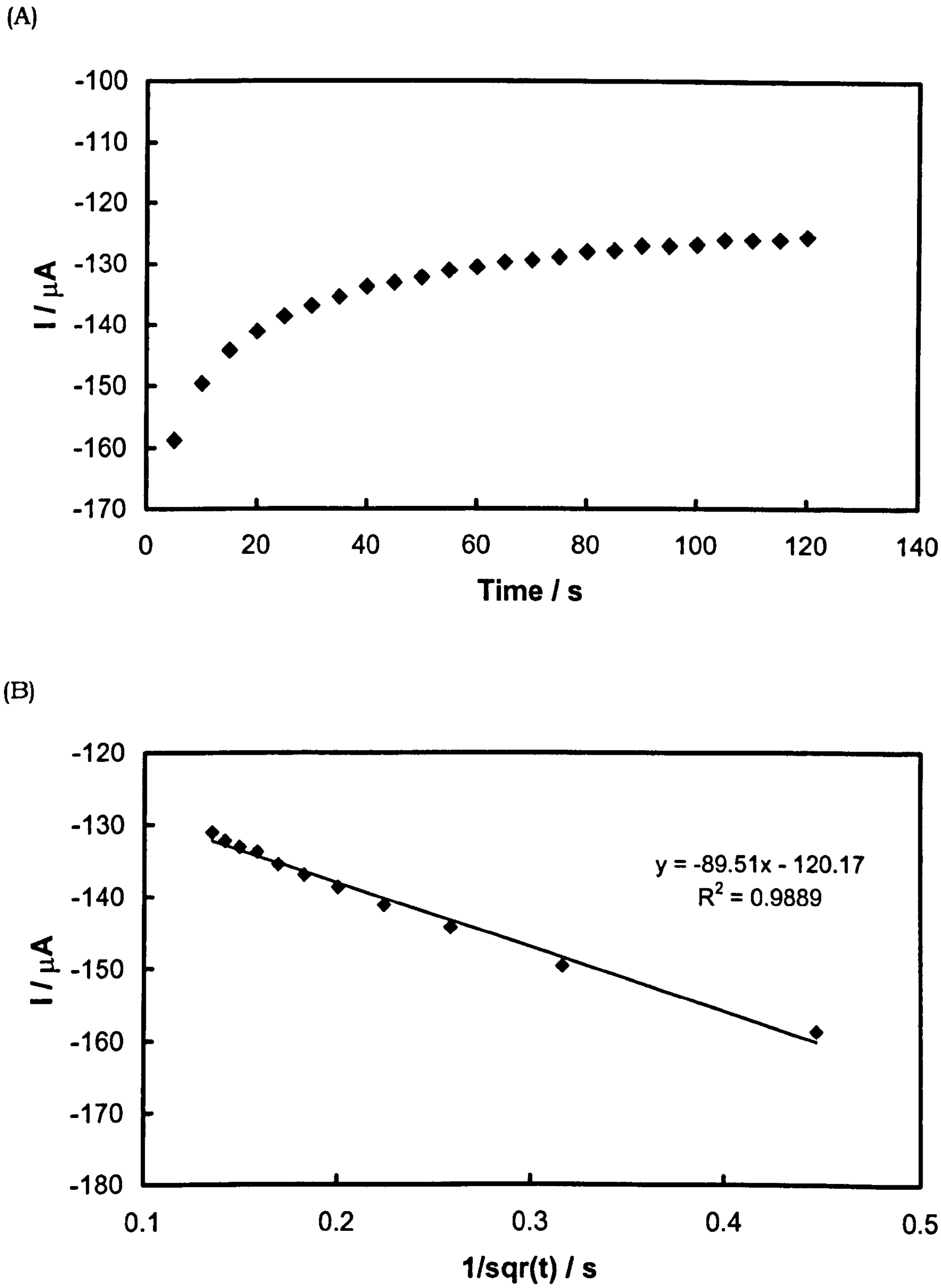

Figure 4.3 (A) The current vs. time transient of potential step experiment at the sandwich-type device in a 60% RH air stream. (B) The current vs. $1/\sqrt{t}$ plot of the same experiment

From the experiments by Sakai et al. (1986) the product for oxygen diffusion in water-saturated Nafion® can be calculated as $9.8*10^{-8}$ mol cm^{-2} $s^{-1/2}$. The above result in the case of the sandwich-type sensor, although not conclusive since the diffusion coefficient thus calculated assumes a homogeneous diffusion barrier without accounting for microporosity, tortuosity etc., rules out a high macro-porosity of the gold film as the value should in that case be close to the product for air. However, a fully continuous film also has to be ruled out as oxygen diffusion and concentration is very small in metals and therefore the product should then be smaller than that of water or Nafion® and not between those, as it has been found.

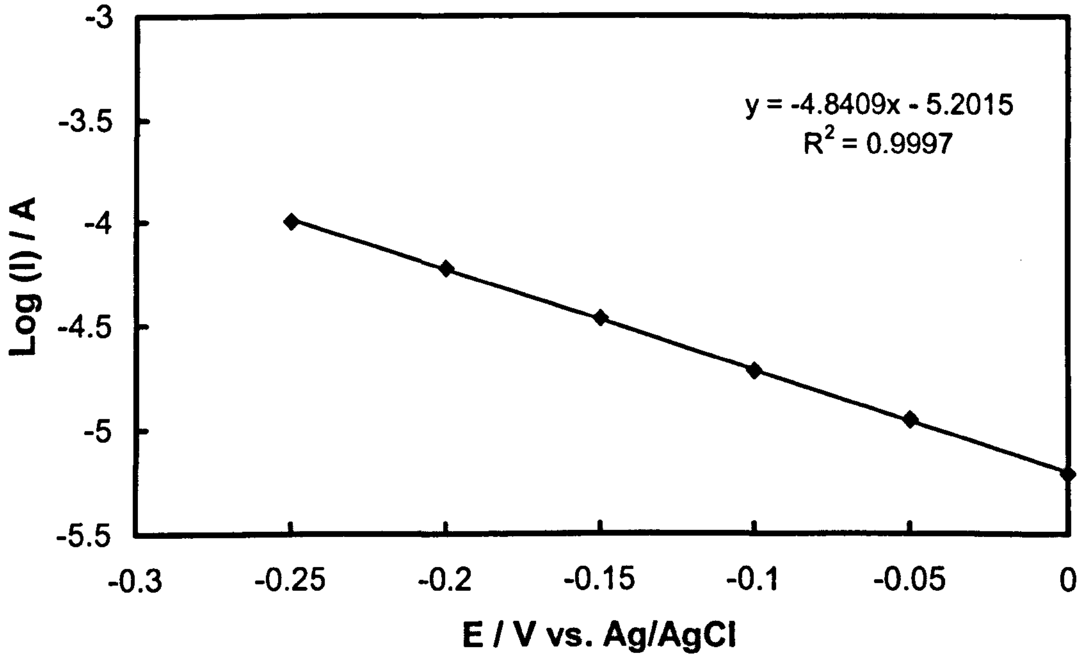

Figure 4.4 Mass transfer corrected Tafel plots for oxygen reduction on a Au (vs. Ag/AgCl)/Nafion®/Au sandwich device in 60% relative humidity

In another set of experiments, near-steady state current data for Tafel analysis were collected at the end of potential steps from open circuit potential to the potential of interest. These values were corrected for possible mass transfer effects (i.e. transformed to purely kinetic currents) using the value of the mass transfer limiting current obtained from slow scan voltammetry (e.g. 0.2 mA for 60% RH in air, see Figure 4.2 above). (For the details of calculating kinetic currents for mass transfer corrected Tafel plots please see Chapter 3 p.92 and 101). Figure 4.4 above shows the mass transfer corrected Tafel plot for oxygen reduction at a sandwich sensor in a 60% RH air stream. The Tafel slope thus estimated is 206 mV/decade i.e. higher than the one reported for aqueous acid solutions (see also discussion in Chapter 3 p.p. 96 and below).

The sandwich-type devices were tested in the entire 20-100% RH range. Figure 4.5 (A) below shows their voltammetry in air streams of varied humidity at a 50 mV/s scan rate whereas Figure 4.5 (B) and its inset their voltammetry at 5 mV/s.

(A)

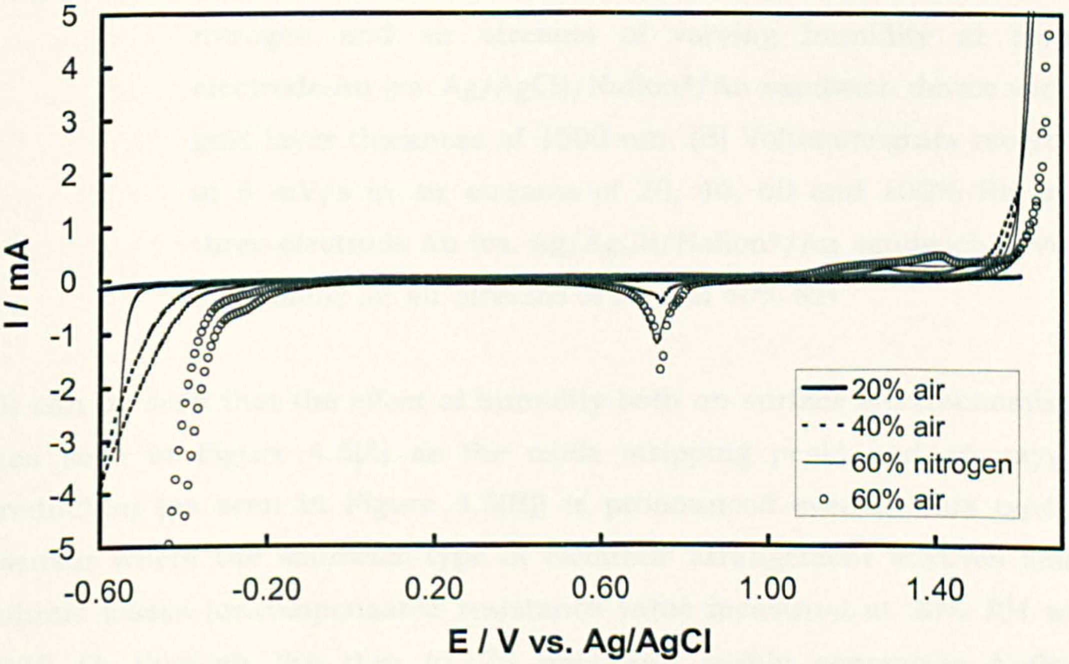

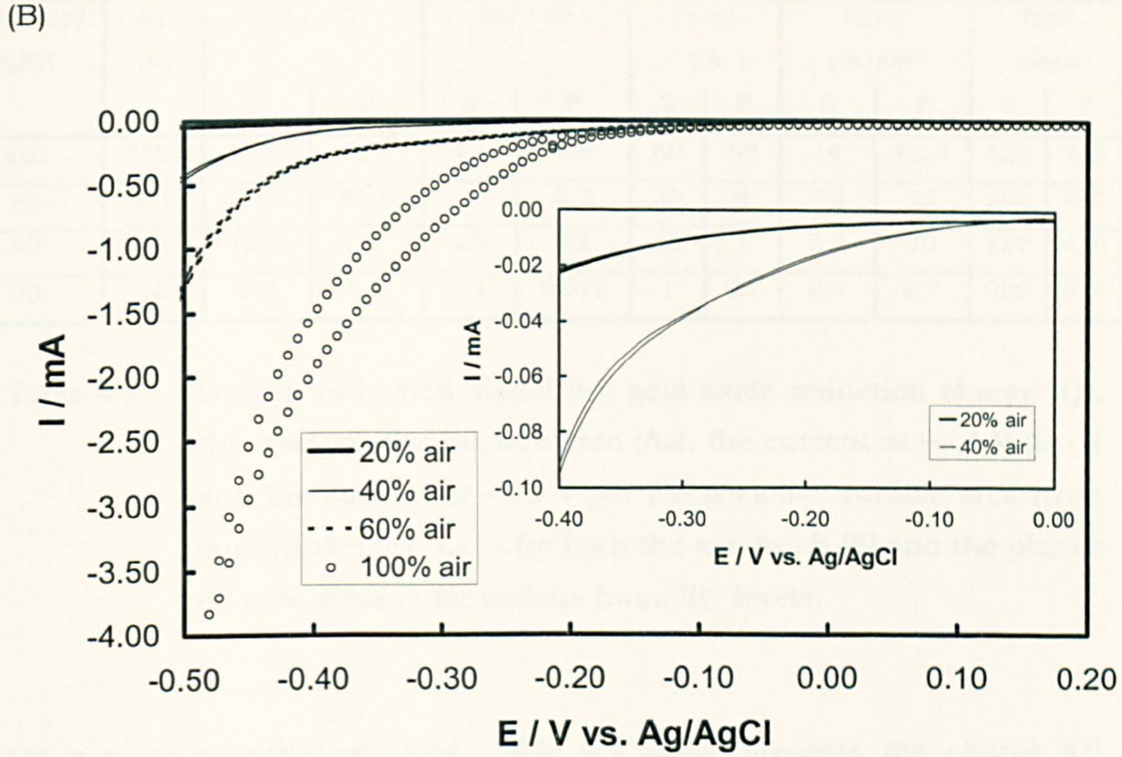

Figure 4.5 (A) Voltammograms recorded at 50 mV/s in water saturated nitrogen and air streams of varying humidity at three-electrode Au (vs. Ag/AgCl)/Nafion®/Au sandwich device with a gold layer thickness of 1500 nm. (B) Voltammogram recorded at 5 mV/s in air streams of 20, 40, 60 and 100% RH at a three-electrode Au (vs. Ag/AgCl)/Nafion®/Au sandwich device. Inset same for air streams of 20 and 40% RH

It can be seen that the effect of humidity both on surface electrochemistry (as seen in Figure 4.5(A) as the oxide stripping peak) and on oxygen reduction (as seen in Figure 4.5(B)) is pronounced even in this type of sensor where the sandwich-type of electrode arrangement ensures small ohmic losses (uncompensated resistance value measured at 20% RH was 320 Ω) through the thin (0.175 mm) and highly contacting Nafion® membrane.

Humidity/ %RH	I_L/ μA	Q / μC		A_{el}/ cm²		$I_{-0.1V}$/ μA		$i_{-0.1V}$/ μA/cm²		Tafel slope	
		S	P	S	P	S	P	S	P	S	P
100	2500	1800	319	4.3	0.8	60	50	14	62.5	129	243
60	210	1700	83.6	4	0.2	30	5	7.5	25	206	467
40	60	1200	39	2.9	0.1	10	1	3.5	10	187	428
20	20	450	5.8	1.1	0.015	1	0.1	0.9	6.7	280	524

Table 4.1 Oxygen reduction signal (I_L), gold oxide reduction charge (Q), the electroactive surface area (A_{el}), the current at –0.1 V ($I_{-0.1V}$) and the current at –0.1 V per electroactive surface area (true current density, $i_{-0.1V}$) for both the sandwich (S) and the planar (P) type sensors for various humidity levels.

On a more quantitative basis, Table 4.1 above presents the charge (Q) corresponding to gold oxide stripping (indicative of electroactive surface area), the electroactive surface area (A_{el}), the current at –0.1 V ($I_{-0.1V}$) and the current at –0.1 V per electroactive surface area (true current density, $i_{-0.1V}$), both for the sandwich-type sensor of Figures 4.5 above (nominal area of 2.01 cm²) and of an all-planar sensor (nominal area of 0.6 cm²), for various humidity levels. For the sandwich-type sensor, the near-limiting current values in the –0.3 to -0.4 V region are also given.

Three points can be made on the results of Table 4.1. First, as it has already been discussed for the planar arrangement in Chapter 3, for both sensors the effect of humidity is more pronounced (especially at high relative humidity values) on the oxygen reduction current ($I_{-0.1}$ and I_L) than on the stripping charge-electroactive surface area (Q-A_{el}), indicating that the effect of water content on oxygen reduction is not merely a gold active site number effect but also due to its influence on reaction kinetics at the Au/Nafion® interface.

Second, the electroactive surface area of the sandwich-type device is generally higher than that of the planar device (after correcting for the 2.01

$cm^2/0.6\ cm^2$ ratio of their nominal working electrode area). This is another indication that, assuming a similar gold layer roughness factor and due to current distribution and ohmic loss considerations, in the planar arrangement some part of the working electrode layer lying far away of the counter electrode, does not contribute much to the observed current. This fact, together with the presence of a much thicker mass transfer barrier in the case of the sandwich arrangement (resulting in partially mixed control at –0.1 V and signs of some current mass transfer limitations) leads to lower current densities at the sandwich sensor.

Third, for both sensors the Tafel-slope values obtained are strongly affected by the humidity, confirming once again that the latter affects the kinetics of oxygen reduction at the Au/Nafion® interface. The higher values observed for the planar sensor may be due to the higher current densities in the corresponding Tafel plots. As it has already been discussed in Section 3.4.2 of Chapter 3, Tafel values higher (double or quadruple) than 120 mV/dec have been reported for oxygen reduction at Pt/Nafion® interfaces and are predicted to depend on humidity (Sena et al. 1999, Jaouen et al. 2002, Ihonen et al. 2002). Hence, the humidity effect is conclusively proven to be due to changes of Au/Nafion® active site number and (mainly)/or catalytic activity with changing water content.

Finally, the response of the sandwich-type sensor to oxygen concentration steps is shown in the current (at -0.25 V) vs. time curves presented for 100% RH and 40% RH gas streams in Figures 4.6(A) and 4.6(B) respectively. The insets in these Figures show the current vs. oxygen concentration calibration plots. Reasonable linearity and detection limits less than 1 % v/v were observed.

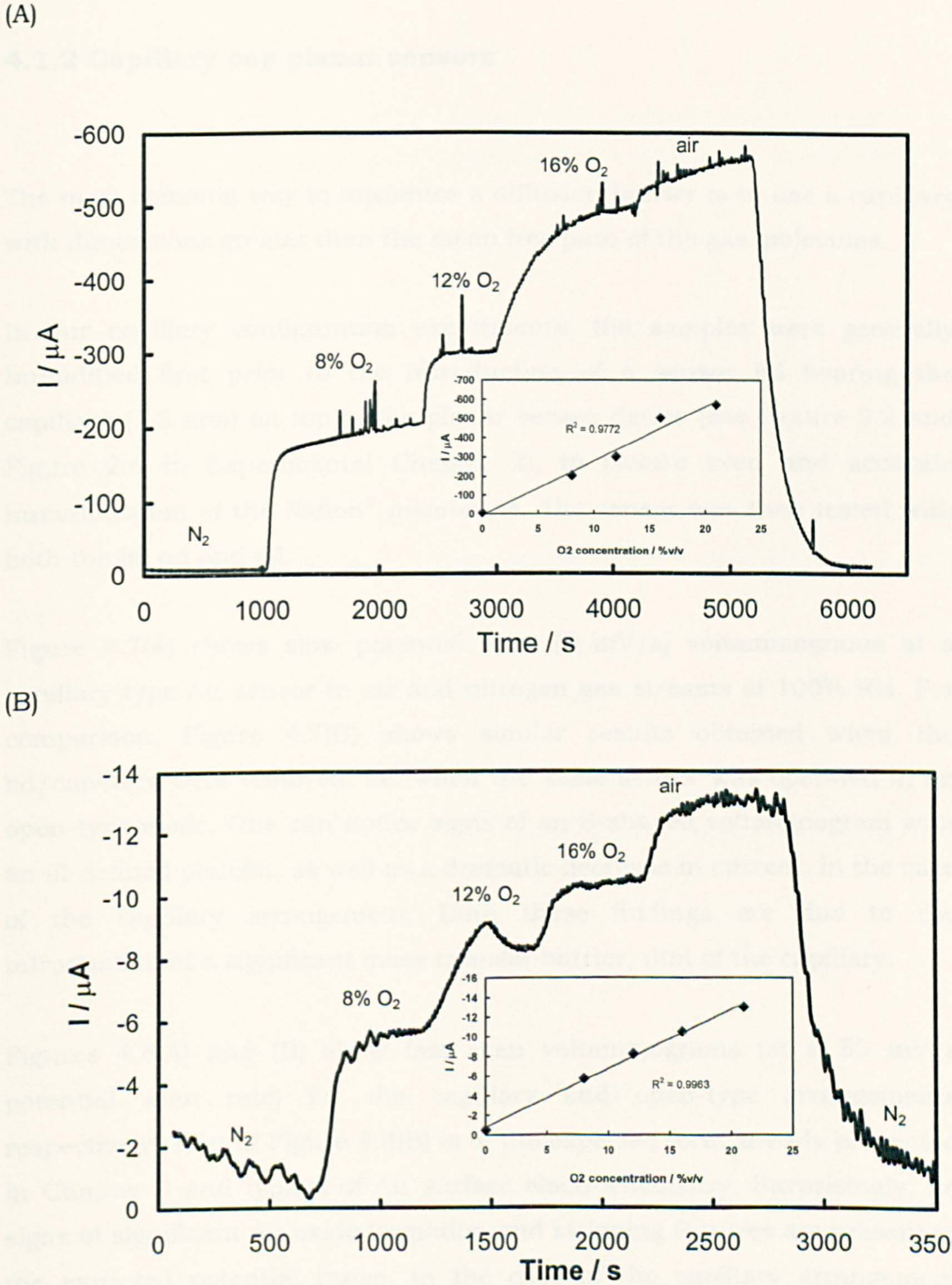

Figure 4.6 Current-time response of the Au (vs. Ag/AgCl)/Nafion®/Au sandwich sensor to oxygen concentration steps at (A) 100% and (B) 40% RH gas samples. The working electrode was held at –0.25 V vs. Ag/AgCl. *Insets:* Variation of the background corrected current with oxygen concentration

4.1.2 Capillary cap planar sensors

The most common way to introduce a diffusion barrier is to use a capillary with dimensions greater than the mean free path of the gas molecules.

In our capillary configuration experiments, the samples were generally humidified first prior to the introduction of a sensor lid bearing the capillary (1.5 mm) on top of the planar sensor device (see Picture 2.2 and Figure 2.4 in Experimental Chapter 2), to ensure even and accurate humidification of the Nafion® membrane. The sensor was then tested with both the lid on and off.

Figure 4.7(A) shows slow potential scan (5 mV/s) voltammograms at a capillary-type Au sensor in air and nitrogen gas streams of 100% RH. For comparison, Figure 4.7(B) shows similar results obtained when the lid/capillary were removed, i.e. when the same sensor was operated in an open-type mode. One can notice signs of an S-shaped voltammogram with an ill-defined plateau, as well as a dramatic decrease in current, in the case of the capillary arrangement. Both these findings are due to the introduction of a significant mass transfer barrier, that of the capillary.

Figures 4.8(A) and (B) show fast scan voltammograms (at a 50 mV/s potential scan rate) for the capillary and open-type arrangements respectively. That of Figure 4.8(B) is of the expected form already presented in Chapter 3 and typical of Au surface electrochemistry. Surprisingly, no signs of significant Au oxide formation and stripping features are present in the expected potential range, in the case of the capillary arrangement (Figure 4.8(A)). Traces only of a Au oxide stripping peak can be seen around +0.3 V in the zoom-into curve of the Inset of Figure 4.8(A). (The current plateau at potentials more negative than –0.6 V will be discussed later).

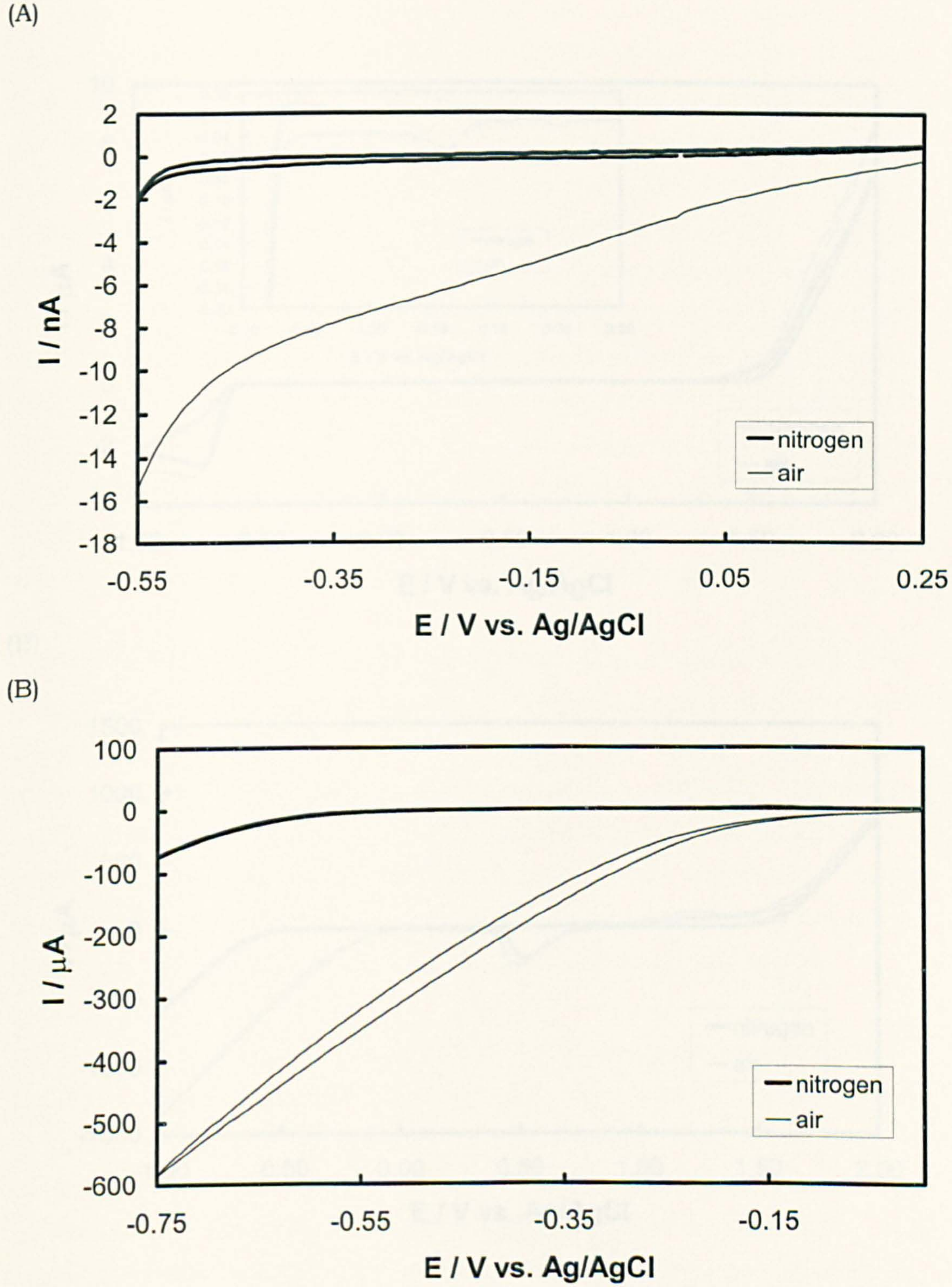

Figure 4.7 Slow scan voltammograms (at a 5 mV/s potential scan rate) for (A) the capillary and (B) open-type arrangements of Au (vs. Ag/AgCl)/Nafion®/Au sensor in air and nitrogen gas streams of 100% RH

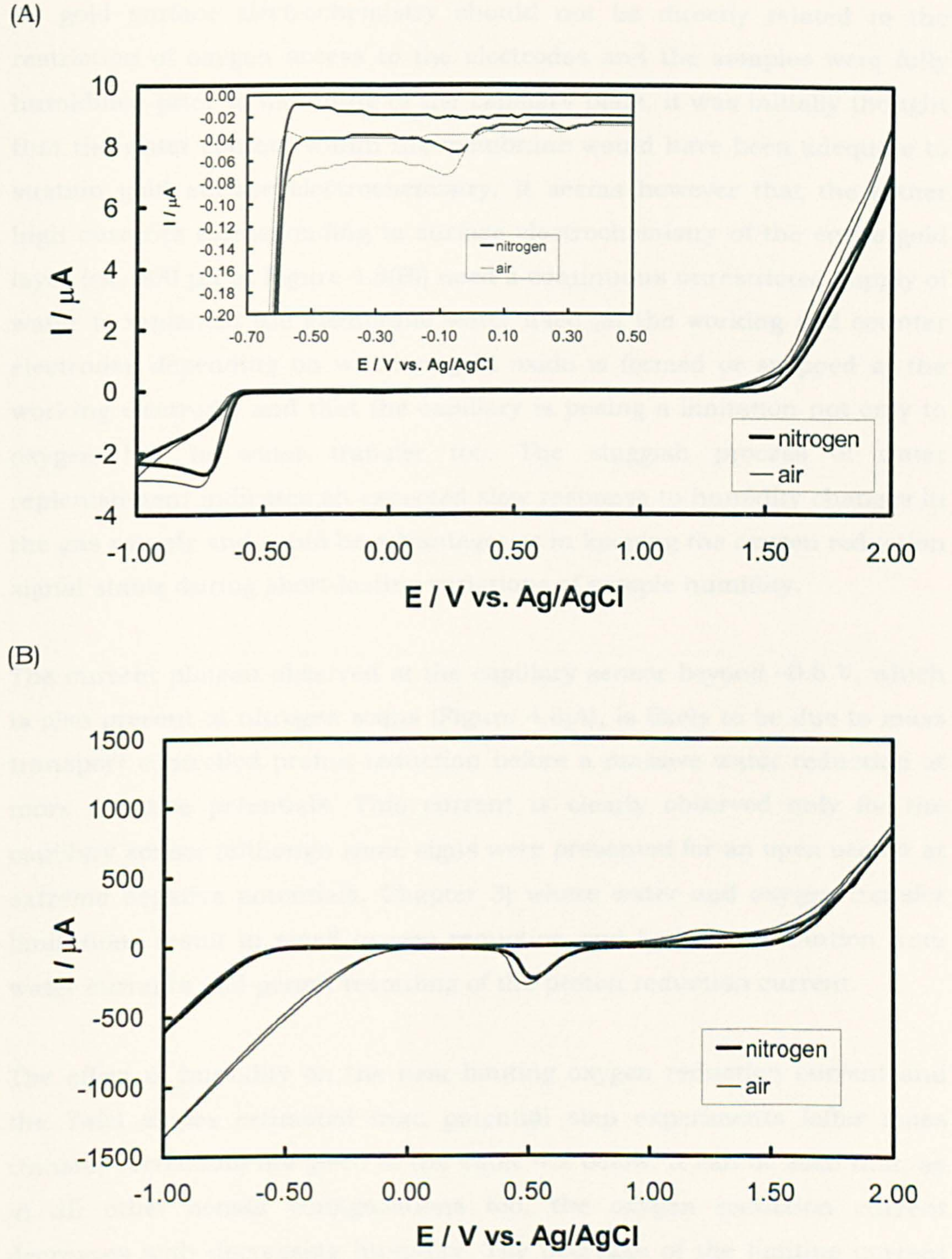

Figure 4.8 Fast scan voltammograms (at a 50 mV/s potential scan rate) for (A) the capillary (Inset: Zoom into oxide stripping region) and (B) open-type arrangements of Au (vs. Ag/AgCl)/Nafion®/Au sensor in air and nitrogen gas streams of 100% RH

As gold surface electrochemistry should not be directly related to the restriction of oxygen access to the electrodes and the samples were fully humidified prior to mounting of the capillary plate, it was initially thought that the water content within the membrane would have been adequate to sustain gold surface electrochemistry. It seems however that the rather high currents corresponding to surface electrochemistry of the entire gold layer (ca. 200 µA in Figure 4.8(B)) need a continuous unrestricted supply of water to replenish the membrane water used (at the working and counter electrodes depending on whether gold oxide is formed or stripped at the working electrode) and that the capillary is posing a limitation not only to oxygen but to water transfer too. The sluggish process of water replenishment indicates an expected slow response to humidity changes in the gas sample and could be advantageous in keeping the oxygen reduction signal stable during short-lasting variations of sample humidity.

The current plateau observed at the capillary sensor beyond -0.6 V, which is also present at nitrogen scans (Figure 4.8(A), is likely to be due to mass transport controlled proton reduction before a massive water reduction at more negative potentials. This current is clearly observed only for the capillary sensor (although some signs were presented for an open sensor at extreme negative potentials, Chapter 3) where water and oxygen transfer limitations result in small oxygen reduction and hydrogen evolution from water currents and permit recording of the proton reduction current.

The effect of humidity on the near-limiting oxygen reduction current and the Tafel slopes estimated from potential step experiments (after mass transfer correction) are given in the Table 4.2 below. It can be seen that, as in all other sensor configurations too, the oxygen reduction current decreases with decreasing humidity. The decrease of the limiting current can only be attributed to a decrease in the electroactive electrode area due to a decrease in active-hydrated Au/Nafion® sites. However, an interesting difference of the capillary-type sensor from both the planar and sandwich-type ones is that the Tafel slope does not seem to vary significantly (within experimental uncertainties) with humidity, indicating a different operative mechanism at the low currents encountered at this type of sensor.

Humidity / %RH	Limiting current / nA	Tafel slope / (mV/dec)
100	10	195
40	2.9	155
20	0.5	182

Table 4.2 Limiting currents and Tafel slopes measured with capillary type sensor for various humidity levels

Finally, Figure 4.9 below shows the variation of current with time during oxygen concentration steps at a capillary-type sensor with the Au WE held at –0.05 V vs. a Ag/AgCl strip reference electrode.

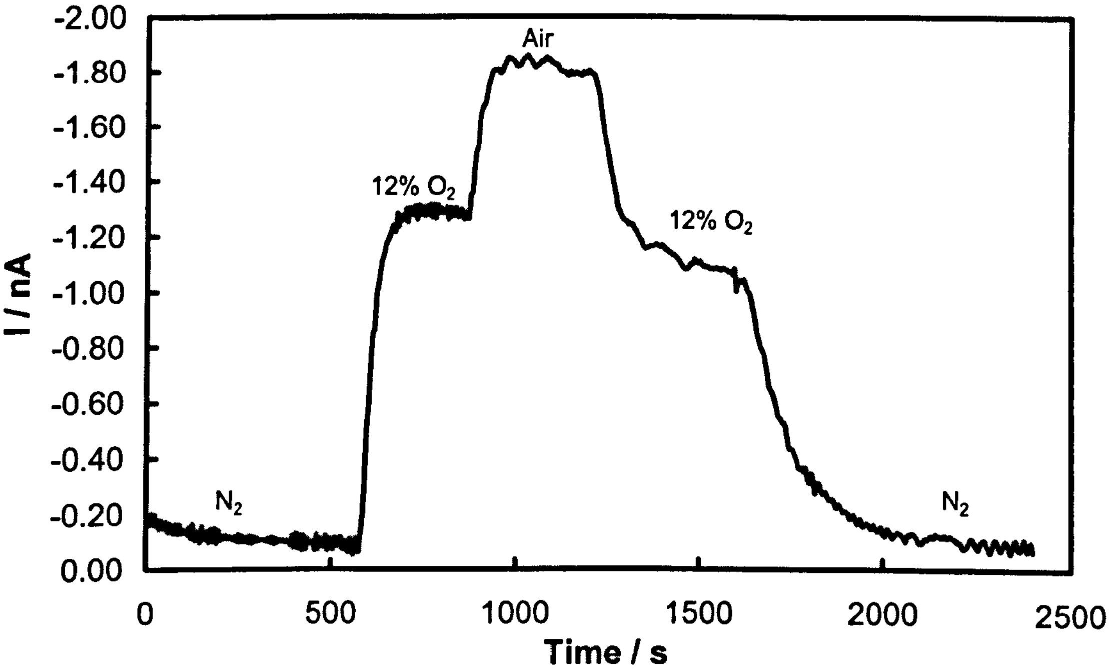

Figure 4.9 Current-time response of the Au (vs. Ag/AgCl)/Nafion®/Au capillary sensor to oxygen concentration steps at 100% RH gas samples. The working electrode was held at –0.05 V vs. Ag/AgCl.

The estimated response time T_{90} of the capillary sensor of 55 s is equivalent of that measured with the planar three-electrode device (65 s). The rather high response times obtained with both devices should be due to the dead volumes of our gas tubing, humidification vessel and test cell as the T_{90} of commercial fuel-cell type CiTiceL® sensor (City Technology Ltd) placed in the test cell simultaneously with the planar device was 60 s (specification of the sensor reports $T_{95} \leq 10$ s). (See Figure 3.16 and discussion). For the sandwich sensor the response time nearly doubled to 125 s as the gas has to diffuse through the electrode layer to the electrode/electrolyte interface.

4.2 Other solid electrolyte materials

4.2.1 Polybenzimidazole polymer electrolyte.

Acid-doped polybenzimidazole (PBI) is a recently introduced polymer electrolyte (Weng et al. 1996) which is an attractive alternative to Nafion® for use in fuel cells (Wang et al. [1] 1996, Wang et al. [2] 1996) since it exhibits good conductivity at temperatures up to 200°C, almost zero electrosmotic drag (Wang et al. [1] 1996) and limited methanol crossover (Wang et al. [2] 1996). The electrochemistry of oxygen at the Pt/PBI interface has been studied (Zecevic et al. 1997) but there is only a single report on its use in potentiometric sandwich-type sensors for hydrogen and oxygen (Bouchet et al. 1997). Therefore, the use of PBI as the electrolyte in the new sensor arrangement would be in line with the trend in sensor technology to use materials developed for the fuel cell industry (Hobbs et al. 1991). The material can also be used to prove the general applicability of the planar sensor design concept and, more importantly, it is useful to investigate whether PBI reduces the strong humidity effects on sensor behaviour that were observed at Nafion®-based devices (Hodgson et al. 1998).

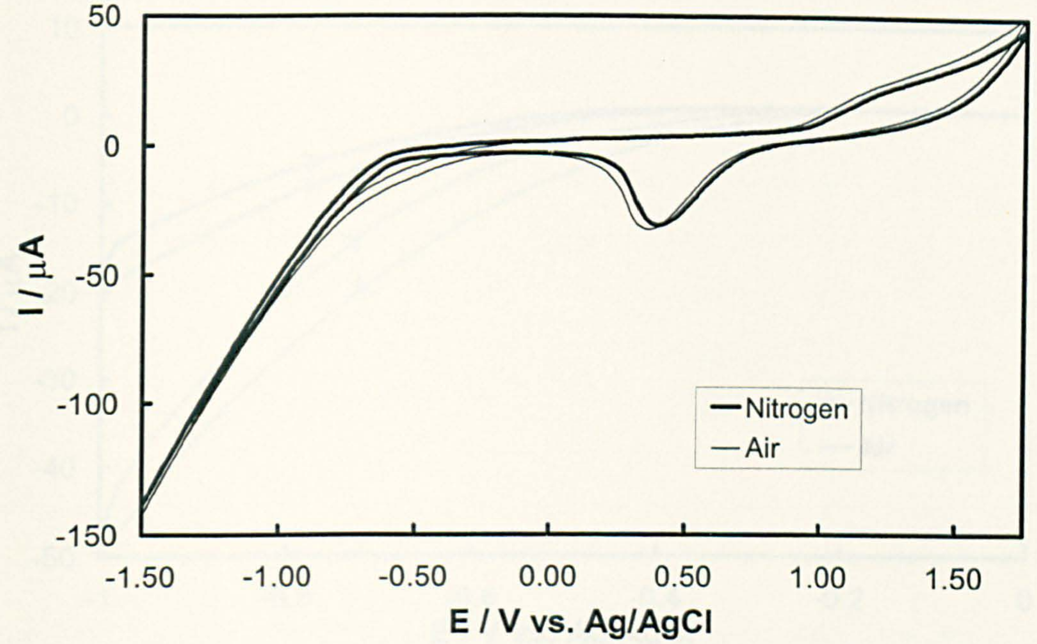

Figure 4.10 Voltammogram recorded at 50 mV/s in water saturated nitrogen and air streams at a three-electrode Au (vs. Ag/AgCl)/PBI/Au planar device

Figure 4.10 shows a cyclic voltammograms recorded at 50 mV/s in water-saturated nitrogen and air streams, with Au (vs. Ag/AgCl)/PBI/Au assembly, while Figure 4.11 shows the slow (at 5 mV/s) potential-sweep voltammogram of oxygen reduction from water-saturated atmospheres. As with Nafion®-based devices, the Au/PBI interface was characterised by well-defined gold electrochemistry but the oxygen reduction (distinguished in the –0.40 to –1.00 V range from the background response in nitrogen) is now closer to the hydrogen evolution reaction in the extremely acidic environment of 11-M phosphoric acid-doped PBI. Once again, the oxygen reduction voltammogram shows no indications for a significant mass transport barrier, which could be explained by the reaction taking place at the Au/PBI/gas line interface and/or through a very thin (when compared to the oxygen reduction kinetics on gold) mass transfer barrier.

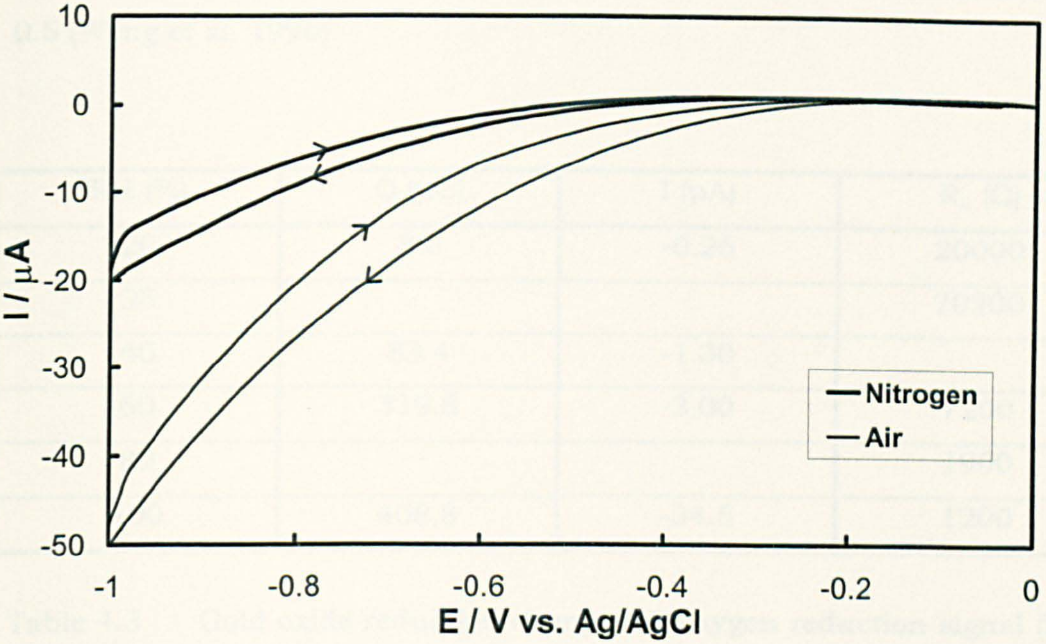

Figure 4.11 Voltammogram recorded at 5 mV/s in water saturated nitrogen and air streams at a three-electrode Au (vs. Ag/AgCl)/PBI/Au planar device

We have studied the behaviour of the Au/Nafion®/Au and Au/PBI/Au devices with respect to both gold surface electrochemistry and oxygen reduction in water-saturated samples of varied relative humidity (RH) in the 15-85 % RH range. The results of a systematic study of the effect of gas relative humidity on uncompensated membrane resistance, the charge corresponding to gold oxide stripping and the oxygen reduction current at a given potential (taken from the slow voltammograms) are all shown in Table 4.3.

The lower values of uncompensated resistance (R_u) for PBI (when compared to those for Nafion®, see Chapter 3) at very low humidity levels (18% RH) which stay constant up to 36% RH are in line with the views that there are additional proton conduction mechanisms in PBI (less dependent on water (Weng et al. 1996)) and the finding that PBI-based fuel cells can operate in a satisfactory manner even at low gas humidification conditions (Wang et al. [1] 1996). The number of water molecules per PBI repeat unit is also reported to increase from 1 to 3 as the water activity increases from 0.1 to 0.5 (Weng et al. 1996).

RH (%)	Q (μC)	I (μA)	R_u (Ω)
20	8.6	-0.26	20000
35			20200
40	83.4	-1.30	
60	319.8	-3.00	7200
80			1900
100	408.8	-34.5	1200

Table 4.3 Gold oxide reduction charge (Q), oxygen reduction signal (I) at –0.5V vs. Ag/AgCl and uncompensated resistance (R_u) in air streams of varied RH for three-electrode Au (vs.Ag/AgCl)/PBI/Au planar device.

As with Nafion® samples in Chapter 3, we normalized the oxygen reduction currents with respect to the corresponding gold oxide stripping charges using values given in Table 4.3. This was done by first translating the charge values into gold electroactive surface areas (based on the 420 μC/cm^2 reported for a AuO monolayer on smooth gold (Capon & Parsons 1972, Kita & Nakajima 1986, Amadelli et al. 1992)) and then converting the currents into current densities (current per electroactive surface area). Figure 4.12 presents the variation of these current densities with relative humidity. It can be seen that, within the experimental uncertainties involved in calculating electroactive surface areas from repetitive cyclic voltammetry, the current density for PBI-based devices (as for Nafion® ones too, see Figure 3.24 in Chapter 3) varies little with humidity at relative humidity less than ca. 60%, indicating that a mere decrease in the number of gold sites in contact with water can explain the variation of both surface electrochemistry and oxygen reduction in the 20-60% RH range. However, at higher humidity levels there is a sharp increase in the current density indicating higher oxygen reduction rates as the type of water in Nafion® changes from "strongly bound" to "free-bulk" water (Zawodzinski et al 1991).

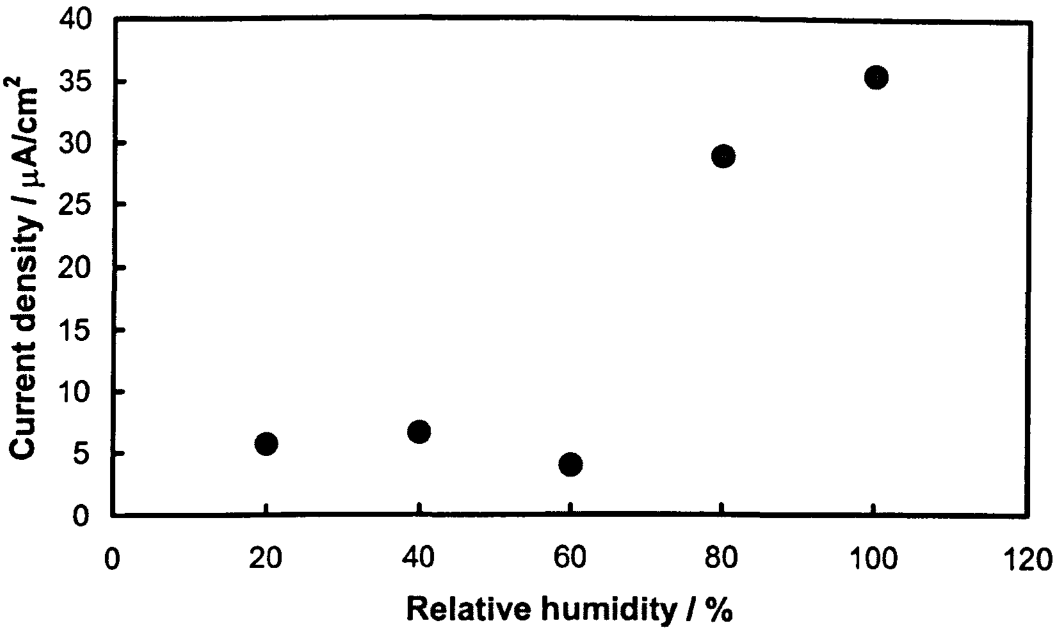

Figure 4.12 Variation of oxygen reduction current density with relative humidity of air streams for a three-electrode Au (vs. Ag/AgCl)/PBI/Au-planar device

4.2.2 β-Alumina

For the following experiments, commercial β/β"-alumina-discs were provided by Ionotec Ltd. The gold electrodes were deposited on the top of the disc by sputtering as was described in chapter 2.1.2 using mask for Device B (Experimental, Figure 2.3). The thickness of gold layers was kept at 360 nm. A strip of Ag-loaded paint served as the reference electrode.

The electrochemistry of β/β"-alumina devices was studied in gas streams of varying oxygen and humidity levels. The fast voltammograms recorded at 50 mV/s (Figure 4.13) contain unclear information with respect to oxygen determination since they are expected to reflect Au/alumina surface electrochemistry phenomena, capacitive charging and large ohmic losses. It is also not clear whether the large difference between the nitrogen and air voltammograms (nitrogen being the first set of curves recorded) is merely due to a continuous activation of the gold electrode as the number of scans and times of exposure at extreme potentials increases or whether the occurrence of oxygen reduction at negative potentials in air containing streams has a beneficial effect on the gold electrode activity.

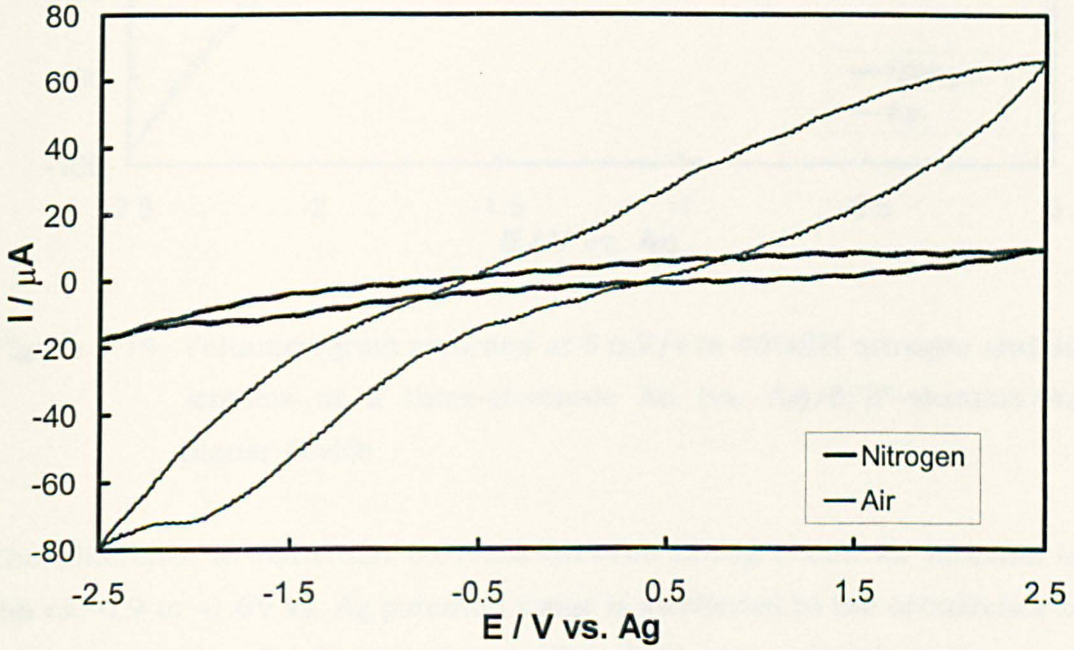

Figure 4.13 Voltammogram recorded at 50 mV/s in 40%RH nitrogen and air streams at a three-electrode Au (vs. Ag)/β/β"-alumina/Au planar device

The slow scan (5 mV/s) voltammogram of Figure 4.14 is much more promising for the use of alumina-based sensors for oxygen determination since it shows a clear difference between nitrogen and air streams at scan rates where the relative contribution of surface electrochemistry and capacitive currents is expected to be small and so is the effect of ohmic losses in the intermediate range potentials presented.

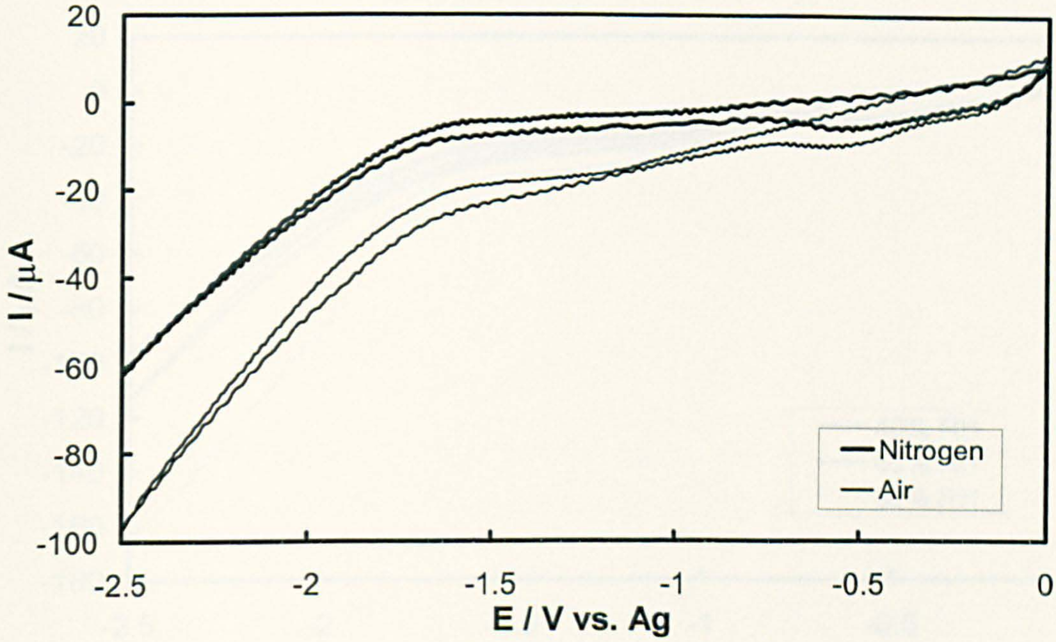

Figure 4.14 Voltammogram recorded at 5 mV/s in 40%RH nitrogen and air streams at a three-electrode Au (vs. Ag)/β/β"-alumina/Au planar device

The difference in reduction currents between nitrogen and air streams in the ca.-0.9 to –1.6V vs. Ag potential range is attributed to the occurrence of oxygen reduction. In the very few studies of alumina cathodic polarisation in the presence of oxygen that appear in literature (Armstrong et al. 1976, Staikov et al. 1990) the reduction of oxygen at Pt and Au/β"-alumina interfaces has already been reported at potentials less negative than the Na^+/Na cathodic deposition (in the absence of water). The further negative current rise beyond c.a. –1.7 V vs. Ag can be attributed to hydrogen evolution from the water adsorbed at the Au/alumina interface from the humidified gas stream. These higher currents are affected by IR drop as reflected in a gradual linearisation of the current-potential curve as the scan moves to extreme negative potentials and higher negative currents. The positive currents at potentials more positive than –0.75 V during positive going scan are likely to reflect traces of gold oxide formation which are stripped off during the reverse scan resulting in a negative current "hump" around –0.7 V.

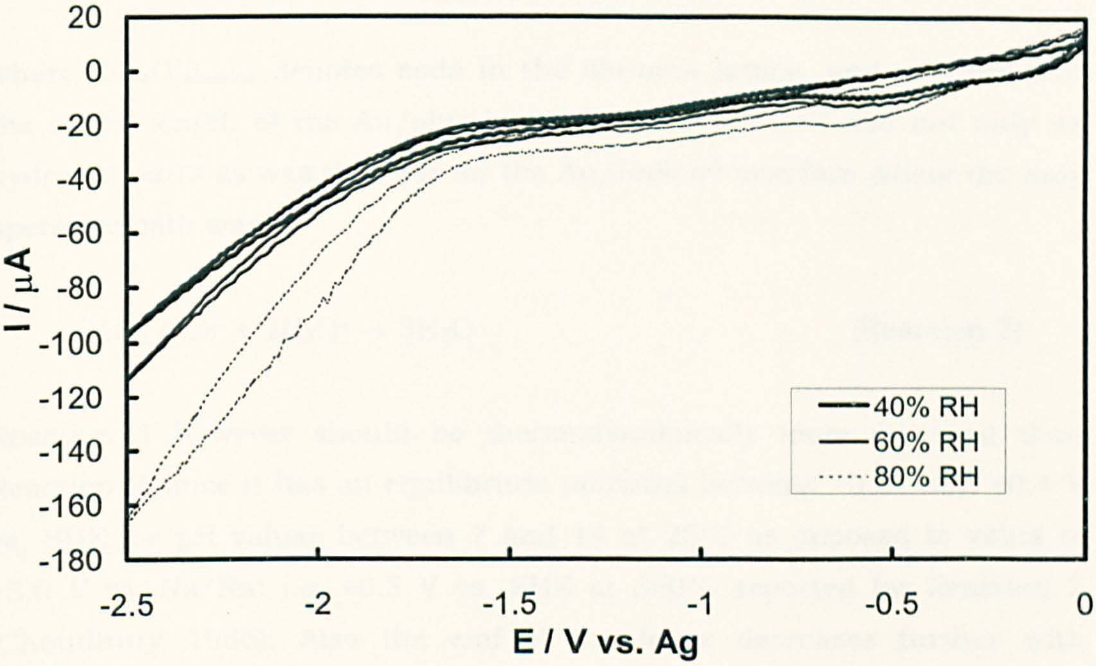

Figure 4.15 Voltammogram recorded at 5 mV/s in air streams of various humidity levels at a three-electrode Au (vs. Ag)/β/β"-alumina/Au planar device

Figure 4.15 shows the effect of different humidity levels in an air stream on the voltammograms recorded at alumina-based devices. There is an increase in the cathodic current attributed to oxygen reduction in the –0.9 to –1.6V range with increasing water content, but this is significantly smaller than the corresponding one for Nafion®-based devices. In fact there is very little humidity effect between 40% RH, which is near ambient conditions, and 60% RH. The moderate to limited increase of the oxygen current in the presence of water at alumina-based devices could be explained by the possibility of an additional oxygen reduction pathway to that of oxygen reduction at sites of adsorbed water along the Au/β/β"-alumina interface:

$\frac{1}{2}O_2 + 2e^- + H_2O \rightarrow 2OH^-$ (Reaction 1)

This additional pathway can be written as:

$\frac{1}{2}O_2 + 2e^- + 2Na^+ \rightarrow [Na_2O]_{\beta/\beta''\text{-alumina}}$ (Reaction 2)

where $[Na_2O]_{alumina}$ denotes soda in the alumina lattice, and ensures that the entire length of the Au/alumina interface is utilised and not only its hydrated parts as was the case for the Au/Nafion® interface where the only operative path was:

$\frac{1}{2}O_2 + 2e^- + 2H_3O^+ \rightarrow 3H_2O$ (Reaction 3)

Reaction 1 however should be thermodynamically more favoured than Reaction 2 since it has an equilibrium potential between +0.81 and +0.4 V vs, SHE for pH values between 7 and 14 at 25°C as opposed to value of +3.0 V vs. Na/Na^+ i.e. +0.5 V vs. SHE at 350°C reported for Reaction 2 (Choudhury 1986). Also the emf of the latter decreases further with decreasing temperature (Gaur & Sethi 1967). Reaction 2 will probably show slower kinetics too since it involves the incorporation of oxide ions into the alumina lattice and might include a nucleation overpotential. Hence an increase in the sites available for Reaction 1, by an increase in water content, slightly increases the oxygen reduction current.

Table 4.4 presents results for the uncompensated resistance (R_u) between the working and reference electrode of β/β"-alumina based devices. For comparison purposes, previous results for Nafion®-based devices are included to the table. The uncompensated resistance values measured by the current interrupt technique can only be used as an indicator of the sample surface conductivity. However the values can indicate the range of ohmic losses expected during oxygen reduction experiments and to identify qualitative trends between materials and humidity levels.

Humidity (%)	Nafion® IR interrupt (Ω)	β-Alumina IR interrupt (Ω)
20		8000
40	650	3000
60	450	
80	250	
100	200	5000

Table 4.4 Uncompensated resistance (R_u) measured by current interrupt and positive feedback techniques in air streams of varied RH for three-electrode Au (vs.Ag/AgCl)/Nafion®/Au and Au (vs. Ag)/β/β"-alumina/Au planar devices.

The results of Table 4.4 show that the uncompensated resistance for the Alumina-based devices is much higher than that of the Nafion®-based ones, but are less sensitive to humidity changes. The observations are in qualitative agreement with the value of Nafion® bulk conductivity in 100% RH of $4 - 8 * 10^{-2}$ ohm^{-1} cm^{-1} and that of Ionotec β/β"-alumina specified as $2 * 10^{-3}$ ohm^{-1} cm^{-1}. The findings are also in accordance with the Ionotec Ltd claim that the specific alumina formulation used in these experiments exhibits a limited dependence of conductivity on humidity.

Figure 4.16 presents slow voltammograms recorded at Au/alumina device in 80% RH streams of three different oxygen concentrations; 0% as nitrogen, 12% and 21% as air. The voltammograms depict a promising increase in the currents within the -0.9 to -1.6 V potential range with increasing oxygen content. The background corrected current at -1.5 V is 14 μA for 12% oxygen and 28 μA for 21% indicating a near-linear variation of the current with oxygen concentration.

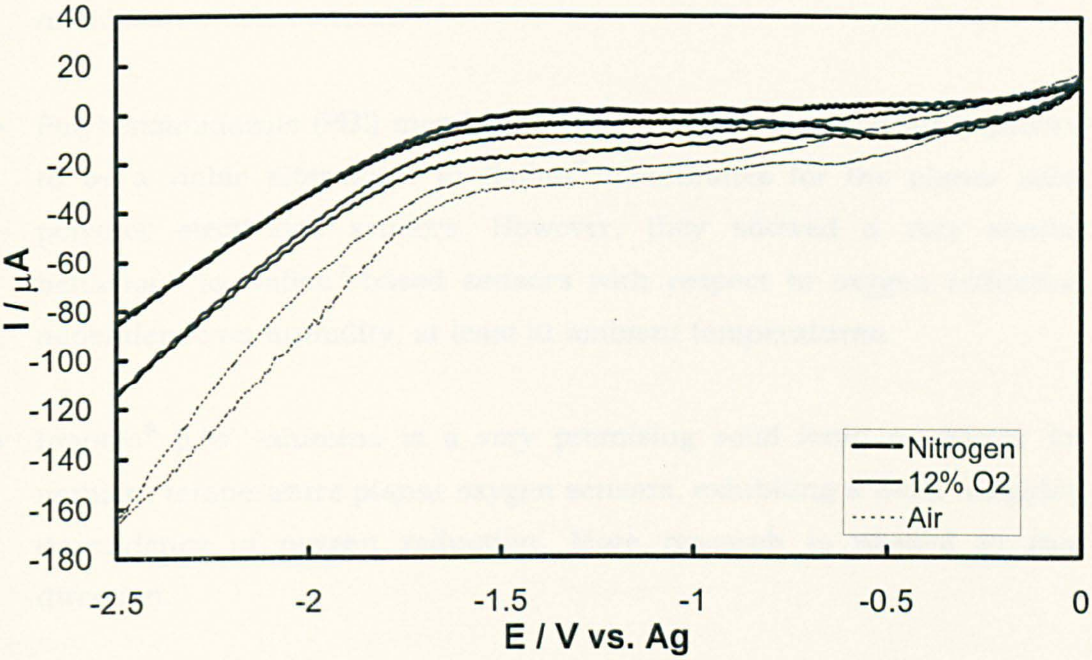

Figure 4.16 Voltammogram recorded at 5 mV/s at a three-electrode Au (vs. Ag)/β/β"-alumina/Au planar device in 80% RH streams of nitrogen, 12% oxygen and air.

4.3 Conclusions

- The use of a sandwich-type electrode arrangement or of a capillary bearing cap on top of the planar electrode arrangement, both introduced a significant mass transfer barrier and resulted in voltammograms showing limiting current signs.

- Despite the much lower ohmic losses encountered in these arrangements (due to a smaller inter-electrode gap or smaller currents), they both exhibited strong humidity dependence of their oxygen reduction signal, providing conclusive evidence that the effect of water on oxygen reduction at Nafion®-based solid polymer sensors is not an ohmic one. Nevertheless, the capillary-type sensor is expected to be less sensitive to humidity fluctuations in the sample, due to water vapour mass transfer limitations resulting in slower equilibration of the membrane water content.

- Polybenzimidazole (PBI) membranes fabricated in our laboratory proved to be a viable alternative to Nafion® membranes for the planar solid polymer electrolyte sensors. However, they showed a very similar behaviour to Nafion®-based sensors with respect to oxygen reduction dependence on humidity, at least at ambient temperatures.

- Ionotec® β/β''-alumina is a very promising solid ionic conductor for ambient temperature planar oxygen sensors, exhibiting a weak humidity dependence of oxygen reduction. More research is needed to that direction.

CHAPTER 5

Nafion® based methanol sensors

5.1 Introduction

The determination of dissolved methanol in a wide concentration range is essential for a variety of cases ranging from plant, foodstuff and drug trace analysis to monitoring industrial process streams and fuel cell feeds. The determination of methanol vapours in equilibrium with methanol solutions provides an alternative way to monitor methanol in many of the above applications.

Examples of analytical methods for dissolved methanol determination include spectrophotometry (Mangos & Haas 1996) with a detection limit of 10^{-3} M, fluorometry (where methanol is derivatised) (Wojciechowski & Fall 1996) with a higher detection limit and GC/MS with a detection limit of 10^{-5} M. Despite the thorough investigations of methanol electro-oxidation as a potential fuel (Parsons & Van der Noot 1988, Wasmus & Küver 1999) few amperometric sensors for dissolved methanol have been developed. An amperometric Nafion®-based platinum sensor of a sandwich-type arrangement has appeared for the much higher concentration range of 0.5 – 3 M (Barton et al. 1998) whereas alcohol oxidase-peroxidase amperometric biosensors with detection limits down to 10^{-5} M have also been proposed (Hasunuma et al. 2004).

Examples of methanol vapour sensors include mainly conductivity sensors, based either on polypyrrole-based devices with detection limits in the 0.1-10 Torr range (Lin et al. 1998, Jun et al. 2003) or on semiconducting oxides with detection limits down to 0.1 Torr (Patel et al. 2003), but also chemically modified quartz microbalance sensors with detection limits lower than 0.1 Torr (Wang et al. 2001). Although galvanic ethanol sensors used for breath alcohol levels testing have long been available (e.g. the "breathalyzer"-Schiavon et al. 1996), alcohol electrochemistry on Nafion®-based electrode assemblies has mainly focused on fuel cell research aspects (even when methanol concentrations down to 0.3 Torr were used (Nakajima & Kita 1998)). Very few all-solid Nafion®-based alcohol vapour amperometric sensors have appeared in the literature and as an example a fuel-cell type ethanol sensor (Millet et al. 1996) and a Nafion®-covered microelectrode methanol sensor (Umeda [2] et al. 2001) can be mentioned here.

In this chapter we present results aiming to develop simple amperometric methods for a rough estimate of methanol vapours in equilibrium with 1-10% w/w aqueous methanolic solutions (equivalent to a methanol vapour range of ca. 1-13 Torr, as calculated using data from Perry's chemical engineers' handbook (Perry et al. 1984) and from Vapor-liquid equilibrium data collection (Gmehling et al. 1981), using Pt/Nafion® all-solid all-planar sensors. We also test crude monitoring of dissolved methanol (in the 0.5-3 M range) in sulfuric acid using bare platinum microdisc electrodes.

A common characteristic of both of these dissolved and gaseous methanol sensors is the high rate of analyte mass transfer to the indicator electrode due to non-planar diffusion in the case of microelectrodes in solution and to the existence of a thin mass transfer barrier in the case of the Nafion®-based all-planar sensors in gas samples. This property is expected to have an additional advantage in the case of amperometric methanol detection in oxygen-containing solutions or gas streams. Oxygen is known to interfere with methanol electrochemistry on platinum in acid since the onset potential of its reduction coincides with the onset potential for methanol oxidation (Chu & Gilman 1994). Although methanol oxidation is known to be always under kinetic control and thus not affected by an increase in mass transfer rates, the mixed control region of oxygen reduction is expected to shift to more negative potentials in that case and the methanol oxidation currents not to need background correction in oxygen-containing samples.

5.2 Dissolved methanol oxidation at platinum microelectrodes in acidic solutions

Of all the single metals platinum has been found to be the best catalyst for methanol oxidation, although its activity is not satisfactory. Detailed studies by Pletcher and Solis in 1982 also proved that the oxidation rate of methanol is critically dependent on the history of the electrode surface, whereby a freshly reduced surface permits more rapid adsorption and oxidation of methanol. Figure 5.1 presents a cyclic voltammogram for methanol oxidation in an air-equilibrated H_2SO_4 solution, at a 50 μm diameter platinum microelectrode. The cyclic voltammograms shown were recorded at a potential scan rate of 5 mV/s in an air-equilibrated 2 M methanol + 3 M H_2SO_4 solution and in an air-equilibrated 3 M H_2SO_4 solution with no methanol (background voltammogram). The peak at ca +0.7 V vs. Ag/AgCl during the positive-going scan in the presence of methanol is the typical methanol oxidation peak on traces of a Pt-O monolayer whereas the waves at more positive potentials correspond to oxidation on a partially and, eventually, complete oxide layer (Pletcher and Solis in 1982). However, during the negative-going scan the presence of methanol is indicated only by a kink at ca. +0.45 V despite the fact that a peak (shifted to less positive potentials) similar to the positive-scan is reported in the literature for nitrogen-purged solutions and for electrodes that have not entered the multilayer oxide formation and oxygen evolution potential range (beyond +1.6 V). As can be seen by closer inspection of the background voltammogram (Inset to Figure 5.1) there is an extended potential range during the negative-going scan (0.5 - 0.2 V) where a reduction current is recorded in the absence of methanol, most likely due to reduction of excessive oxide formed at the extreme potential limits (up to +1.75 V) of the positive-going scan and, partially, to oxygen reduction too.

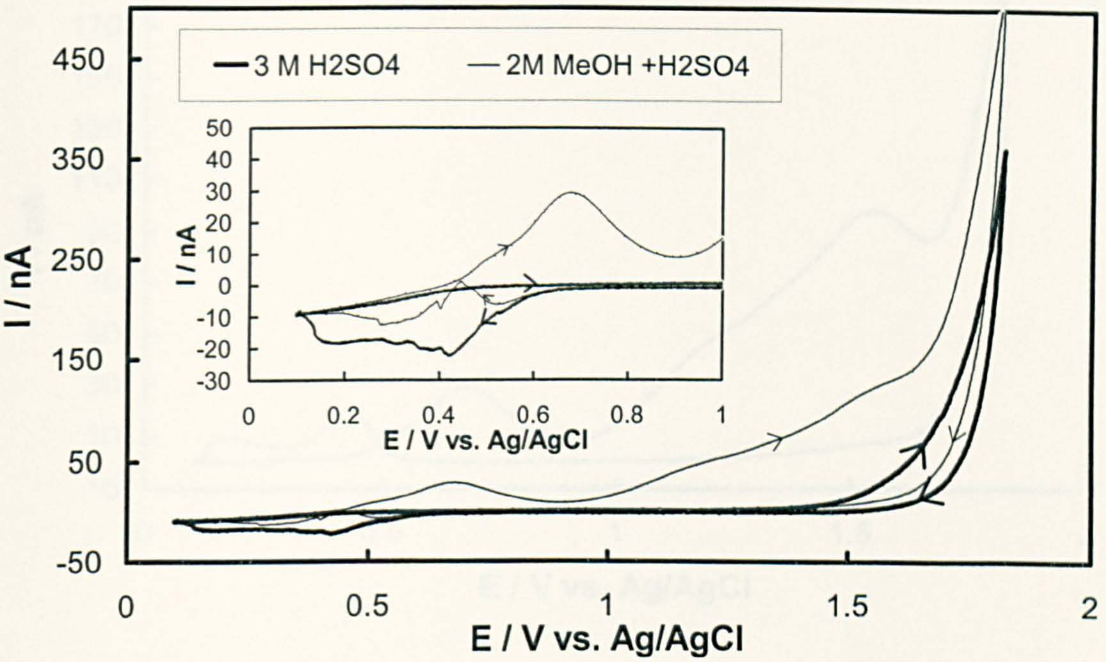

Figure 5.1 Voltammograms recorded at 5 mV/s in aerated H_2SO_4 solution and in a 2 M methanol + 3 M H_2SO_4 solution at a 50 μm diameter platinum microelectrode. Inset: magnification of the voltammogram in the 0-1 V vs. Ag/AgCl range.

Figure 5.2 presents the background-corrected voltammogram of methanol oxidation resulting from the subtraction of the voltammograms of Figure 5.1 above. It can be seen that, when the background features are removed, after the excessive oxide starts to strip off at potentials more negative than 0.5 V during the reverse scan, the methanol oxidation peak appears on that scan too, showing the typical methanol oxidation picture of de-aerated solutions. That is, the positive-going scan shows the typical bell-shaped methanol oxidation peak at ca. +0.7 V vs. Ag/AgCl and two overlapping voltammetric waves in the platinum oxide formation potential region at more positive potentials. On the reverse scan the peak at 0.2-0.4 V vs. Ag/AgCl is due to methanol oxidation on a freshly exposed surface just after the stripping of platinum oxides.

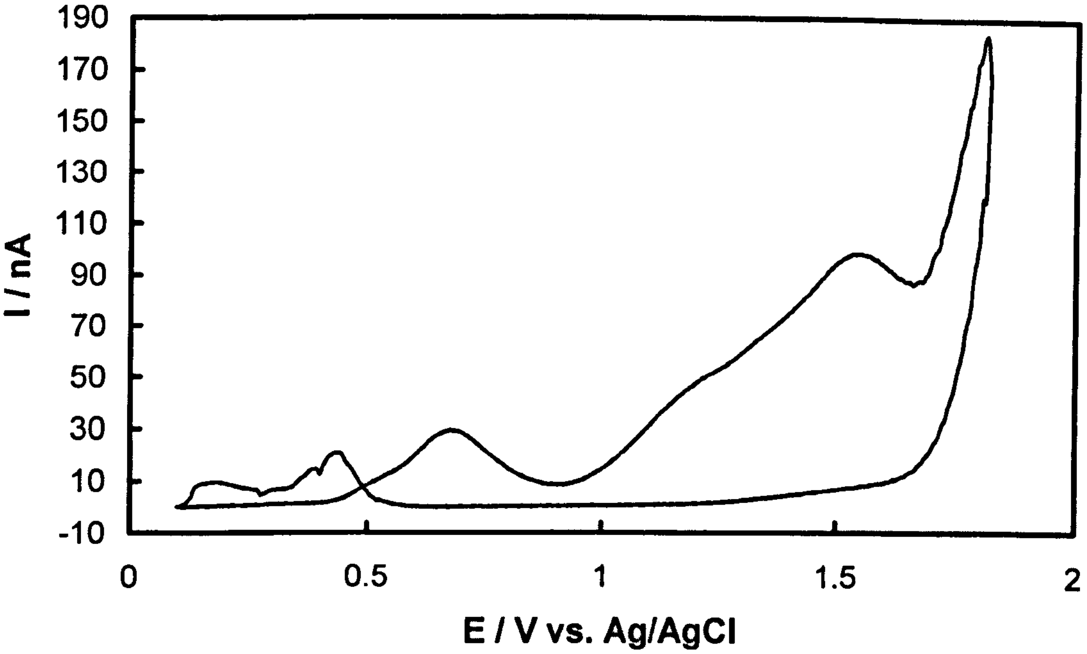

Figure 5.2 Background - corrected voltammogram of Figure 5.1 above.

The form of the background-corrected voltammogram is a direct indication that the methanol oxidation mechanism is not affected by the reduction of oxygen (in air-equilibrated solutions) or of multilayer platinum oxides (at positively exposed electrodes) and that the voltammetric response of Figure 5.1 results from a simple superposition of corresponding currents. What is however important is that the current of the 0.7 V (forward peak) is almost the same (ca 30 nA in this case) both in the air- and nitrogen saturated methanolic solutions, a useful feature from an electroanalysis point of view. In other words, the important feature shown is the separation of the forward methanol oxidation peak from oxygen/oxide reduction peak.

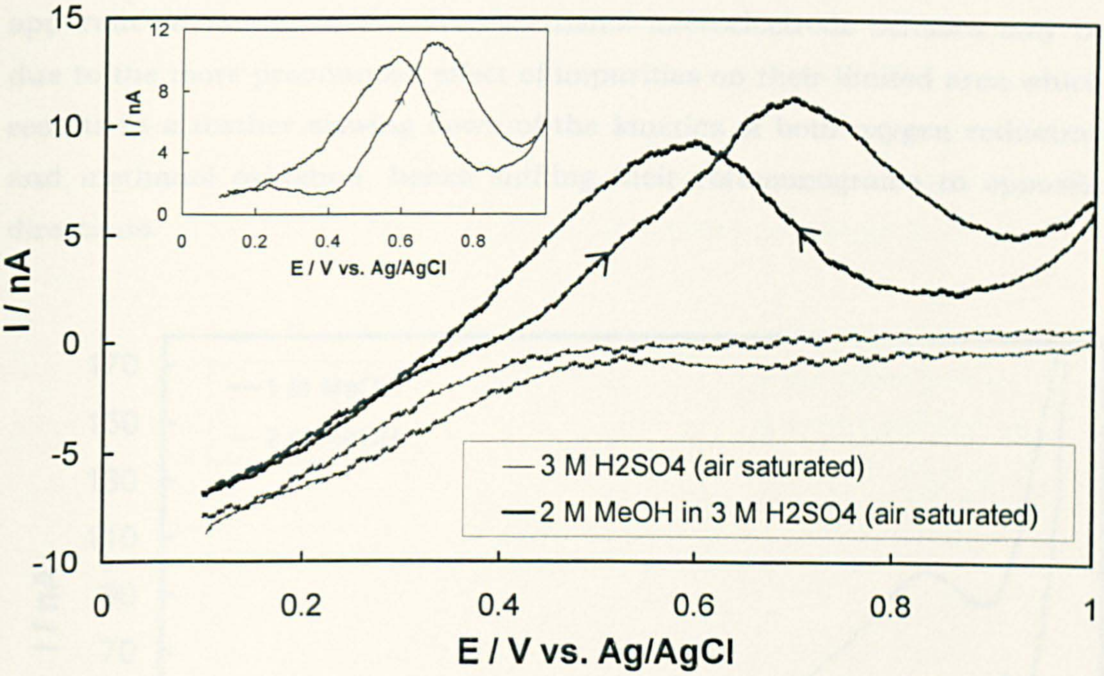

Figure 5.3 Voltammograms recorded at 5 mV/s in aerated H_2SO_4 solution and in a 2 M methanol + 3 M H_2SO_4 solution at a 50 μm diameter platinum microelectrode with limited positive potential. Inset: Background - corrected voltammogram.

When the positive potential was limited before the oxygen evolution and oxide multilayer formation region, as in Figure 5.3, the oxygen reduction, recorded as a S-shaped wave, did not affect either of the two methanol peaks and the separation of the reverse peak from oxygen/oxide reduction peak is further extended. This allowed experiments in air to be studied with no great need for background correction. As has also been mentioned in the opening paragraphs of this chapter, a significant separation of methanol oxidation and oxygen reduction voltammograms is already expected at the high mass transfer rates of microelectrodes. This is because oxygen reduction is known to show (apart from the kinetic control) mixed control and mass transfer control regions on platinum and its voltammogram is expected to shift to more negative potentials upon increased mass transfer rates (Pletcher & Sotiropoulos 1993). However, during similar experiments on rotating platinum disc macroelectrodes (Chu & Gilman 1994), even at the highest rotation rates (2500 rpm) used therein, the separation was not as pronounced as in the case of our microelectrode experiments. This apparent advantage of dissolved methanol microelectrode sensors may be due to the more pronounced effect of impurities on their limited area which results in a further slowing down of the kinetics of both oxygen reduction and methanol oxidation, hence shifting their voltammograms to opposite directions.

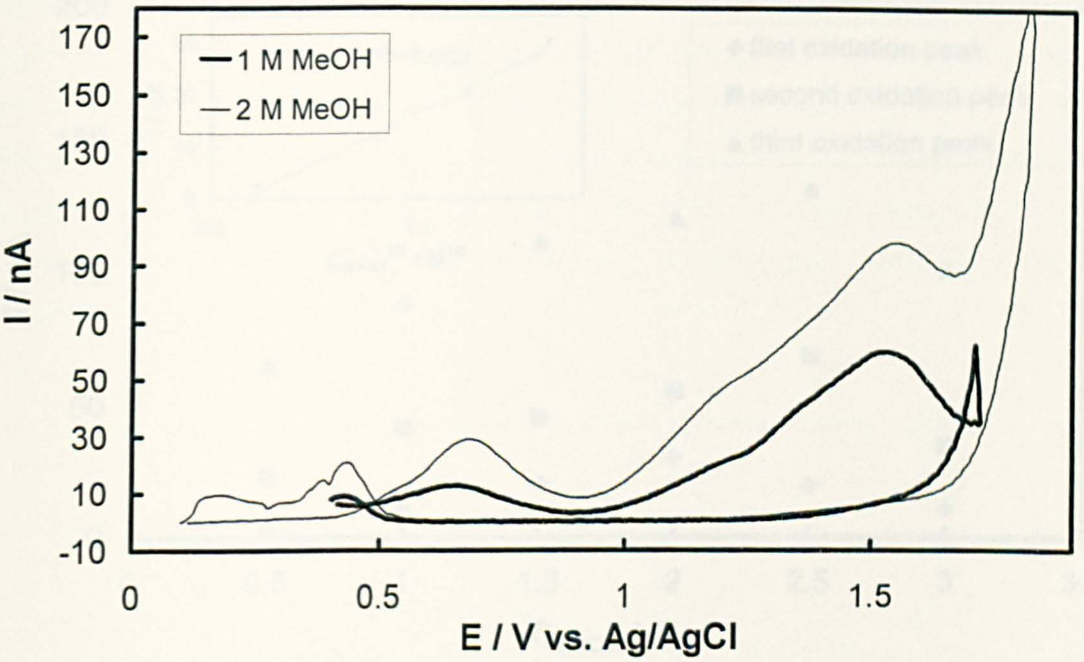

Figure 5.4 Background - corrected voltammograms recorded at 2 mV/s on a 50 µm platinum microelectrode in 1 and 2M MeOH + 3M H_2SO_4 air-saturated solutions

Figure 5.4 presents cyclic voltammograms recorded in two different methanol concentrations. These voltammograms were recorded in several methanol concentrations and Figure 5.5 presents the variation of the three oxidation peak currents measured at 0.7 V, 1.25 V and 1.5 V with methanol concentration. It can be seen that there is no linear current-concentration dependence. Furthermore, at concentrations above 2 M the current starts to fall, possibly due to increased electrode poisoning at high methanol concentrations, via the formation of strongly adsorbed intermediates, that slows down the reaction rate (Bagotzky & Vassilyev 1967). The variation of the first peak current (at ca 0.65-0.7 V vs. Ag/AgCl) with the square root of methanol concentration (Figure 5.5 inset) exhibits reasonable linearity, in accordance with literature from Bagotzky and Vassilyev 1967 (on platinum electrodes) and Chu and Gilman 1996 (on unsupported Pt-Ru electrodes), which reports a 0.5 reaction order with respect to methanol concentration from aqueous solutions. A fractional reaction order is often observed in the case of oxidation of organic compounds (Bagotzky and Vassilyev 1967).

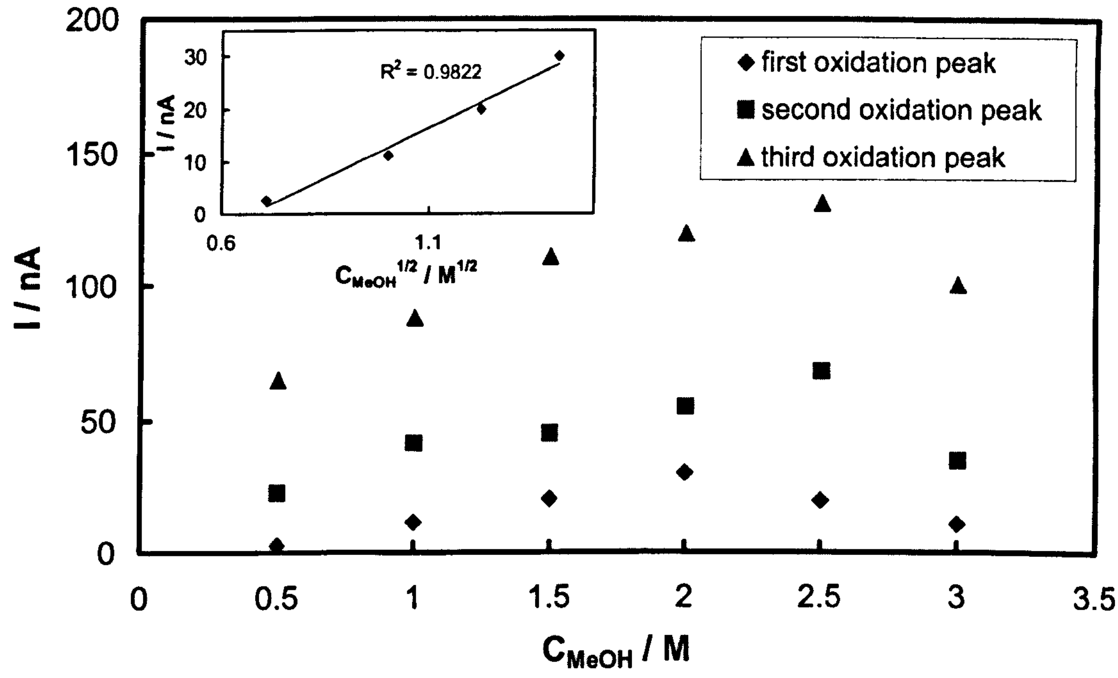

Figure 5.5 Variation of voltammogram oxidation peak currents with dissolved methanol concentration on a 50 μm platinum microelectrode measured at ca. 0.7 V, 1.25 V and 1.5 V Inset: First peak current vs. the square root of methanol concentration.

The oxidation rate of methanol on a clean platinum anode is initially large but decays quickly due to partial oxidation products, which build up on the surface and effectively poison the electrode. In their experiments Pletcher and Solis (1982) used cycling or pulsing of the electrode through the potential range where platinum oxide is formed to activate the platinum surface. Fedkiw et al (1988) introduced a pulsed potential measurement of methanol oxidation, which on average increased the currents by nearly two orders of magnitude above the steady-state current of the same potential. To avoid this current deterioration during the continuous monitoring at constant potential and to improve the linearity of the current vs. $C^{1/2}$ curve, a potential sequence consisting of +1.6 V for 10s (cleaning pulse) / 0 V for 120 s (equilibration pulse) / +0.6 V for 180 s (measurement pulse) was applied to the electrodes. During the cleaning pulse all adsorbed organic intermediates and products are expected to be oxidized and removed from the surface while the onset of oxygen evolution should offer mechanical cleaning too. The equilibration pulse at 0 V is necessary for the stripping-reduction of platinum oxides formed during the cleaning pulse and methanol adsorption on a clean platinum surface. Finally, the measurement pulse was chosen on the potential range of the first oxidation peak, which is generally more reproducible and shows a stronger variation with concentration.

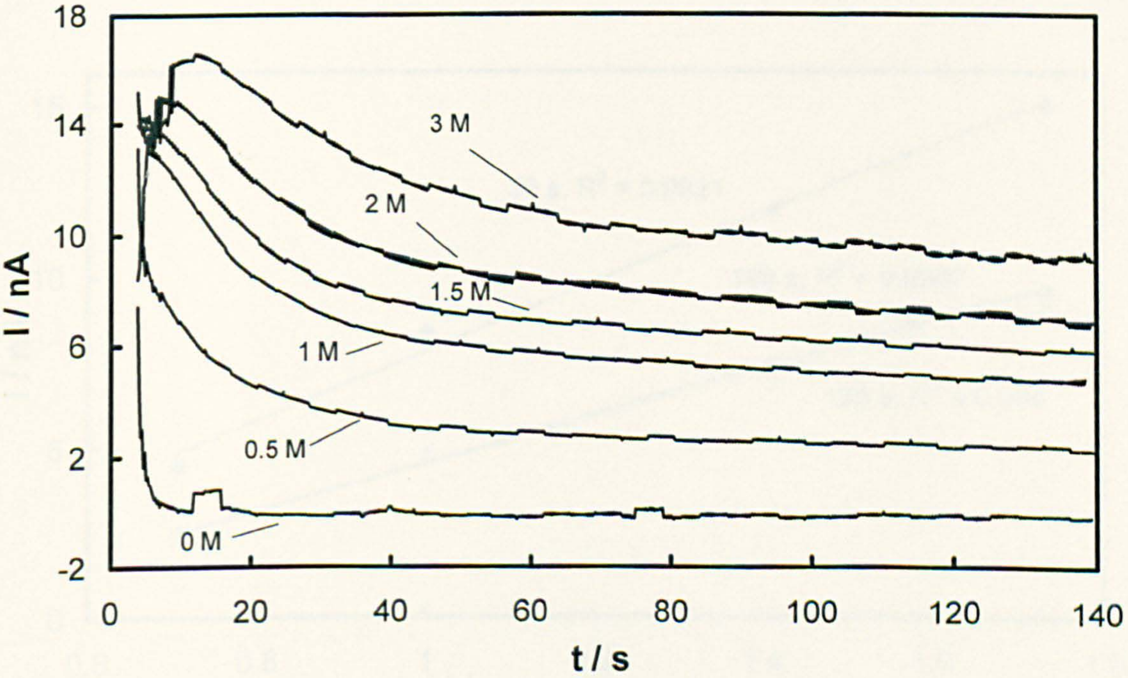

Figure 5.6 Current / time transients at 50 μm platinum microelectrode at the measurement potential of +0.6 V vs. Ag/AgCl (within the pulse sequence used) in MeOH + 3M H_2SO_4 air saturated solutions.

The resulting current-time transients seen at Figure 5.6 were reproducible upon periodic application of the sequence for at least 8 hours. The method proved to be sensitive to methanol concentrations above 0.1 M and thus potentially applicable to crude monitoring of high methanol levels. It should also be noted that an electronic filter of 1 s was employed during the recording of the chronoamperometric transients to cut off oscillations that are known to occur during the potentiostatic and galvanostatic oxidation of organics at high concentrations (Vielstich et al. 2001)

The peak of the current transient observed at short times for the higher concentrations studied is similar to that reported by Pletcher and co-workers (Pletcher & Solis 1982) and can be attributed to the oxidation of methanol pre-adsorbed during the equilibration step following which the current reaches a steady state value corresponding to methanol oxidation from the bulk.

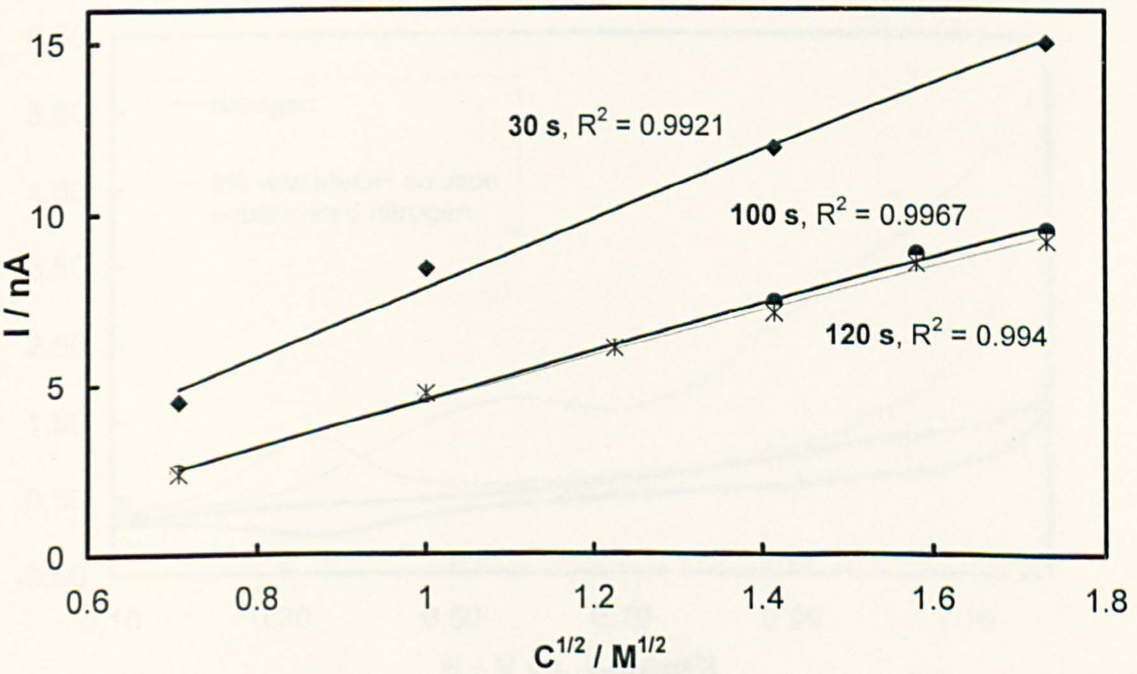

Figure 5.7 Variation of current collected at various time intervals vs. the square root of methanol concentration.

Figure 5.7 shows the square root correlations collected at various time intervals between the oxidation current at +0.6 V and methanol concentration that extends from 0.5 M to beyond 3 M. A good linearity is observed in all the measurements ($r^2 > 0.99$) and a steady state response is acquired for times longer than 100 s.

5.3 Methanol vapour oxidation at three-electrode Nafion® sensors

A three-electrode Pt/Nafion® type B device (see Experimental 2.1.4) similar to those used in oxygen sensors was prepared for experiments in water saturated methanol-enriched nitrogen and air streams. Preliminary experiments of surface electrochemistry showed clear changes in the currents associated with methanol oxidation in nitrogen streams.

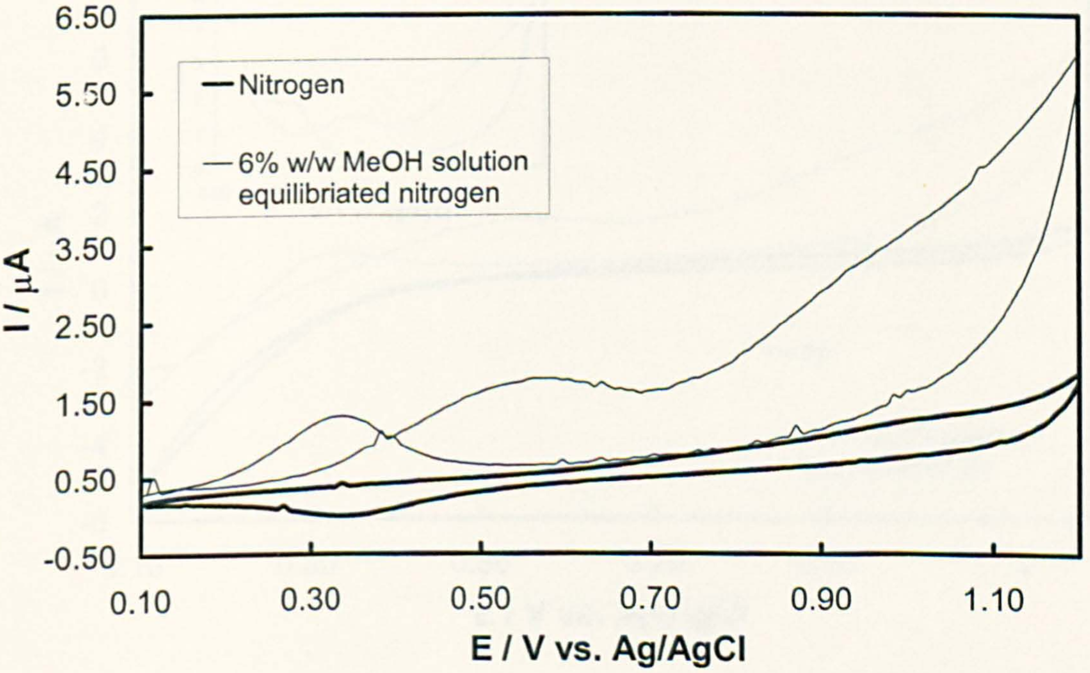

Figure 5.8 Voltammograms recorded at 5 mV/s in a pure water saturated nitrogen stream and in a 6% w/w methanol/water solution-equilibrated nitrogen stream at a three-electrode Pt (vs. Ag/AgCl)/Nafion®/Pt planar device.

Figure 5.8 presents a cyclic voltammogram recorded at 5 mV/s in a 6% w/w methanol/water solution equilibrated nitrogen stream passing over the Pt/Nafion® detector, together with the background voltammogram of a pure water-saturated nitrogen stream. It can be seen that the positive-going scan shows the overall methanol oxidation picture of dissolved methanol oxidation with a bell-shaped peak at ca. +0.6 V vs. Ag/AgCl and a voltammetric wave in the platinum oxide formation potential region at more positive potentials. Another feature of the voltammogram is the increased oxidation currents when compared to similar dissolved methanol sensors; result that was also reported by Nakajima and Kita in 1988. They used metal electrodes bonded to solid polymer electrolyte membranes to study methanol vapor oxidation at various partial pressures from 0.3 to 6 Torr and also found oxidation currents of 10^3 times larger than the equivalent dissolved methanol sensor.

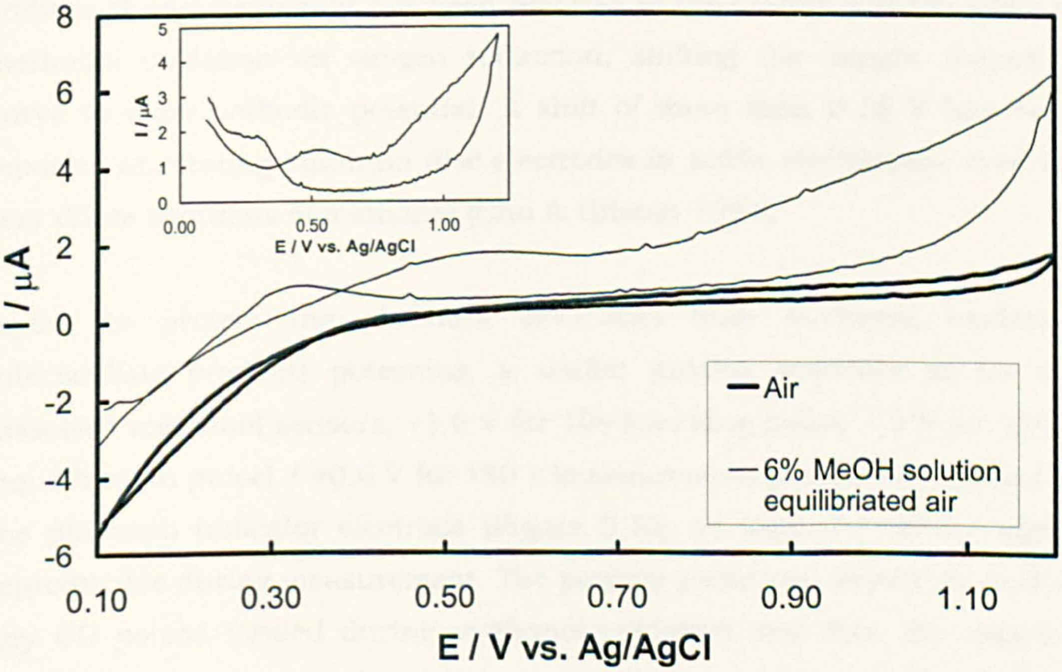

Figure 5.9 Voltammograms recorded at 5 mV/s in pure water saturated air stream and in a 6% w/w methanol/water equilibrated air stream at a three-electrode Pt (vs. Ag/AgCl)/Nafion®/Pt planar device. Inset: Background-corrected voltammogram.

A clear signal for methanol oxidation above the background current can also be seen in samples containing air (Figure 5.9). However the background reduction current (observed at potentials less positive than +0.5 V) is now higher , due in this case not only to the reduction of platinum oxides formed when the electrode is exposed to positive potentials but also to oxygen reduction. This current only affects the methanol oxidation picture during the reverse, negative-going potential scan, suppressing the peak usually observed on an oxide-free platinum surface. The interference of background currents especially from oxygen reduction means, that the results recorded need to be background corrected (Figure 5.9 inset) if the reverse peak is to be identified. However, from an electroanalytical point of view it is important again that the methanol oxidation current at potentials above +0.5 V is hardly influenced by oxygen reduction. Similar arguments holding for the discussion in the case of microelectrodes (high mass transfer rates from the gas phase and effect of membrane impurities) can interprete the separation of the two signals. An additional parameter that has been reported in the literature is the effect of methanol oxidation on oxygen reduction, shifting the oxygen reduction curve to more cathodic potential. A shift of more than 0.15 V has been reported at rotating platinum disc electrodes in acidic electrolytes, even for very dilute solutions of methanol (Chu & Gilman 1994).

Again, to protect the platinum electrodes from methanol oxidation intermediate products poisoning, a similar pulsing sequence as for the dissolved methanol sensors, +1.6 V for 10s (cleaning pulse) / 0 V for 110 s (equilibration pulse) / +0.6 V for 180 s (measurement pulse), was applied to the platinum indicator electrode (Figure 5.10), to keep the sensor signal reproducible during measurement. The positive pulse was applied to oxidise any CO poison formed during methanol oxidation and then the negative pulse to hydrogen evolution region (equilibration pulse) to strip platinum oxides from the sensor's indicator electrode before measurement.

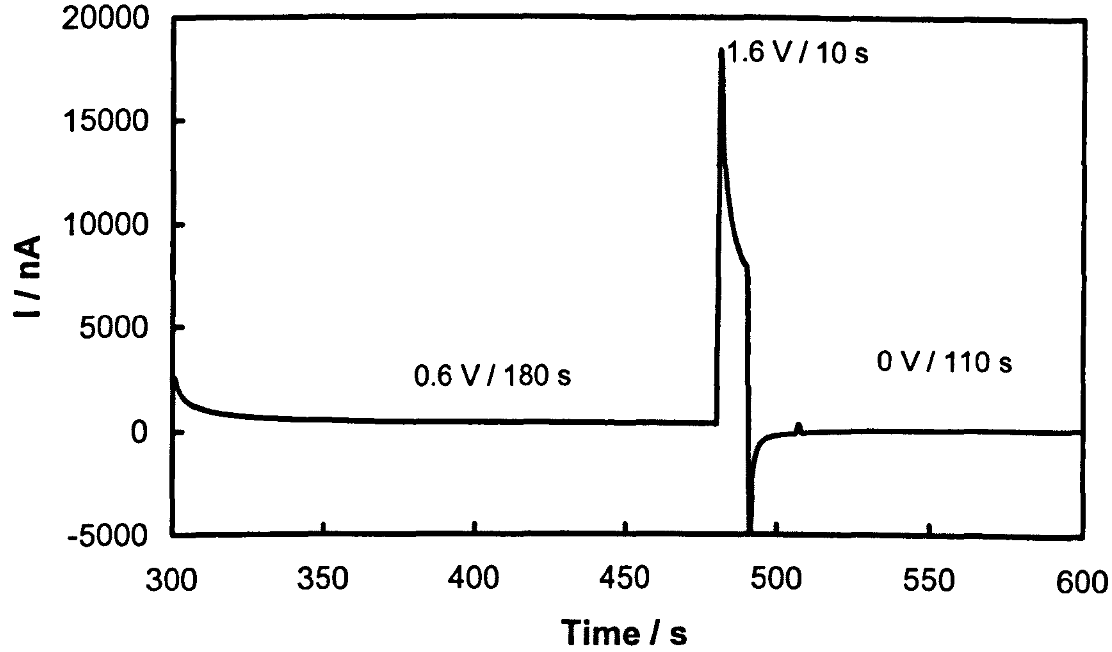

Figure 5.10 Potential pulsing sequence showing the measurement, cleaning and equilibration pulses

Using the potential sequence of Figure 5.10 the current-time transients of Figure 5.11 and 5.12 were obtained from which a variation of the steady state current from the background value is observed for methanol concentrations higher than 2% w/w. For gaseous methanol oxidation at the Pt/Nafion® interface in nitrogen, a linear correlation between the oxidation current at +0.6 V (collected 120 s after the application of the pulse) and methanol concentration fits marginally better the experimental data (Figure 5.11 Inset).

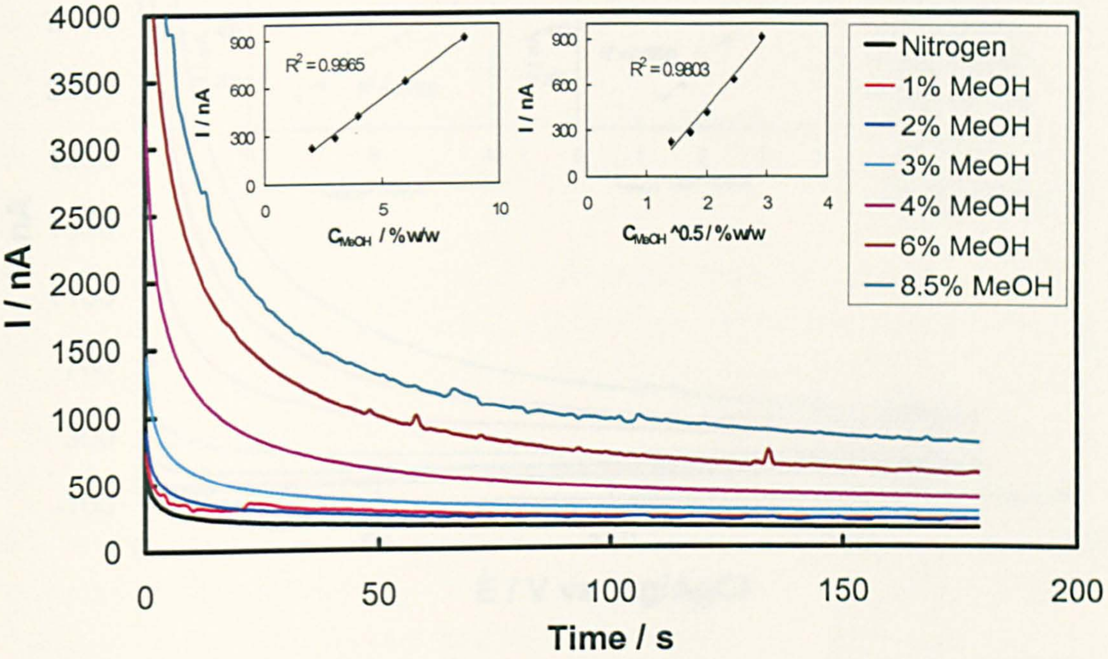

Figure 5.11 Current / time transients at Pt (vs. Ag/AgCl)/Nafion®/Pt planar device at the measurement potential of +0.6 V (within the pulse sequence used) in water equilibrated nitrogen and methanol vapour streams. Inset: Variation of the currents collected at 120 s vs. the methanol concentration and the square root of the methanol concentration in the solution phase (for concentrations higher than 2% w/w).

For oxygen containing samples a square root correlation seems to be more appropriate (Figure 5.12 Inset). However, we consider the differences in the correlation coefficients within the experimental error of these devices and hence we cannot speculate a different mechanism and reaction rate for methanol oxidation at the Pt/Nafion® interface in the absence of oxygen from that holding at the same interface but in the presence of oxygen or in all cases of platinum electrodes in acid solutions.

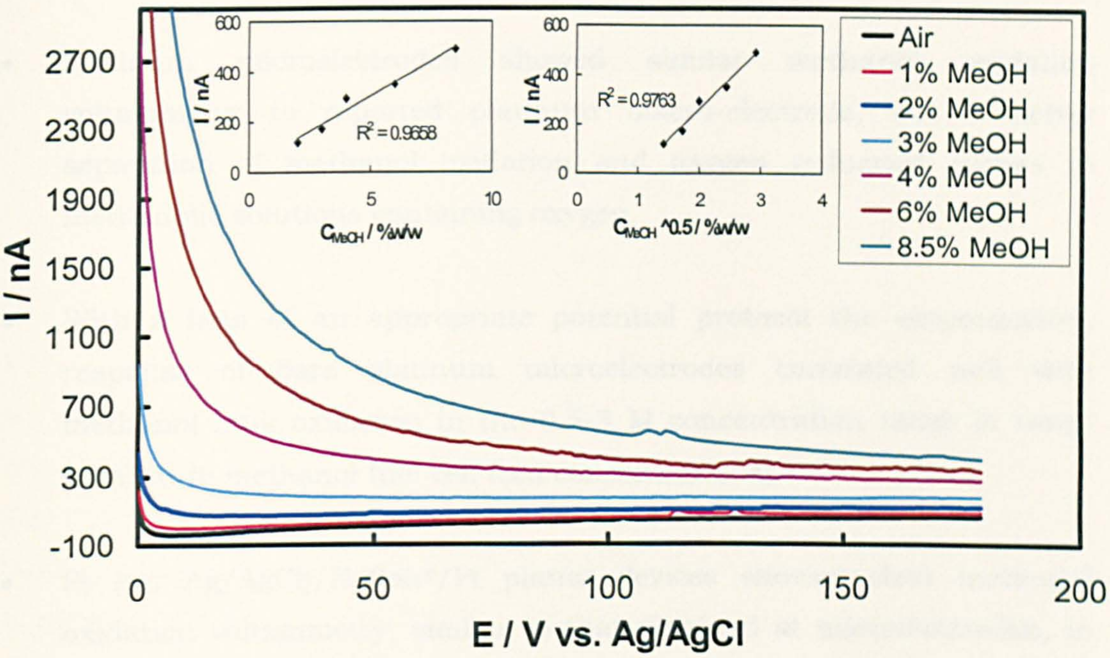

Figure 5.12 Current / time transients at Pt (vs. Ag/AgCl)/Nafion®/Pt planar device at the measurement potential of +0.6 V (within the pulse sequence used) in water saturated air and methanol streams. Inset: Variation of the currents collected at 120 s vs. the methanol concentration and the square root of the methanol concentration.

It should be noted that plotting the methanol oxidation current of these solid-state sensors vs. methanol concentration in the purged solutions assumes that gaseous methanol in equilibrium with these solutions re-dissolves into the water regions of Nafion® before reacting at the Pt/Nafion® interface and that water in Nafion® retains bulk water properties. The first assumption is supported by the fact that inferior correlation coefficients were obtained when the current was plotted vs. corresponding methanol vapour pressures while the second is also true for the high %RH values of these aqueous solution-saturated gaseous streams (measured as >90%).

5.4 Conclusions

- Platinum microelectrodes showed similar methanol oxidation voltammetry to reported platinum macro-electrode, but a better separation of methanol oxidation and oxygen reduction curves in methanolic solutions containing oxygen.

- With a help of an appropriate potential protocol the amperometric response of bare platinum microelectrodes correlated well with methanol bulk oxidation in the 0.5-3 M concentration range (a range relevant to methanol fuel cell feed concentrations).

- Pt (vs. Ag/AgCl)/Nafion®/Pt planar devices showed clear methanol oxidation voltammetry, similar to that obtained at microelectrodes, in methanol containing nitrogen and air streams.

- The application of an appropriate potential protocol ensured a good correlation between the amperometric response of the Pt (vs. Ag/AgCl)/Nafion®/Pt planar devices with dissolved methanol concentration in the 2-10% w/w range (ca 0.6-3 M), when operated in methanol-containing nitrogen and air streams equilibrated with these solutions.

CHAPTER 6

Conclusions

During the course of this research program all-planar solid-state amperometric devices, fabricated with thin sputtered metal layers on the same face of a solid protonic conductor, were successfully used as gas sensors in gaseous samples. Gold or platinum served as the indicator and counter electrodes, the solid polymer electrolytes of Nafion® or polybenzimidazole (PBI) served as ionic conductors and oxygen or methanol were the test gases used. The amperometric sensors were operated in a two-electrode or, mainly, in a three-electrode mode with the addition of a Ag/AgCl reference electrode.

A clear voltammetric picture could be obtained for all three-electrode devices operated in gaseous streams of controlled humidity (20-100% RH), both with respect to gold and platinum surface electrochemistry and with respect to the sensing reactions of oxygen reduction and methanol oxidation. All devices responded in a step-wise pattern upon step changes of gas concentration. It was proven that significant contribution to the measured current originated from the edge of the deposit (where a metal/polymer electrolyte/gas interface exists), due to high mass transfer rates and minimum ohmic losses prevailing there. A significant systematic dependence of sensor response on humidity was found and attributed to the participation of water in the mechanism of the sensing reactions at the metal/ionic polymer electrolyte interface.

The main advantages of the design are the simplification of the manufacturing process (all components on the same plane) and the minimisation of precious electrocatalyst needed (significant contribution from the edge of the metal deposit). The planar sensor design concept with all electrodes on the same face of a solid electrolyte could be used both as oxygen and a methanol sensor, supporting the general applicability and potential of this design principle.

6.1 Nafion® - based planar oxygen sensors

The behaviour of both two- and three-electrode oxygen sensors based on the design where all the electrodes are deposited or attached on the same face of the ionic conductor, separated by an uncovered strip of the electrolyte, and in direct contact with the gas sample, was investigated in controlled humidity (20-100% RH) and ambient gas samples. Although both gold and platinum indicator electrodes were used, gold was chosen as the primary electrode material as it is cheaper than platinum and it provides a larger potential window for oxygen reduction.

In all gas streams the voltammetry of three-electrode Au (vs. Ag/AgCl)/Nafion®/Au planar device was found to be well defined and typical of aqueous Au electrochemistry. When voltammograms were recorded at 5 mV/s in water-saturated air and nitrogen streams with the same device, a clear exponential rise of the current in the presence of oxygen could be seen with no signs of a limiting current even at extreme negative potentials.

Experiments with two-electrode gold sensors (where the current flowing through can be determined by either one or both of the processes occurring at the working and counter electrodes, if these are of comparable dimensions) in water saturated air streams, showed signs that, at least at high oxygen concentrations the oxygen reduction current is not solely determined by oxygen reduction at the sensing electrode, but also by the extent of oxygen evolution at the counter electrode. Replacing the counter electrode to platinum, which is a better catalyst for oxygen evolution, the voltammograms approached those recorded with three-electrode Au (vs. Ag/AgCl)/Nafion®/Au planar sensors.

When used as oxygen sensor the three-electrode Au (vs. Ag/AgCl)/Nafion®/Au planar device showed good linearity with oxygen concentration and similar response times to those of a commercial fuel cell type sensor (CiTiceL, City Technology Ltd.), with traces only of signal saturation at high oxygen levels, making the sensor suitable for crude environmental monitoring in the 2-20% v/v range. For two electrode sensors the observed higher signal saturation poses a serious limitation leaving the sensor suitable only for monitoring of threshold oxygen levels.

The humidity dependence on the conductivity and physical properties of Nafion® is well known. However, the clear surface electrochemistry obtained for both gold and platinum working electrodes in varied humidity conditions (down to 20% RH) indicated that the fall of oxygen reduction signal with decreasing humidity could not be solely due to ohmic losses (which were only observed at high overpotentials). The dependence of surface electrochemistry and oxygen reduction on humidity followed similar pattern below 70% RH. In this case the variation in both surface electrochemistry and oxygen reduction can be explained simply with changes with the number of working electrode sites in contact with water. For relative humidities above 70% RH, the increase in water content enhanced significantly the reduction of oxygen. At higher humidities the additional water is filling the polymer channels and pinholes and swells the membrane. This free water is believed to enhance the catalytic activity of the electrode with respect to oxygen reduction at the metal/Nafion® interface. The strong dependence of oxygen reduction signal on humidity levels was proven to be the major drawback for this type of sensor if it were to be operated as a solution-free all-solid state device. For future experiments, adding a small water reservoir or water-filled porous support underneath the device and in contact with the polymer electrolyte, signal stability could be achieved and the other sensor advantages (easy to fabricate and cheap) maintained.

The shape of the current-potential curves for oxygen reduction at three-electrode Au/Nafion®/Au-devices showed no signs of a mass transport limiting current plateau. The study of Tafel slopes at three-electrode

Au/Nafion®/Au-device at various humidities gave values higher than those reported in acidic aqueous solutions (even after ohmic correction) and indicated that the kinetics were not controlled by simple electron transfer. The dependence of Tafel-slope on humidity levels for both high and low oxygen concentrations indicated a chemical step, which is affected by water content. The reaction limitations were not simply the oxygen evolution at the counter electrode, but were rather related to the water content needed for creating active sites at the cathode/Nafion® interface.

Changing the thickness of the sensing electrode by nearly five-fold had no significant effect on the oxygen reduction current giving evidence that oxygen diffusing through the metal layers does not contribute to the reduction current in the planar type of sensor. However, a significant part of the current on the sensor is due to diffusion of oxygen from the back of the sensor and through the Nafion® membrane. For gold sensing electrodes the contribution of the deposit perimeter (metal/polymer/gas line interface), that has no significant mass transport barrier, is still high and blurs the appearance of a mass transport limiting current plateau. In the case of a platinum working electrode where oxygen reduction kinetics are faster, a limiting current was observed revealing the existence of a thin mass transfer barrier.

6.2 Other sensor arrangements

Sandwich-type and capillary-type sensor configurations were tested to introduce a mass transport barrier and an oxygen reduction plateau when using gold electrodes. In the former design the working and counter electrodes were deposited on different sides of the polymer membrane whereas in the latter a cap with a capillary opening was fitted on top of the all-planar device of the previous section. For the capillary-type configuration the capillary cap was provided by City Technology Ltd.

In the sandwich design the thickness of the gold layers on the electrode were doubled from the normally used ~300 nm to 600 nm. The results already suggested a mass transport barrier, which became even more prominent as the thickness of the gold layers was increased to 1500 nm, since the gas has to diffuse through the working electrode layer to the electrode/electrolyte interface in this type of electrode arrangement. In the capillary configuration the samples were generally humidified without lid to ensure even and accurate humidification through the sample and then tested both with the lid on and off. Signs of S-shaped voltammograms were observed for gold, indicating a significant mass transfer barrier. The capillary was also found to pose a limitation to water transfer resulting in diminished surface electrochemistry.

Both these alternative arrangements exhibited strong humidity dependence of the oxygen signal too proving that the effect is not a simple conductivity effect (as these electrode arrangements ensured small ohmic losses due to a small interelectrode gap or small currents respectively), but rather a decrease in active-hydrated Au/Nafion® sites. For sandwich type sensor, as was also seen for the planar sensor, the changes in humidity were strongly affecting the kinetics of the oxygen reduction at the Au/Nafion® interface. With the capillary-type sensor the Tafel slope did not seem to vary significantly with humidity indicating a possible modification of the reaction mechanism at the lower currents recorded on this device.

6.3 Other sensor materials

Polybenzimidazole (PBI) membranes fabricated in our laboratory proved to be a viable alternative to Nafion® membranes for the planar sensors. The Au/PBI interface was characterised with well-defined gold electrochemistry with no indications of a significant mass transport barrier. Although PBI was found to be less humidity-dependent, it still exhibited similar behaviour with humidity to Nafion® at least at ambient temperatures.

To avoid polymer electrolytes, that seem to require water for oxygen reduction, the electrochemistry of Ionotec® β/β"-alumina devices was studied in gas streams of varying oxygen and humidity levels. The preliminary investigations on the material exhibited a change in the amperometric signal with oxygen concentration and only a weak humidity dependency on oxygen reduction making it an interesting candidate for future research.

6.4 Methanol sensors

A simple amperometric method was developed for crude monitoring of dissolved methanol (0.5-3 M) in acidic solutions using bare platinum microdisc electrodes and in vapours (in equilibrium with 2-10 % w/w or 0.6-3 M solutions) using Nafion®-based planar platinum sensors. These levels of dissolved methanol are relevant to the continuous monitoring and adjustment of methanol concentration in the feed of a direct methanol fuel cell (Barton et al. 1998).

Voltammetry using 50 µm diameter platinum microelectrodes in aerated methanol acidic solutions gave typical methanol oxidation peaks, separated from the oxygen reduction wave. The current-time transients recorded after the application of an appropriate potential protocol in different methanol concentrations gave steady state currents whose plot vs. the square root of methanol concentration exhibited good linearity. Hence the method can be considered suitable for crude monitoring of dissolved methanol levels.

The same experiments were repeated for methanol vapour oxidation at a three-electrode Pt (vs. Ag/AgCl)/Nafion®/Pt planar device. A similar voltammetric picture to that of dissolved methanol at microelectrodes was obtained and the sensor's amperometric response exhibited reasonable linearity to the variations in methanol concentration of aqueous solutions in equilibrium with the test gas. For both types of sensors methanol oxidation currents were not affected by oxygen reduction making the method suitable for methanol determination in the presence of oxygen without the need for background correction.

References

Alber K.S., Cox J.A. & Kulesza P.J (1997) Solid-state amperometric sensors for gas phase analytes : A review of recent advances, Electroanalysis, 9, 2, pp. 97-101

Alberti G. & Casciola M. (2001) Solid state protonic conductors, present main applications and future prospects, Solid State Ionics, 145, 1-4, pp. 3-16

Alberti G., Cherubini F. & Palombari R. (1995) Potentiometric and amperometric gas sensors based on the protonic conduction of layered zirconium phosphates and phosphonates, Sensord and Actuators B, 24-25, pp. 270-272

Alberti G. & Palombari R. (1989) All solid state hydrogen sensors based on pellicular alpha-zirconium phosphate as a protonic conductor, Solid State Ionics, 35, pp. 153-156

Amadelli R., De Battisti A. & Enea O. (1992) Gas-phase electroreduction of O_2 on gold-Nafion® and (underpotential deposition, gold)- Nafion® electrodes, Journal of Electroanalytical Chemistry, 339, pp. 85-100

Anantaraman A.V. & Gardner C.L. (1996) Studies on ion-exchange membranes. 1. Effect of humidity on conductivity of Nafion ®, Journal of Electroanalytical Chemistry, 414, 2, pp. 115-120

Armstrong R.D., Burnham R.A. & Willis P.M. (1976) Breakdown of beta-alumina at positive and negative potentials, Journal of Electroanalytical Chemistry, 67, 1, pp. 111-120

Azad A.M, Akbar S.A., Mhaisalkar S.G., Birkefeld L.D. & Goto K.S. (1992) Solid-state gas sensors: A review, Journal of Electrochemical Society, 139, 12, pp. 3690-3704

Bagotzky V.S. & Vassilyev Yu.B. (1967) Mechanism of electro-oxidation of methanol on the platinum electrode, Electrochimica Acta, 12, 9, pp. 1323-1343

Bakker E. & Telting-Diaz M. (2002) Electrochemical sensors, Analytical Chemistry, 74, pp. 2781-2800

Barton S.A.C., Murach B.L., Fuller T.F. & West A.C. (1998) A methanol sensor for portable direct methanol fuel cells, Journal of the Electrochemical Society, 145, 11, pp. 3783-3788

Bazinet L., Lamarche F. & Ippersiel D. (1998) Bipolar-membrane electrodialysis: Applications of electrodialysis in the food industry, Trends in Food Science & Technology, 9, 3, pp. 107-113

Beden B., Kadirgan F., Lamy C. & Leger J. (1981) Electrocatalytic oxidation of methanol on platinum-based binary electrodes, Journal of Electroanalytical Chemistry, 127, 1-3, pp. 75-85

Bergman I. (1970) Metallised membrane sensors, British patent 1200595

Bianchi G., Massa F. & Mussini T. (1966) Oxygen and hydrogen-peroxide processes on gold electrodes in acid solutions, Electrochimica Acta, 11, 10, pp. 1509-1523

Bontempelli G., Comisso N., Toniolo R. & Schiavon G. (1997) Electroanalytical sensors for nonconducting media based on electrodes supported on perfluorinated ion-exchange membranes, Electroanalysis, 9, 6, pp. 433-443

Bouchet R., Siebert E. & Vitter G. (1997) Acid-doped polybenzimidazole as the membrane of electrochemical hydrogen sensors, Journal of Electrochemical Society, 144, 5, pp. 95-97

Bouchet R. & Siebert E. (1999) Proton conduction in acid doped polybenzimidazole, Solid State Ionics, 118, 287-299

Bouchet R. [1], Miller S., Duclot M. & Souquet J.L. (2001) A thermodynamic approach to proton conductivity in acid-doped polybenzimidazole, Solid State Ionics, 145, pp. 69-78

Bouchet R. [2], Rosini S., Vitter G. & Siebert E. (2001) Solid-state hydrogen sensor based on acid-doped polybenzimidazole, Sensors and Actuators B, 76, 1-3, pp. 610-616

Brina R., Pons S. & Fleischmann M. (1988) Ultramicroelectrode sensors and detectors - Considerations of the stability, sensitivity, reproducibility and mechanism of ion-transport in gas-phase chromatography and in high-performance liquid-phase chromatography, Journal of Electroanalytical Chemistry, 244, 1-2, pp. 81-90

Brodd R.J., Huang W.W. & Akridge J.R. (2000) Polymer battery R&D in the US, Macromolecular Symposia, 159 pp. 229-245

Broka K. & Ekdunge P. (1997) Oxygen and hydrogen permeation properties and water uptake of Nafion 117 membrane and recast film for PEM fuel cell, Journal of Applied Electrochemistry, 27, pp. 117-123

Brooks N.W., Duckett R.A., Rose J. & Ward I.M. (1993) An NMR study of absorbed water in polybenzimidazole, Polymer, 34, 19, pp. 4038-4042

Bruce P.G. (1995) Solid state electrochemistry, Cambridge University Press, Cambridge

Cao D.X. & Bergens S.H. (2003) A direct 2-propanol polymer electrolyte fuel cell, Journal of Power Sources, 124, 1, pp. 12-17

Capon A. & Parsons R. (1972) Effect of strong acid on reactions of hydrogen and oxygen on noble metals - study using cyclic voltammetry and a new teflon electrode holder, Journal of Electroanalytical Chemistry, 39, 2, p. 275-286

Chen R.H., Chen T.M. & Shern C.S. (1998) Structural phase transitions and electrical conductivity studies of $(NH_4)_3H(SeO_4)_2$ crystal, Journal of Physics and Chemistry of Solids, 59, 6-7, pp. 1009-1013

Cheng W.-H & Kung H.H. (1994) Methanol production and use (edited by Cheng W.-H & Kung H.H.) Marcel Dekker inc., New York

Choudhury N. (1986) Thermochemical stability of beta-alumina and beta"-alumina electrolytes in Na/S cells. 1. The activities of Na_2O and Al_3O_3, Journal of the Electrochemical Society, 133, 2, pp. 425-429

Chu D. (1998) O_2 reduction at the Pt/Nafion interface in 85% concentrated H_3PO_4, Electrochimica Acta, 43, 24, pp. 3711-3718

Chu D. & Gilman S. (1994) The influence of methanol on O(2) electroreduction at a rotating Pt disk electrode in acid electrolyte, Journal of the Electrochemical Society, 141, 7, pp. 1770-1773

Chu D. & Gilman S. (1996) Methanol electro-oxidation on unsupported Pt-Ru alloys at different temperatures, Journal of the Electrochemical Society, 143, 5, pp. 1685-1690

Chung T.S. (1997) A critical review of polybenzimidazoles: Historical development and future R&D, Journal of Macromolecular Science – Reviews in Macromolecular Chemistry and Physics, C37, 2, pp. 277-301

Chviruk V.P., Linyucheva O.V. & Buket A.I. (1997) On the nature of transition processes in ammetric gas sensors based on solid proton electrolytes, Electrochimica Acta, 42, 20-22, pp. 3155-3165

Colomban P. (1992) Proton conductors, Cambridge University Press, Cambridge, UK

Colomban P. & Novak A. (1992) in Proton conductors (edited by Colomban P.) Cambridge University Press, Cambridge, UK

CRC Handbook of Chemistry and Physics, CRC Press.

Damjanovic A., Genshaw M.A. & Bockris J.O'M. (1966) The role of hydrogen peroxide in the reduction of oxygen at platinum electrodes, Journal of Physical Chemistry, 70, 11, pp. 3761-3762

Davies A., Fray D.J. & Witek S.R (1995) Measurement of oxygen in steel using beta-alumina electrolytes, Ironmaking & Steelmaking, 22, 4, pp. 310-315

Davis T.A, Genders J.D & Pletcher D. (1997) A first course in ion permeable membranes, The Electrochemical Consultancy, Romsey, England

Dimitrova P., Friedrich K.A., Stimming U. & Vogt B. (2002) Modified Nafion®-based membranes for use in direct methanol fuel cells, Solid State Ionics, 150, 1-2, pp. 115-122

Divisek J., Eikerling M., Mazin V., Schmitz H., Stimming U. & Volfkovich Yu.M. (1998) A study of capillary porous structure and sorption properties of Nafion proton-exchange membranes swollen in water, Journal of Electrochemical Society, 145, 8, pp. 2677-2683

El-Deab M.S. & Ohsaka T.[1] (2002) An extraordinary electrocatalytic reduction of oxygen on gold nanoparticles-electrodeposited gold electrodes, Electrochemistry Communications, 4, 4, pp. 288-292

El-Deab M.S. & Ohsaka T.[2] (2002) Hydrodynamic voltammetric studies of the oxygen reduction at gold nanoparticles-electrodeposited gold electrodes, Electrochimica Acta, 47, 26, pp. 4255-4261

Evans J., Pletcher D., Warburton P.G. & Gibbs T.K. (1989) Amperometric sensor for carbon dioxide - design, characteristics and performance, Analytical Chemistry 61, 6, pp. 577-580

Fedkiw P.S., Traynelis C.L. & Wang S.-R. (1988) Pulsed-potential oxidation of methanol, Journal of the Electrochemical Society, 135, 10, pp. 2459-2465

Fleischmann M. & Pons S. (1991) in Microelectrodes: theory and applications (edited by Montenegro M.I., Queiros M.A. & Daschbach J.L.), NATO ASI Series, Kluwer, Dordrecht

Floriano J.B., Ticianelli E.A. & Gonzales E.R. (1994) Influence of the supporting electrolyte on the oxygen reduction reaction at the platinum proton-exchange membrane interface, Journal of Electroanalytical Chemistry, 367, 1-2, pp. 157-164

Fontanella J.J., Wintersgill M.C., Chen R.S., Wu Y. & Greenbaum S.G. (1995) Charge transport and water molecular motion in variable molecular weight Nafion membranes: High pressure electrical conductivity and NMR, Electrochimica Acta, 40, 13-14, pp. 2321-2326

Fontanella J.J., Wintersgill M.C., Wainright J.S., Savinell R.F. & Litt M. (1998) High pressure electrical conductivity studies of acid doped polybenzimidazole, Electrochimica Acta, 43, 10-11, pp. 1289-1294

Futerko P. & Hsing I-M. (1999), Thermodynamics of water vapour uptake in perfluorosulfonic acid membranes, Journal of Electrochemical Society, 146, 6, pp. 2049-2053

Gaur H.C. & Sethi R.S. (1967) Calculated emf of galvanic cells containing a single solid or molten oxide electrolyte, Indian Journal of Chemistry, 5, 10, pp. 485-

Gavach C. & Pourcelly G. (1992) in Proton conductors (edited by Colomban P.) Cambridge University Press, Cambridge

Geniès L., Faure R. & Durand R. (1998) Electrochemical reduction of oxygen on platinum nanoparticles in alkaline media, Electrochimica Acta, 44, 8-9, pp. 1317-1327

Glipa X., Bonnet B., Mula B., Jones D.J. & Rozière J. (1999) Investigation of the conduction properties of phosphoric and sulphuric acid doped polybenzimidazole, Journal of Materials Chemistry, 9, pp. 3045-3049

Gmehling J., Onken U. & Arlt W. (1981) Vapor-liquid equilibrium data collection 1a, Aqueous-organic systems: supplement 1, (data by Uchida S. & Kato H.), DECHEMA, Schön & Wetzel GmbH, Frankfurt

Gnanamuthu D.S. & Petrocelli J.V. (1967) A generalized expression for the Tafel slope and the kinetics of oxygen reduction on noble metals and alloys, Journal of the Electrochemical Society, 114, pp. 1036-1041

Gottesfeld S., Raistrick I.D. & Srinivasan S. (1987) Oxygen reduction kinetics on a platinum RDE coated with a recast Nafion film, Journal of the Electrochemical Society 134, pp. 1455-1462

Hamann C.H., Hamnett A. & Vielstich W (1998) Electrochemistry, Wiley-VCH, Weinheim, Germany

Hasunuma T., Kuwabata S., Fukusaki E. & Kobayashi A. (2004) Real-time quantification of methanol in plants using a hybrid alcohol oxidase-peroxidase biosensor, Analytical Chemistry, 76, 5, pp. 1500-1506

He G., Goto T., Narushima T. & Iguchi Y. (1999) Electrical conductivity of alkaline earth metal β-aluminas and their application to a CO_2 gas sensor, Solid State Ionics, 40/41, pp. 313-319

Heineman W.R. (1989) Chemical sensors and microinstrumentation (edited by Murray R.W., Dessy R.E., Heineman W.R., Janata J. & Seitz W.R.) American Chemical Society, Washington DC

Hinatsu J.T., Mizuhata M. & Takenaka H. (1994) Water uptake of perfluorosulfonic acid membranes from liquid water and water vapour, Journal of Electrochemical Society, 141, 6, pp. 1493-1498

Hoare J.P. (1968) The electrochemistry of oxygen, Wiley-Interscience, NY

Hobbs B.S., Tantram A.D.S. & Chan-Henry R. (1991) Techniques and mechanisms in gas sensing (edited by Moseley P.T., Norris J.O.W. & Williams D.E.), Adam Hilger, Bristol

Hodgson A.W.E, Pletcher D & Sotiropoulos S. (1998) A new approach to the design of amperometric gas sensors, Sensors and Actuators B – Chemical, 50, pp. 181-185

Hrncirova P., Opekar F & Stulik K. (2000) An amperometric solid-state NO_2 sensor with a solid polymer electrolyte and a reticulated vitreous carbon indicator electrode, Sensors and Actuators B – Chemical, 69, 1-2, pp. 199-204

Hwang B-J, Liu Y-C & Hsu W-C (1998) Nafion based solid-state gas sensors: Pt/Nafion electrodes prepared by an impregnation-reduction method in sensing oxygen, 2, pp. 378-385

Ihonen J., Jaouen F., Lindberg G., Lundblad A. & Sundholm G. (2002) Investigation of mass-transport limitations in the solid polymer fuel cell cathode – II. Experimental, Journal of the Electrochemical Society, 149, 4, pp. A448-A454

Inzelt G., Pineri M., Schultze J.W. & Vorotyntsev M.A. (2000) Electron and proton conducting polymers: recent developments and prospects, Electrochimica Acta, 45, pp. 2403-2421

Ivers-Tiffée E., Härdtl K.H., Menesklou W. & Riegel J. (2001) Principles of solid state oxygen sensors for lean combustion gas control, Electrochimica Acta, 47, 5, pp. 807-814

Iwasita T. (2002) Electrocatalysis of methanol oxidation, Electrochimica Acta, 47, pp. 3663-3674

James P.J., Elliott J.A., McMaster T.J., Newton J.M., Elliott A.M.S., Hanna S. & Miles M.J. (2000) Hydration of Nafion® studied by AMF and X-ray scattering, Journal of Materials Science, 35, pp. 5111-5119

Janata J. (1989) Principles of chemical sensors, Plenum Press, New York

Janata J. (1990) Chemical sensors, Analytical Chemistry, 62, 12, pp. 33R-44R

Janata J. (1992) Chemical sensors, Analytical Chemistry, 64, 12, pp. 196R-219R

Janata J. & Bezegh A (1988) Chemical sensors, Analytical Chemistry, 60, 12, pp. 62R-74R

Janata J., Josowicz M. & DeVaney D.M. (1994) Chemical sensors, Analytical Chemistry, 66, 12, pp. 207R-228R

Janata J., Josowicz M., Vanýsek P. & DeVaney D.M. (1998) Chemical sensors, Analytical Chemistry, 70, 12, pp.

Janz G.J. (1961) Reference electrodes theory and practice (edited by Ives D.J.G & Janz G.J.) Academic Press, New York and London

Jaouen F., Lindberg G. & Sundholm G. (2002) Investigation of mass-transport limitations in the solid polymer fuel cell cathode – I. Mathematical model, Journal of the Electrochemical Society, 149, 4, pp. A437-A447

Jun H.K., Jiang L.S., Lee K.M., Hohl Y.S., Lim J.O. & Huh J.S (2003) Polypyrrole-based methanol sensors prepared by chemical and vapor state polymerisation, Eco-Materials Processing & Design, Materials Science Forum, 439, pp. 326-330

Jung D.H., Cho S.Y., Peck D.H., Shin D.R. & Kim J.S. (2003) Preparation and performance of a Nafion®/montmorillonite nanocomposite membrane for direct methanol fuel cell, Journal of Power Sources, 118, 1-2, pp. 205-211

Kalhammer F.R (2000) Polymer electrolytes and the electric vehicle, Solid State Ionics, 135, 1-4, pp. 315-323

Kawahara M., Morita J., Rikukawa M., Sanui K. & Ogata N. (2000) Synthesis and proton conductivity of thermally staple polymer electrolyte: Poly(benzimidazole) complexes with strong acid molecules, Electrochimica Acta, 45, pp. 1395-1398

Kinoshita K. (1992) Electrochemical oxygen technology, John Wiley & Sons, USA

Kita H. & Nakajima H. (1986) Metal-electrodes bonded on solid polymer electrolyte membranes (SPE). 3. Co oxidation at Au-SPE electrodes, Electrochimica Acta, 31, 2, pp. 193-200

Kocache R. (1986) The measurement of oxygen in gas mixtures, Journal of Physics E: Scientific Instruments, 19, 6, pp. 401-412

Kordali V., KyriacouG & Lambrou C (2000) Electrochemical synthesis of ammonia at atmospheric pressure and low temperature in a solid polymer electrolyte cell, Chemical Communications, 17, pp. 1673-1674

Koter S. & Warszawski A. (2000) Electromembrane processes in environment protection, Polish Journal of Environmental Studies, 9, 1, pp. 45-56

Kozawa A. (1964) Effects of anions and cations on oxygen reduction and oxygen evolution reactions on platinum electrodes, Journal of Electroanalytical Chemistry, 8, 1, pp. 20-39

Kung H.H & Smith K.J (1994) Methanol production and use (edited by Cheng W.-H & Kung H.H.) Marcel Dekker inc., New York

Laporta M., Pegoraro M. & Zanderighi L. (1999) Perfluorosulphonated membrane (Nafion): FT-IR study of the state of water with increasing humidity, Physical Chemistry Chemical Physics, 1, pp. 4619-4628

Lawson D.R. Whiteley L.D. Martin C.R. Szentirmay M.N. & Song J.I. (1988) Oxygen reduction at Nafion film-coated platinum electrodes: transport and kinetics, Journal of the Electrochemical Society, 135 pp. 2247-2253

Léger J.-M. (2001) Mechanistic aspects of methanol oxidation on platinum-based electrocatalysts, Journal of Applied Electrochemistry, 31, pp. 767-771

Lin A.S., Kowalak A.D. & O'Grady W.E. (1996) Studies of the role of water in the electrocatalysis of methanol oxidation, Journal of Power Sources, 58, pp. 67-72

Lin C.W., Hwang B.J. & Lee C.R. (1998) Methanol sensors based on the conductive polymer composites from polypyrrole and poly(vinyl alcohol), Materials Chemistry and Physics, 55, 2, pp. 139-144

Linek V., Vacek V., Sinkule J. & Beneš P. (1998) Measurement of oxygen by membrane-covered probes: Guidelines for applications in chemical and biochemical engineering, Ellis Horwood Ltd. England

Lingane J.J. (1961) Chronopotentiometric study of oxygen reduction at a platinum wire cathode, Journal of Electroanalytical Chemistry, 2, 4, pp. 296-309

Liu Y-C, Hwang B-J & Tzeng I-J (2001) Characteristics of solid-state amperometric oxygen sensor using Pt/C film hot-pressed onto Nafion membrane, Electroanalysis, 13, 17, pp. 1441-1446

Liu Y-C, Hwang B-J & Tzeng I-J (2002) Solid-state amperometric hydrogen sensor using Pt/C/Nafion composite electrodes prepared by a hot-pressed method, Journal of the Electrochemical Society, 149, 11, pp. H173-H178

Lufrano F., Gatto I., Staiti P., Antonucci V. & Passalacqua E. (2001) Sufonated polysulfone ionomer membranes for fuel cells, Solid State Ionics, 145, 1-4, pp. 47-51

Lyon S.B. & Elgbar F.A. (1989) Electrochemical detection of hydrogen using a solid-state probe, Corrosion Science, 29, 7, pp. 833-837

Lyon S.B & Fray D.J. (1983) Hydrogen measurement using hydrogen uranyl phosphate tetrahydrate, Solid State Ionics, 9-10, 2, pp. 1295-1298

Mangos T.J. & Haas M.J. (1996) Enzymatic determination of methanol with alcohol oxidase, peroxidase and the chromogen 2,2'-azinobis(3-ethylbenzthiazoline-6-sulfonic acid) and its application to the determination to the methyl ester content of pectins, Journal of Agricultural and Food Chemistry, 44, 10, pp. 2977-2981

Mari C.M & Barbi G.B. (1992) Gas sensors (edited by Sberveglieri), Kluwer Academic Publishers, the Netherlands

Maruyama J., Inaba M. & Ogumi Z. (1998) Rotating ring-disc electrode study on the cathodic oxygen reduction at Nafion®-coated gold electrodes, Journal of Electroanalytical Chemistry, 458, pp. 175-182

Millet P., Michas A. & Durand R. (1996) A solid polymer electrolyte based ethanol gas sensor, Journal of Applied Electrochemistry, 26, 9, pp. 933-937

Minh N.Q. (1993) Ceramic fuel-cells, Journal of the American Ceramic Society, 76, 3, pp. 563-588

Mitsushima S., Araki N., Kamiya N. & Ota K. (2002) Analysis of oxygen reduction on Pt microelectrode with polymer electrolytes of various exchange capacities, Journal of the Electrochemical Society, 149, 10, pp. A1370-A1375

Miura N., Kato H., Ozawa Y., Yamazoe N. & Seiyama T. (1984) Amperometric gas sensor using solid-state proton conductor sensitive to hydrogen in air at room-temperature, Chemical Letters, 11, pp. 1905-1908

Morisawa M., Amemiya Y., Kohzu H., Liang C.X. & Muto S. (2001) Plastic optical fibre sensor for detecting vapour phase alcohol, Measurement Science and Technology, 12, pp. 877-881

Müller L. & Nekrassow L. (1964) Untersuchung des elektrochemischen reduktionsprozesses von sauerstoff an platin mit hilfe der rotierenden scheibenelektrode mit Ring, Electrochimica Acta, 9, 7, pp. 1015-1023

Nakajima H. & Kita H. (1988) Metal-electrodes bonded on solid polymer electrolyte membranes (SPE). 5. Methanol oxidation on Pt-SPE electrode, Electrochimica Acta, 33, 4, pp. 521-526

Narayanan S.R., Valdez T.I. & Chun W. (2000) Design and operation of an electrochemical methanol concentration sensor for direct methanol fuel cell systems, Electrochemical and Solid-State Letters, 3, 3, pp. 117-120

National Research Council (US) (1926-1930) International critical tables of numerical data, physics, chemistry and technology vol. III (edited by Washburn E.W., West C.J. & Dorsey N.E.) McGraw-Hill, New York

Nogami M. Daiko Y., Goto Y., Usui Y. & Kasuga T. (2003) Sol-gel preparation of fast proton-conducting P_2O_5-SiO_2 glasses, Journal of Sol-gel Science and Technology, 26, 1-3, pp. 1041-1044

Nãfe H. (1994) The feasibility of a potentiometric CO_2 sensor based on Na-beta-alumina in the light of the electronic conductivity of the electrolyte, Sensors and Actuators B, 21, pp. 79-82

Ogumi Z., Takehara Z. & Yoshizawa S. (1984) Gas permeation in SPE method. 1. Oxygen permeation through Nafion and Neosepta, Journal of the Electrochemical Society, 131, 4, pp. 769-773

Ogumi Z., Kuroe T. & Takehara Z. (1985) Gas permeation in SPE method. 2. Oxygen and hydrogen permeation through Nafion, Journal of the Electrochemical Society, 132, 11, pp. 2601-2605

Okada T., Xie G., Gorseth O., Kjelstrup S., Nakamura N. & Arimura T. (1998) Ion and water transport characteristics of Nafion membranes as electrolytes, Electrochimica Acta, 43, 22, pp. 3741-3747

Opekar F. (1989) Detection of hydrogen in air with a detector containing a Nafion membrane metallized on both sides, Journal of Electroanalytical Chemistry, 260, pp. 451-455

Opekar F. (1992) An amperometric solid-state sensor for nitrogen dioxide based on a solid polymer electrolyte, Electroanalysis, 4, pp. 133-138

Opekar F., Langmaier J. & Samec Z. (1994) Indicator and reference platinum | solid polymer electrolyte electrodes for a simple solid-state amperometric hydrogen sensor, Journal of Elecroanalytical Chemistry, 379, pp. 301-306

Opekar F. & Štulík K. (1999) Electrochemical sensors with solid polymer electrolytes, Analytica Chimica Acta, 385, pp. 151-162

Opekar F. & Štulík K. (2002) Amperometric solid-state gas sensors: Materials for their active components, Critical Reviews in Analytical Chemistry 32, 3, pp. 253-259

Ota K.I., Nakagawa Y. & Takahashi M, (1984) Reaction-products of anodic oxidation of methanol in sulphuric-acid solution, Journal of Electroanalytical Chemistry, 179, 1-2, pp. 179-186

Paik W., Springer T.E. & Srinivasan S. (1989) Kinetics of fuel cell reactions at the platinum/solid polymer electrolyte interface, Journal of the Electrochemical Society, 136, 3, pp. 644-649

Parsons R. & VanderNoot T. (1988) The oxidation of small organic molecules: A survey of recent fuel cell related research, Journal of Electroanalytical Chemistry, 257, 1-2, pp. 9-45

Parthasarathy A., Martin C.R. & Srinivasan S. (1991) Investigations of the O_2 reduction reaction at the platinum/Nafion® interface using a solid-state electrochemical cell, Journal of the Electrochemical Society, 138, 4, pp. 916-921

Parthasarathy A., Srinivasan S., Appleby A.J. & Martin C.R. (1992) Electrode kinetics of oxygen reduction at carbon-supported and unsupported platinum microcrystallite / Nafion® interfaces, Journal of Electroanalytica Chemistry, 339, pp. 101-121

Patel N.G., Patel P.D. & Vaishnav V.S. (2003) Indium tin oxide (ITO) thin film gas sensor for detection of methanol at room temperature, Sensors and Actuators B – Chemical, 96, 1-2, pp. 180-189

Perry R.H., Green D.W. & Maloney J.O. (1984) Perry's chemical engineers' handbook, 6th edition McGraw-Hill, New York

Phillips H.M., Smayling M.C. & Sauerbrey D. (1993) Modification of electrical conductivity and surface structure in polymers using ultraviolet laser radiation, Microelectronic Engineering, 20, pp. 73-88

Pivovar B.S., Wang Y.X. & Cussler E.L. (1999) Pervaporation membranes in direct methanol fuel cells, Journal of Membrane Science, 154, 2, pp. 155-162

Pletcher D. (1991) A first course in electrode processes, The Electrochemical Consultancy, England

Pletcher D. & Solis V. (1982) The effect of experimental parameters on the rate and mechanism of oxidation of methanol at a platinum anode in aqueous acid, Electrochimica Acta, 27, 6, 775-782

Pletcher D. & Sotiropoulos S. (1993) A study of cathodic oxygen reduction at platinum using microelectrodes, Journal of Electroanalytical Chemistry, 356, 1-2, pp. 109-119

Pourcelly G., Oikonomou A., Gavach G. & Hurwitz H.D. (1990) Influence of the water content on the kinetics of counter-ion transport in perfluorosulphonic membranes, Journal of Electroanalytical Chemistry, 287, pp. 43-59

Pourcelly G. & Gavach G. (1992) in Proton conductors (edited by Colomban P.) Cambridge University Press, Cambridge, UK

Qingfeng L., Hjuler H.A. & Bjerum N.J. (2001) Phosphoric acid doped polybenzimidazole membranes: Physicochemical characterization and fuel cell applications, Journal of Applied Electrochemistry, 31, pp. 773-779

Ramamoorthy R., Dutta P.K. & Akbar S.A. (2003) Oxygen sensors: Materials, methods, designs and applications, Journal of Material Science, 38, 21, pp. 4271-4282

Ren X., Springer T.E & Gottesfeld S. (2000) Water and methanol uptakes in Nafion membranes and membrane effects on direct methanol cell performance, Journal of Electrochemical Society, 147, 1, pp. 92-98

Reucroft P.J., Rivin D. & Schneider N.S. (2002) Thermodynamics of Nafion™ – vapor interactions. I. Water vapor, Polymer, 43, pp. 5157-5161

Sakai T., Takenaka H. & Torikai E. (1986) Gas-diffusion in the dried and hydrated Nafions, Journal of the Electrochemical Society, 133, 1, pp. 88-92

Samms S.R., Wasmus S & Savinell R.F (1996) Thermal stability of Nafion® in simulated fuel cell environments, Journal of the Electrochemical Society, 143, 5, pp. 1498-1504

Sarapuu A., Tammeveski K., Tenno T.T., Sammelselg V., Kontturi K. & Schiffrin D.J. (2001) Electrochemical reduction of oxygen on thin-film Au electrodes in acid solution, Electrochemistry Communications 3, 8, pp. 446-450

Schiavon G., Comisso N., Toniolo R. & Bontempelli G. (1996) Pulsed amperometric detection of ethanol in breath by gold electrodes supported on ion exchange membranes (solid polymer electrolytes), Electroanalysis, 8, 6, pp. 544-548

Schiavon G., Zotti G. & Bontempelli G. (1989) Electrodes supported on ion-exchange membranes as sensors in gases and low-conductivity solvents, Analytica Chimica Acta, 221, pp. 27-41

Schiavon G., Zotti G., Bontempelli G., Farnia G. & Sandoná G. (1990) Amperometric monitoring of ozone in gaseous media by gold electrodes supported on ion exchange membranes (solid polymer electrolytes), Analytical Chemistry, 62, 3, pp. 293-298

Schmidt T.J., Stamenkovic V., Ross P.N. & Markovic N.M. (2003) Temperature dependent surface electrochemistry on Pt single crystals in alkaline electrolyte – Part 3. The oxygen reduction reaction, Physical Chemistry Chemical Physics, 5, 2, pp. 400-406

Scott K., Taama W. & Cruickshank J. (1998) Performance of a direct methanol fuel cell, Journal of Applied Electrochemistry, 28, 3, pp. 289-297

Sena D.R., Ticianelli E.A., Paganin V.A. & Gonzales E.R. (1999) Effect of water transport in a PEFC at low temperatures operating with dry hydrogen, Journal of Electroanalytical Chemistry, 477, 2, pp. 164-170

Short G.D (1994) Methanol production and use (edited by Cheng W.-H & Kung H.H.) Marcel Dekker inc., New York

Sone Y., Ekdunge P. & Simonsson D. (1996), Proton conductivity of Nafion 117 as measured by a four-electrode AC impedance method, Journal of Electrochemical Society, 143, 4, pp. 1254-1259

Sotiropoulos S. (1994) The cathodic reduction of oxygen at microelectrodes, PhD Thesis, University of Southampton

Spry R.J., Alexander M.D., Bai S.J., Dang T.D., Price G.E., Dean D.R., Kumar B., Solomon J.S & Arnold F.E. (1997) Anisotropic ionic conductivity of lithium-doped sulfonated PBI, 35, 17, pp. 2925-2933

Staikov G., Yancheva B., Mindjov K. & Yankylov P.D. (1990) Electrochemical behaviour of β"-alumina in presence of oxygen, Solid State Ionics, 40-41, 1, pp. 103-106

Štrbac S. & Adžić R.R. (1996) The influence of pH on reaction pathways for O_2 reduction on the Au (100) face, Electrochimica Acta, 41, 18, pp. 2903-2908

Sumner J.J., Creager S.E., Ma J.J. & DesMarteau D.D. (1998), Proton conductivity of Nafion(R) 117 and in a novel Bis[(perfluoroalkyl)sulfonyl]imide ionomer membrane, Journal of Electrochemical Society, 145, 1, pp. 107-110

Tammeveski K., Tenno T., Claret J. & Ferrater C. (1997) Electrochemical reduction of oxygen on thin-film Pt electrodes in 0.1M KOH, Electrochimica Acta, 42, 5, pp. 893-897

Ticianelli E.A., Derouin C.R & Srinivasan S. (1988) Localization of platinum in low catalyst electrodes to attain high power densities in SPE fuel cells, Journal of Electroanalytical Chemistry, 251, 2, pp. 275-295

Trikhachev S.Yu., Serebryakova N.V, Sokolova N.P., Trukhan E.M. & Boguslavskii L.I. (1989) Stimulation of the protonic conduction of polybenzimidazole membranes by water molecules and Cl^- - ions, Soviet Electrochemistry, 25, 7, pp. 871-876

Umeda M. [1], Kabasawa A., Kokubo M., Mohamedi M., Itoh T. & Uchida I. (2001) methanol gas sensing using ultramicroelectrodes: Studies on sensing mechanism and its enhancement, Japanese Journal of Applied Physics, 40, 1, 8, pp. 5141-5144

Umeda M. [2], Mohamedi M. & Uchida I. (2001) Gas-phase methanol electrooxidation using a Nafion-coated integrated ultramicroelectrode, Langmuir, 17, pp. 7970-7972

Uribe F.A, Springer T.E. & Gottesfeld S. (1992) A microelectrode study of oxygen reduction at the platinum / recast Nafion film interface, Journal of the Electrochemical Society, 139, 3, pp. 765-773

Vielstich W., Paganin V.A., Lima F.H.B. & Ticianelli E.A. (2001) Nonelectrochemical pathway of methanol oxidation at a platinum-catalyzed oxygen gas diffusion electrode, Journal of the Electrochemical Society, 148, 5, pp. A502-A505

Wainright J.S., Wang J-T, Weng D., Savinell R.F. & Litt M. (1995) Acid doped polybenzimidazoles: A new polymer electrolyte, Journal of Electrochemical Society, 142, 7, pp. 121-123

Wang C., Chen F., He X.W., Kang S.Z., You C.C. & Liu Y. (2001) Cyclodextrin derivative-coated quartz crystal microbalances for alcohol sensing and application as methanol sensors, Analyst, 126, 10, pp. 1716-1720

Wang J.-T. [1], Savinell R.F., Wainright J., Litt M. & Yu H. (1996) A H_2/O_2 fuel cell using acid doped polybenzimidazole as polymer electrolyte, Electrochimica Acta, 41, 2, pp. 193-197

Wang J.-T. [2], Wainright J.S., Savinell R.F & Litt M. (1996) A direct methanol fuel cell using acid-doped polybenzimidazole as polymer electrolyte, Journal of Applied Electrochemistry, 26, 7, pp. 751-756

Wasmus S. & Küver A. (1999) Methanol oxidation and direct methanol fuel cells: a selective review, Journal of Electroanalytical Chemistry, 461, 1-2, pp. 14-31

Weng D., Wainright J.S., Landau U. & Savinell R.F. (1996), Electro-osmotic drag coefficient of water and methanol in polymer electrolytes at elevated temperatures, Journal of the Electrochemical Society 143, 4, pp. 1260-1263

West A.R. (1995) Solid state electrochemistry (edited by Bruce P.G) Cambridge University Press, Cambridge

Willett M. (1999) Sensors and their applications X, Proceedings of the Tenth Conference on Sensors and their Applications (edited by White N.M. & Augousti A.T.), Institute of Physics Publishing, Bristol

Wintersgill M.C. & Fontanella F.F. (1998) Complex impedance measurements on Nafion, Electrochimica Acta, 43, 10-11, pp. 1533-1538

Wojciechowski C.L. & Fall R. (1996) A continuous fluorometric assay for pectin methylesterase, Analytical Biochemistry, 237, 1, pp. 103-108

Wroblowa H.S., Pan Y.C. & Razumney G. (1976) Electroreduction of oxygen a new mechanistic criterion, Journal of Electroanalytical Chemistry, 69, 2, pp. 195-201

Xing B. & Savadogo O. (1999) The effect of acid doping on the conductivity of polybenzimidazole (PBI), Journal of New Materials for Electrochemical Systems, 2, pp. 95-101

Yamamoto O. (1995) in Solid state electrochemistry (edited by Bruce P.G) Cambridge University Press, Cambridge

Yan H.Q. & Lu J.T. (1989) Solid polymer electrolyte-based electrochemical oxygen sensor, Sensors and Actuators, 19, pp. 33-40

Yan H.Q. & Lu J.T. (1997) A solid polymer electrolyte based oxygen sensor for portable oxygen meters, Field Analytical Chemistry and Technology, 1, 3, pp. 175-178

Yasuda A. & Shimidzu T. (1999) Electrochemical carbon monoxide sensor with a Nafion® film, Reactive & Functional Polymers, 41, 1-3, pp. 235-243

Yu C., Wang Y., Hua K., Xing W. & Lu T. (2002) Electrochemical H_2S sensor with H_2SO_4 pre-treated Nafion membrane as solid polymer electrolyte, Sensors and Actuators B, 86, pp. 259-265

Zawodzinski Jr T.A., Springer T.E., Davey J., Valerio J. & Gottesfeld S. (1991), Water transport properties of fuel cell ionomers in Modelling of batteries and fuel cells (edited by White R.E., Verbrugge M.W. & Stockel J.F.) The Electrochemical Society Softbound Proceedings Series, Pennington, NJ, vol. 9-10

Zawodzinski Jr T.A., Derouin C., Radzinski S., Sherman R.J., Smith V.T., Springer T.E. & Gottesfeld S. (1993) Water uptake by and transport through Nafion 117 membranes, Journal of the Electrochemical Society, 140, 4, pp. 1041-1047

Zecevic S.K., WainrightJ.S., Litt M., Gojkovic S.L & Savinell R.F. (1997) Kinetics of O-2 reduction on a Pt electrode covered with a thin film of solid polymer electrolyte, Journal of the Electrochemical Society, 144, 9, pp. 2973-2982